SAR Marine Applications (oil spill and ship detection)

Dr. Domenico Velotto, MARUM – Univ. Bremen, Germany

ESA Training Course on Earth Observation 2022

Friday 1 July 2022, Riga Technical University

AGENDA

- Introduction to SAR marine applications
- Fundamentals – Part I & II
  - Basic concepts ocean waves
  - Basic concepts SAR polarimetry
- SAR oil spill detection
  - Marine oil spill source and facts
  - SAR oil spill interpretation
  - Oil spill detection in single and multi-polarization SARs
- SAR ship detection
  - Introduction to Automatic Identification System
  - SAR ship detection interpretation
  - Ship detection in single and multi-polarization SARs

INTRODUCTION

- About **70%** of the Earth's surface is covered by saline waters, e.g. oceans and seas.
- Oceans and seas provide **non-renewable** and **renewable** energy **sources.**
- **About** 72% of Earth's biodiversity live in the oceans and seas

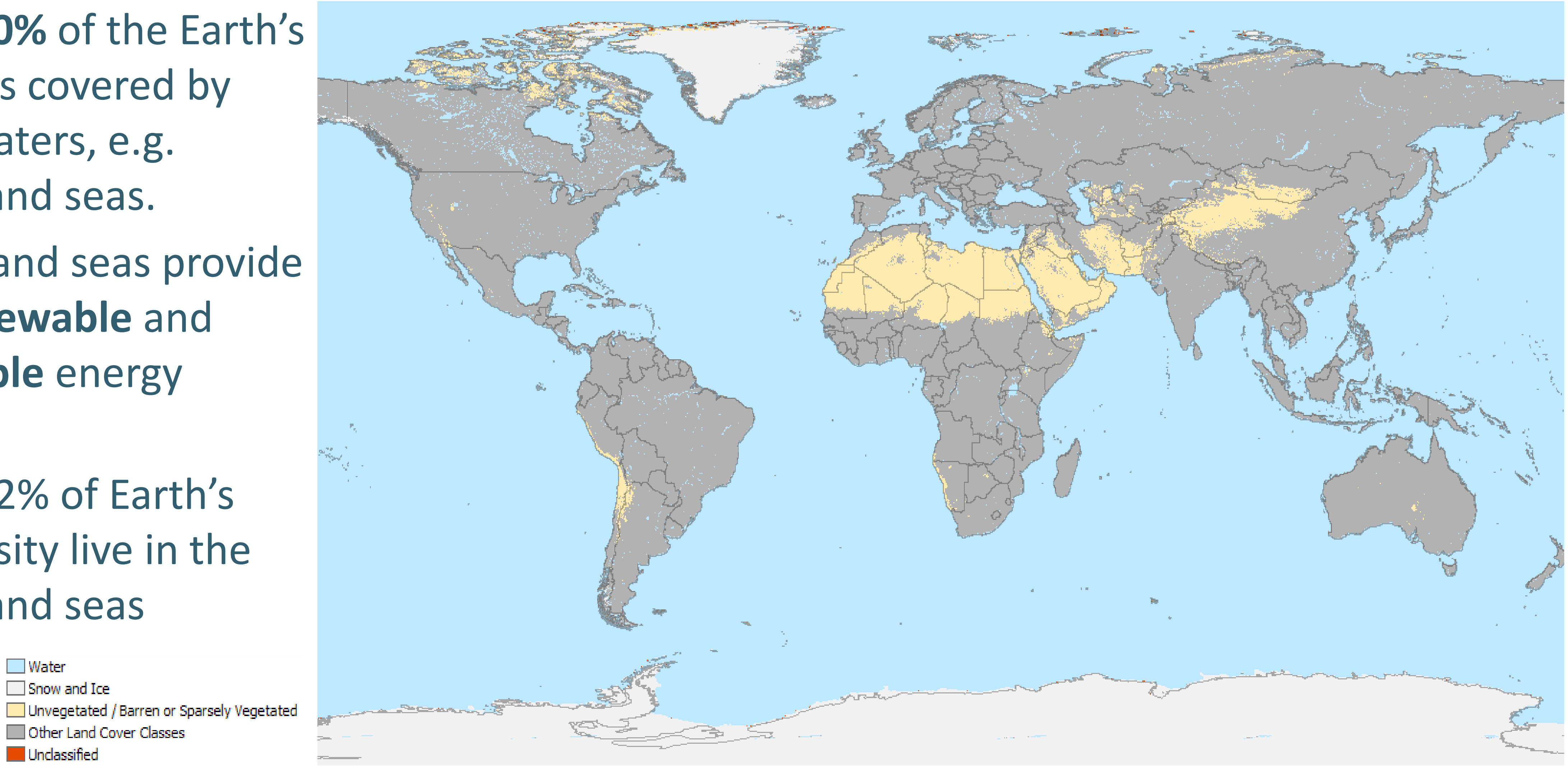

OCEAN MONITORING

Besides Models and In-Situ, there are **Satellites** that help monitoring the Earth’s Oceans!

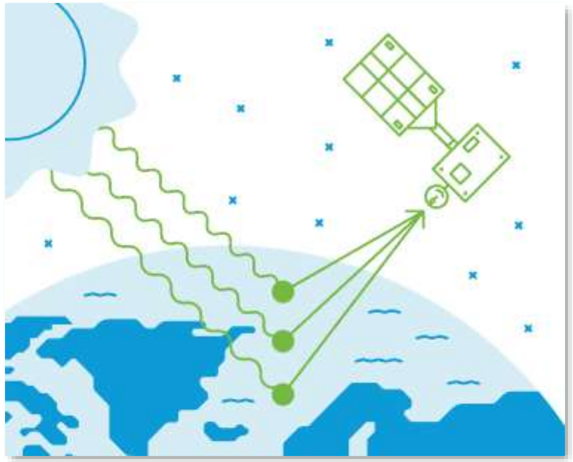

Spectroradiometer

Measures the light in a wide wavelength spectrum. *Chlorophyll content, mineral and organic content, sea surface temperature, sea ice cover*

Microwave radiometer

Measures the energy emitted in microwaves spectrum. *Atmospheric water content, rain rates, sea ice concentration, sea surface temperature, salinity*

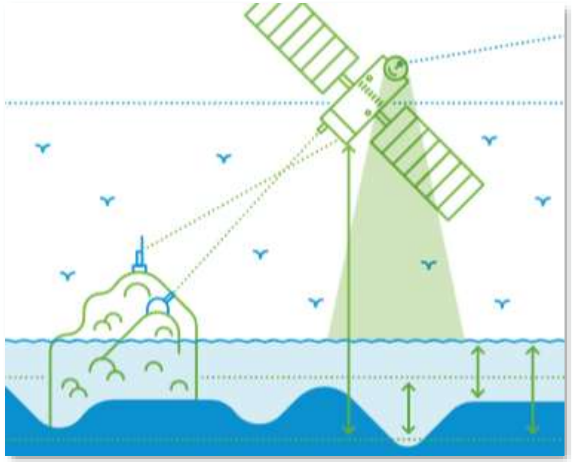

Satellite altimeter

Measures turnaround time delay of short electromagnetic pulse. *Sea surface height, ocean surface wind speed, wave height and sea ice.*

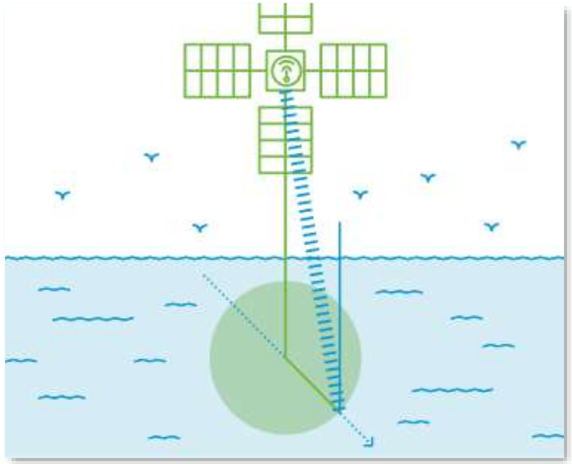

Satellite scatterometer

Measures the scattering energy produced while scanning the surface of the Earth. *Wind speed and direction, as well as rainfall and sea ice concentration*

Infrared radiometer

Measures the radiation being reflected by surfaces using infrared light . *Sea surface temperature*

Synthetic Aperture Radar

Measures the two dimensional scattering energy while scanning the surface of the Earth. *Wind, waves, oil, ship, current, ice*

SAR MARINE APPLICATIONS

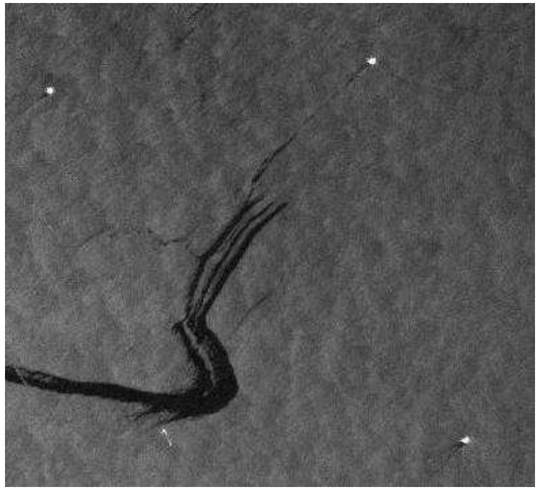
Oil spill, Seepage, Oil drift, Eddies


Ship detection, Wake

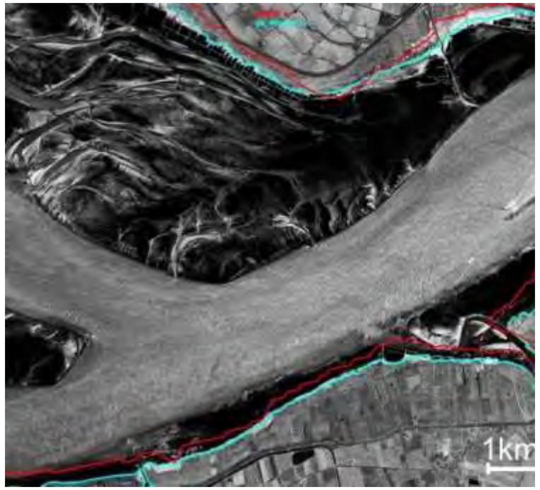

Land-Water line, Coastal erosion

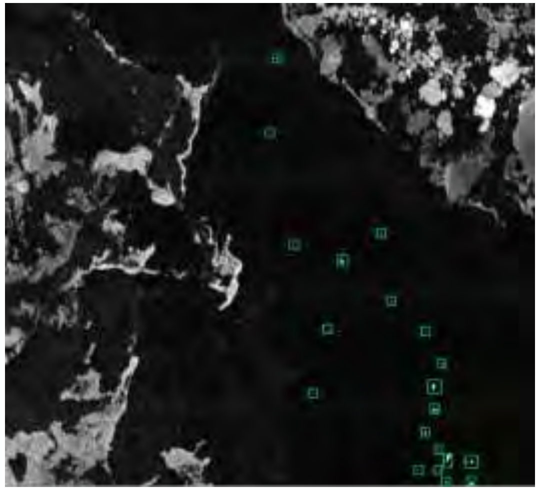
Icebergs detection

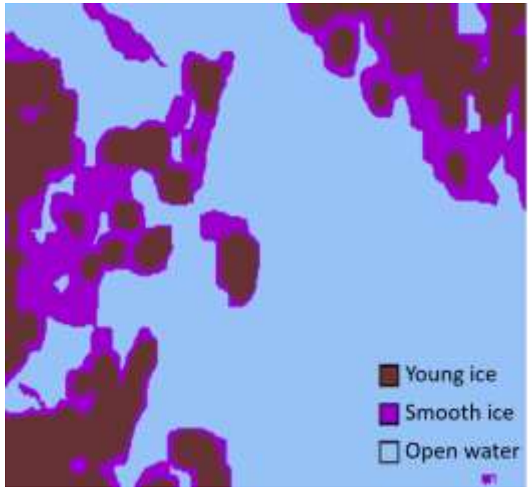

Ice classification

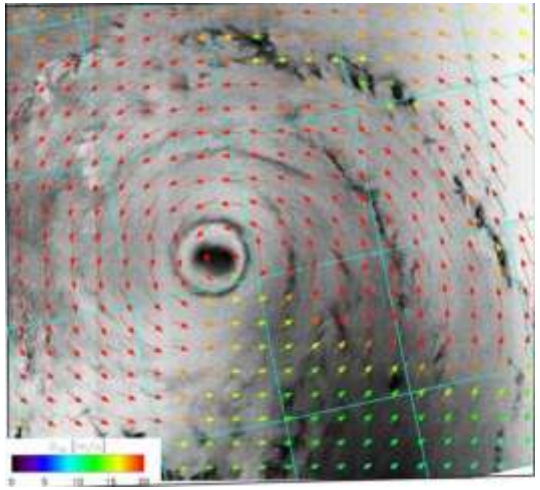
Wind, Hurricane/Cyclone, Windfarm

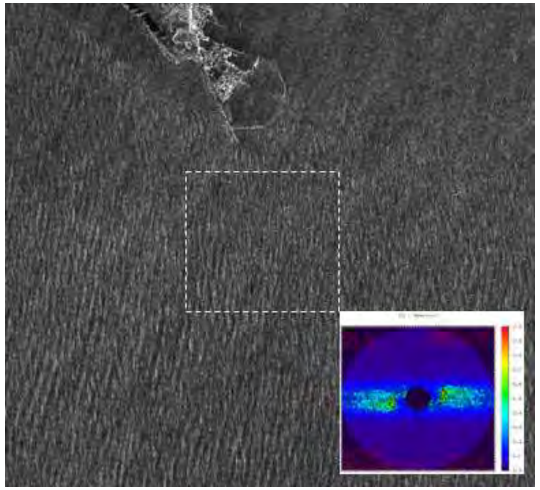
Sea state, Wave breaking, Bathymetry

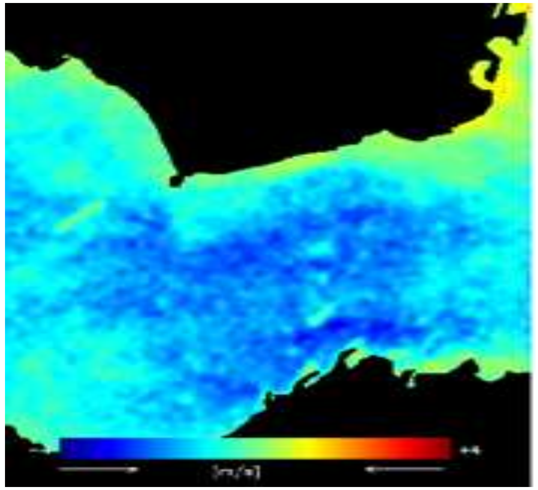
Surface current

FUNDAMENTALS – PART I

Ocean waters have a high dielectric constant which makes radio waves penetration at microwave frequency negligible.

Surface scattering

The roughness of the scattering surface is the main driver defining the observed radar return

Fraunhofer criterion

$$h_{rough} > \lambda/(32 \cdot \cos\theta_i)$$

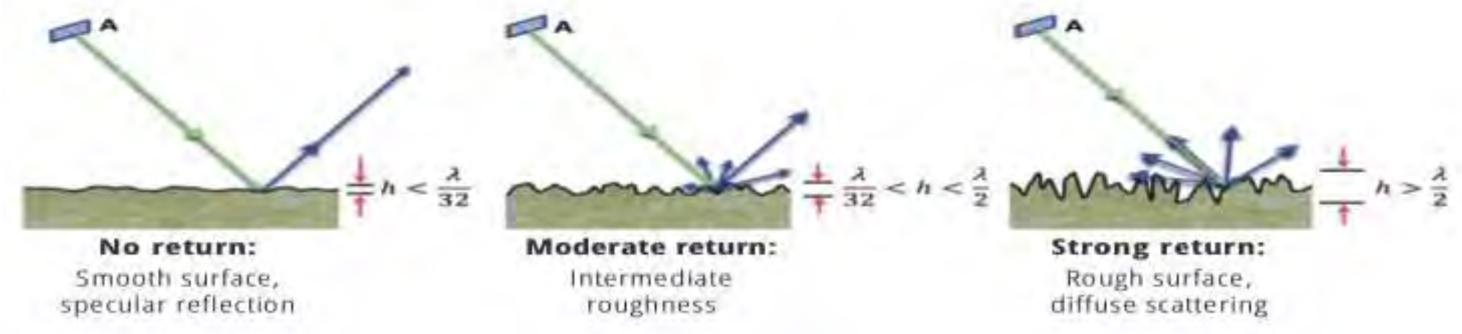

Ocean waves

FUNDAMENTALS – PART I

Ocean waves are classified by the force that creates them and the force that tries to flatten them.

1. **Disturbing forces**: energy that cause waves
   - Wind, gravity, seismic activity, landslides

2. **Restoring forces**: energy that returns the surface to being flat
   - Surface tension, cohesion, gravity

FUNDAMENTALS – PART I

Wind is the primary disturbing force for generating capillary waves and wind waves.
Wind speed, duration and fetch are the wind factor affecting the wave development:

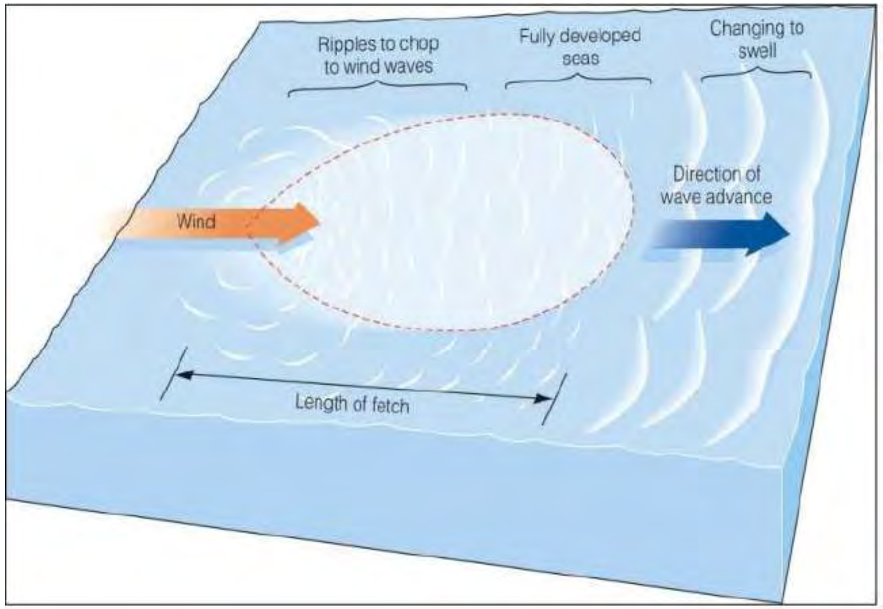

Note I: wind-wave interaction and the physical description of sea state is a complex topic which deserves a dedicated seminar and is not covered here.
Note II: the ocean surface is not static. Theoretical description of SAR imaging of ocean surface wave is out of the scope and not covered here.

FUNDAMENTALS – PART II

For a plane electromagnetic (EM) wave, **polarisation** refers to the behavior of the electric field vector in time observed at a fixed point in space.

Elliptical polarisation

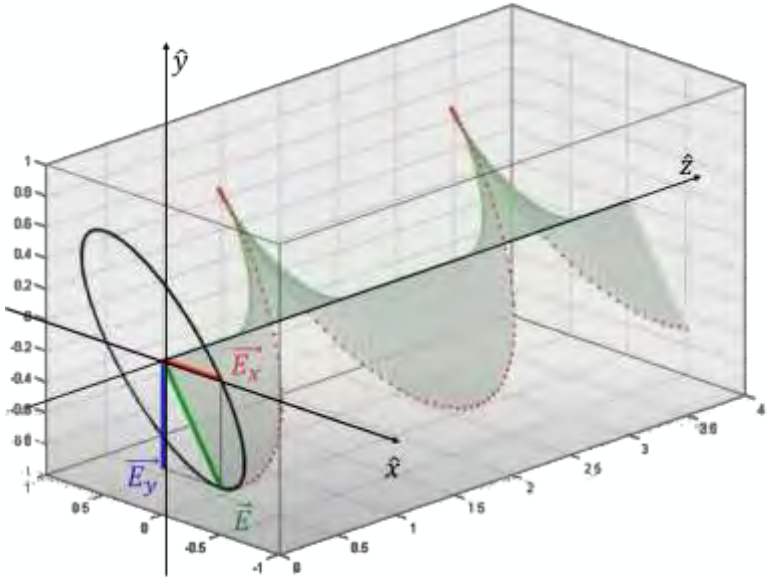

x, y component unequal in amplitude with relative phase $\neq 0^\circ, 90^\circ$

Circular polarisation

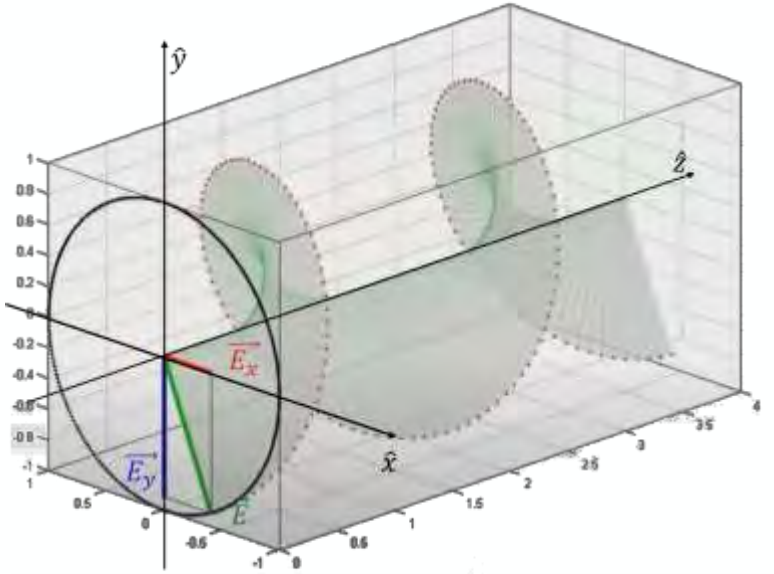

x, y component equal in amplitude with relative phase $= \pm 90^\circ$

Linear polarisation

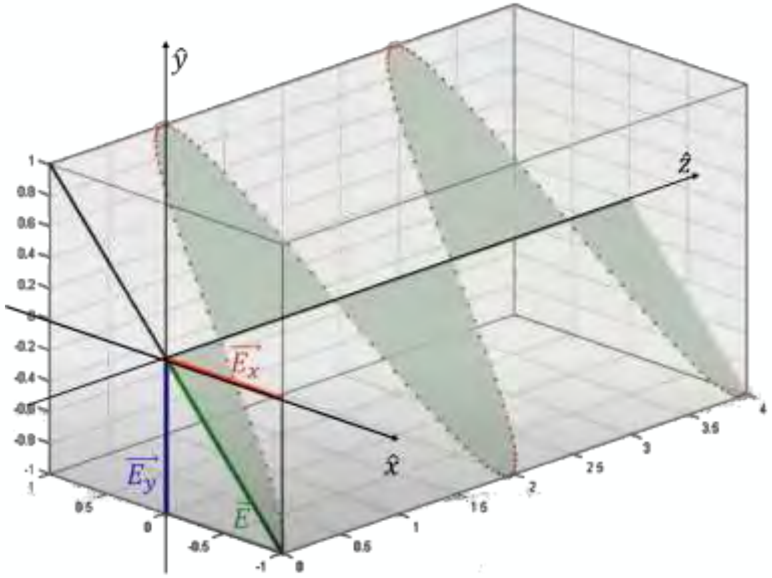

x, y component equal in amplitude and phase

x only -> horizontal; y only -> vertical

FUNDAMENTALS – PART II

The scattering problem: the scatterer changes the polarization of the incident wave

$$\begin{bmatrix} E_h^s \\ E_v^s \end{bmatrix} = F(s) \begin{bmatrix} \dot{S}_{hh} & \dot{S}_{hv} \\ \dot{S}_{vh} & \dot{S}_{vv} \end{bmatrix} \begin{bmatrix} E_h^i \\ E_v^i \end{bmatrix}$$

Spherical factor far field zone $F(s)$

2x2 scattering matrix $S = \begin{bmatrix} \dot{S}_{hh} & \dot{S}_{hv} \\ \dot{S}_{vh} & \dot{S}_{vv} \end{bmatrix}$

Cross-pol channels Co-pol channels

Complex scattering amplitude $\dot{S}_{tr} = |S_{tr}| e^{-j\varphi_{tr}}$

t=transmit r=receive

Bistatic case $\dot{S}_{hv} \neq \dot{S}_{vh}$ Monostatic case $\dot{S}_{hv} = \dot{S}_{vh}$

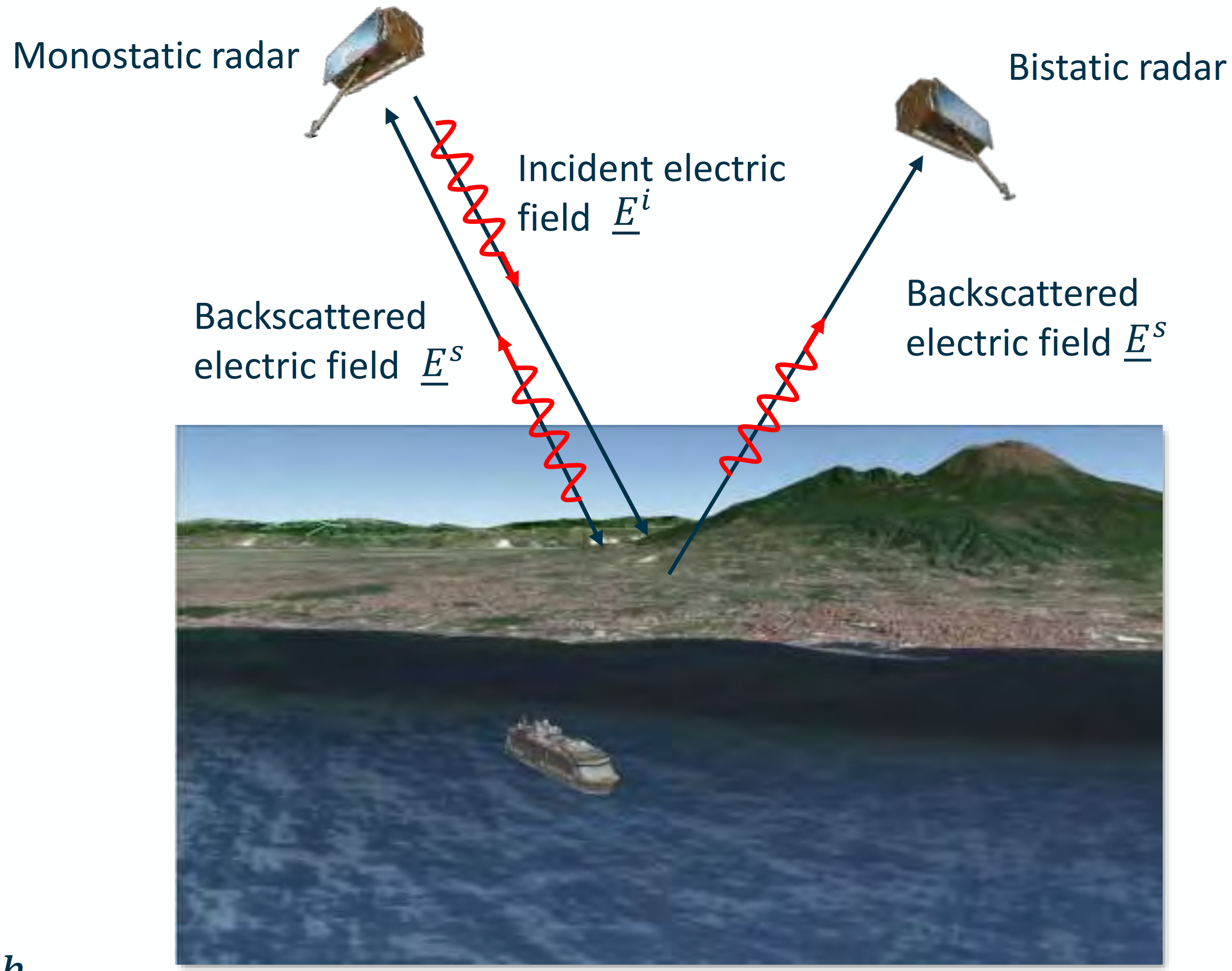

FUNDAMENTALS – PART II

Canonical scatterers and interpretation of polSAR data

Vertical dipole

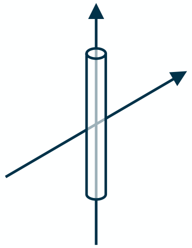

$S = \begin{bmatrix} 0 & 0 \\ 0 & 1 \end{bmatrix}$

Horizontal dipole

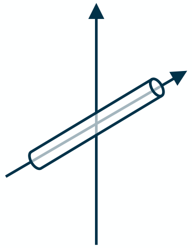

$S = \begin{bmatrix} 1 & 0 \\ 0 & 0 \end{bmatrix}$

Dihedral

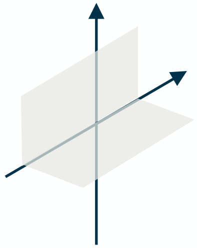

$S = \begin{bmatrix} 1 & 0 \\ 0 & -1 \end{bmatrix}$

HH and VV out of phase

Trihedral

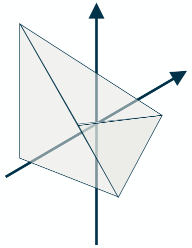

$S = \begin{bmatrix} 1 & 0 \\ 0 & 1 \end{bmatrix}$

HH and VV in phase

Surface scattering (bare soils, sea surface)

$$|\dot{S}_{hv}| \sim 0 \qquad |\dot{S}_{vv}| > |\dot{S}_{hh}|$$

$$\varphi_{vv} - \varphi_{hh} = 0$$

$$|\dot{S}_{hh} + \dot{S}_{vv}| \text{ high}$$

Volume scattering (dense forest)

$$|\dot{S}_{vv}|, |\dot{S}_{hh}| \text{ high}$$

$$|\dot{S}_{hv}| \text{ high}$$

Double bounce (urban area)

$$|\dot{S}_{hh}| > |\dot{S}_{vv}|$$

$$\varphi_{vv} - \varphi_{hh} = \pi$$

$$|\dot{S}_{hh} - \dot{S}_{vv}| \text{ high}$$

FUNDAMENTALS – PART II

Vectoral formulation of the scattering problem. Lexicographic and Pauli scattering vectors

The vectorization of S is needed to extract physical information and is achieved by constructing a system vectors as follows:

$$S = \begin{bmatrix} \dot{S}_{hh} & \dot{S}_{hv} \\ \dot{S}_{vh} & \dot{S}_{vv} \end{bmatrix} \qquad \vec{k} = \frac{1}{2} Tr(S\Psi)$$

For monostatic backscattering case $\dot{S}_{hv} = \dot{S}_{vh}$ two sets of orthogonal spin matrixes are defined

$$\{\Psi_L\} = \left\{ 2\begin{bmatrix} 1 & 0 \\ 0 & 0 \end{bmatrix} \quad 2\sqrt{2}\begin{bmatrix} 0 & 1 \\ 0 & 0 \end{bmatrix} \quad \sqrt{2}\begin{bmatrix} 0 & 0 \\ 0 & 1 \end{bmatrix} \right\}$$

$$\{\Psi_P\} = \left\{ \sqrt{2}\begin{bmatrix} 1 & 0 \\ 0 & 1 \end{bmatrix} \quad \sqrt{2}\begin{bmatrix} 1 & 0 \\ 0 & -1 \end{bmatrix} \quad \sqrt{2}\begin{bmatrix} 0 & 1 \\ 1 & 0 \end{bmatrix} \right\}$$

so the corresponding Lexicographic and Pauli target vectors are

$$\overrightarrow{k_L} = \begin{bmatrix} \dot{S}_{hh} & \sqrt{2}\dot{S}_{hv} & \dot{S}_{vv} \end{bmatrix}^T$$

$$\overrightarrow{k_P} = \frac{1}{\sqrt{2}} \begin{bmatrix} \dot{S}_{hh} + \dot{S}_{vv} & \dot{S}_{hh} - \dot{S}_{vv} & 2\dot{S}_{hv} \end{bmatrix}^T$$

The factors 2, $\sqrt{2}$, $2\sqrt{2}$ ensure the invariane of the total power

$$\mathrm{Span}(S) = |\dot{S}_{hh}|^2 + 2|\dot{S}_{hv}|^2 + |\dot{S}_{vv}|^2$$

Distributed targets. Covariance and Coherency matrixes

S describes the scattering from a point target, but insufficient for distributed targets. Statistically based matrices are used in the latter case

$$C_3 = \langle k_L \cdot k_L^H \rangle = \begin{bmatrix} \langle |\dot{S}_{hh}|^2 \rangle & \sqrt{2}\langle \dot{S}_{hh}\dot{S}_{hv}^* \rangle & \langle \dot{S}_{hh}\dot{S}_{vv}^* \rangle \\ \sqrt{2}\langle \dot{S}_{hv}\dot{S}_{hh}^* \rangle & 2\langle |\dot{S}_{hv}|^2 \rangle & \sqrt{2}\langle \dot{S}_{hv}\dot{S}_{vv}^* \rangle \\ \langle \dot{S}_{vv}\dot{S}_{hh}^* \rangle & \sqrt{2}\langle \dot{S}_{vv}\dot{S}_{hv}^* \rangle & \langle |\dot{S}_{vv}|^2 \rangle \end{bmatrix}$$

$$T_3 = \langle k_P \cdot k_P^H \rangle = \frac{1}{2}\begin{bmatrix} \langle |\dot{S}_{hh} + \dot{S}_{vv}|^2 \rangle & \langle (\dot{S}_{hh}+\dot{S}_{vv})(\dot{S}_{hh}-\dot{S}_{vv})^* \rangle & 2\langle (\dot{S}_{hh}+\dot{S}_{vv})\dot{S}_{hv}^* \rangle \\ \langle (\dot{S}_{hh}-\dot{S}_{vv})(\dot{S}_{hh}+\dot{S}_{vv})^* \rangle & \langle |\dot{S}_{hh} - \dot{S}_{vv}|^2 \rangle & 2\langle (\dot{S}_{hh}-\dot{S}_{vv})\dot{S}_{hv}^* \rangle \\ 2\langle \dot{S}_{hv}(\dot{S}_{hh}+\dot{S}_{vv})^* \rangle & 2\langle \dot{S}_{hv}(\dot{S}_{hh}-\dot{S}_{vv})^* \rangle & 4\langle |\dot{S}_{hv}|^2 \rangle \end{bmatrix}$$

where $(\cdot)^H$ is the adjoint, $(\cdot)^*$ is the conjugate and $\langle \cdot \rangle$ is the averaging operator

Covariance matrix polarimetric features

$$C_3 = \sigma \begin{bmatrix} 1 & \beta\sqrt{\delta} & \rho\sqrt{\gamma} \\ \beta^*\sqrt{\delta} & \delta & \varepsilon\sqrt{\gamma\delta} \\ \rho^*\sqrt{\gamma} & \varepsilon^*\sqrt{\gamma\delta} & \gamma \end{bmatrix}$$

Channel power

$$\sigma = \langle |\dot{S}_{hh}|^2 \rangle$$

Cross- and Co-pol polarization ratio

$$\delta = 2\frac{\langle |\dot{S}_{hv}|^2 \rangle}{\sigma}$$

$$\gamma = \frac{\langle |\dot{S}_{vv}|^2 \rangle}{\sigma}$$

Inter-correlation parameters

$$\rho = \frac{\langle \dot{S}_{hh}\dot{S}_{vv}^* \rangle}{\sigma\sqrt{\gamma}} = \frac{\langle \dot{S}_{hh}\dot{S}_{vv}^* \rangle}{\sqrt{\langle |\dot{S}_{hh}|^2 \rangle \langle |\dot{S}_{vv}|^2 \rangle}}$$

$$\beta = \frac{\sqrt{2}\langle \dot{S}_{hh}\dot{S}_{hv}^* \rangle}{\sigma\sqrt{\delta}} = \frac{\langle \dot{S}_{hh}\dot{S}_{hv}^* \rangle}{\sqrt{\langle |\dot{S}_{hh}|^2 \rangle \langle |\dot{S}_{hv}|^2 \rangle}}$$

$$\varepsilon = \frac{\sqrt{2}\langle \dot{S}_{hv}\dot{S}_{vv}^* \rangle}{\sigma\sqrt{\gamma\delta}} = \frac{\langle \dot{S}_{hv}\dot{S}_{vv}^* \rangle}{\sqrt{\langle |\dot{S}_{hv}|^2 \rangle \langle |\dot{S}_{vv}|^2 \rangle}}$$

FUNDAMENTALS – PART II

Eigenvalue decomposition polarimetric features

With the eigenvalue analysis of the coherency (covariance) matrix it is possible to valuate the dominant average scattering mechanism in each cell. λ_j and e_j are the j-th eigenvalue, eigenvector

$$\mathrm{T}_3 = \sum_{j=1}^{3} \lambda_j \, \underline{e}_j \cdot \underline{e}_j^{\,H}$$

$$\lambda_1 > \lambda_2 > \lambda_3$$

From single scattering mechanism $(\lambda_1 \neq 0, \lambda_2 = \lambda_3 = 0)$ to de-correlated random scattering $(\lambda_1 = \lambda_2 = \lambda_3 \neq 0)$ there is the case of distributed or partially polarized scatterers.

Entropy

$$H = -\sum_{j=1}^{3} P_j \log_3 P_j \quad H \in [0, 1] \qquad P_j = \frac{\lambda_j}{\lambda_1 + \lambda_2 + \lambda_3} \quad P_j \in [0, 1]$$

Average alpha angle

$$\bar{\alpha} = P_1 \alpha_1 + P_2 \alpha_2 + P_3 \alpha_3 \quad \bar{\alpha} \in [0°, 90°]$$

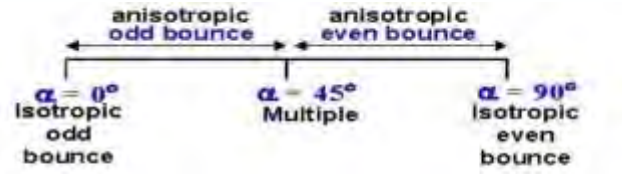

Anisotropy

$$A = \frac{\lambda_2 - \lambda_3}{\lambda_2 + \lambda_3} = \frac{P_2 - P_3}{P_2 + P_3} \qquad 0 \leq A \leq 1$$

Note: there are many more polarimetric parameters which have been introduced in literature for different applications, as well as a whole set of model-based decomposition technique not covered.

FUNDAMENTALS – PART II

PolSAR in a nutshell

Schematic representation of PolSAR radar system composed of two receiver chains and T/R timing diagram

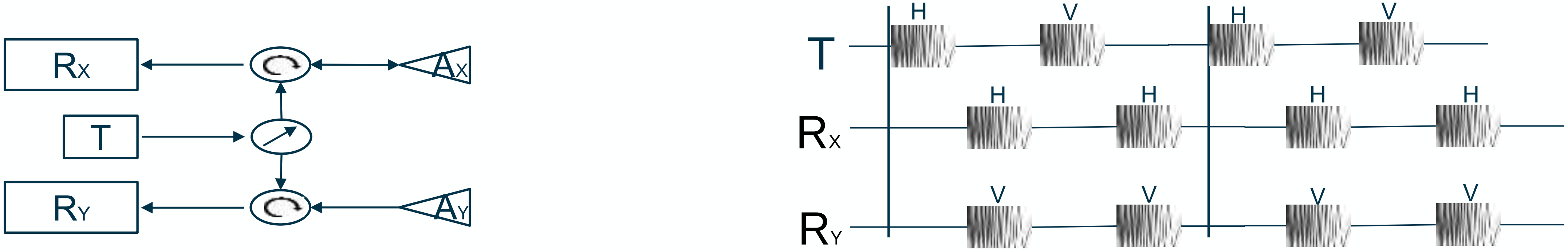

Quad-pol: 4 combinations $[\dot{S}_{hh}, \dot{S}_{hv}, \dot{S}_{vh}, \dot{S}_{vv}]$ ⟶ Doubling of the PRF

Dual-pol: 2 combinations $[\dot{S}_{hh}, \dot{S}_{hv}]$ or $[\dot{S}_{vh}, \dot{S}_{vv}]$ and the combination $[\dot{S}_{hh}, \dot{S}_{vv}]$[1] doubling the PRF

► **PolSAR side effects**: reduced swath width (half coverage in range), reduced spatial resolution (doubled in azimuth).

[1] Different SAR missions have different implementations of the $[\dot{S}_{hh}, \dot{S}_{vv}]$: twin, alternating polarization, ping pong. PRF doubling is needed to keep the inter-channel correlation

Effects of the PolSAR reduced swath width for the oil spill observation

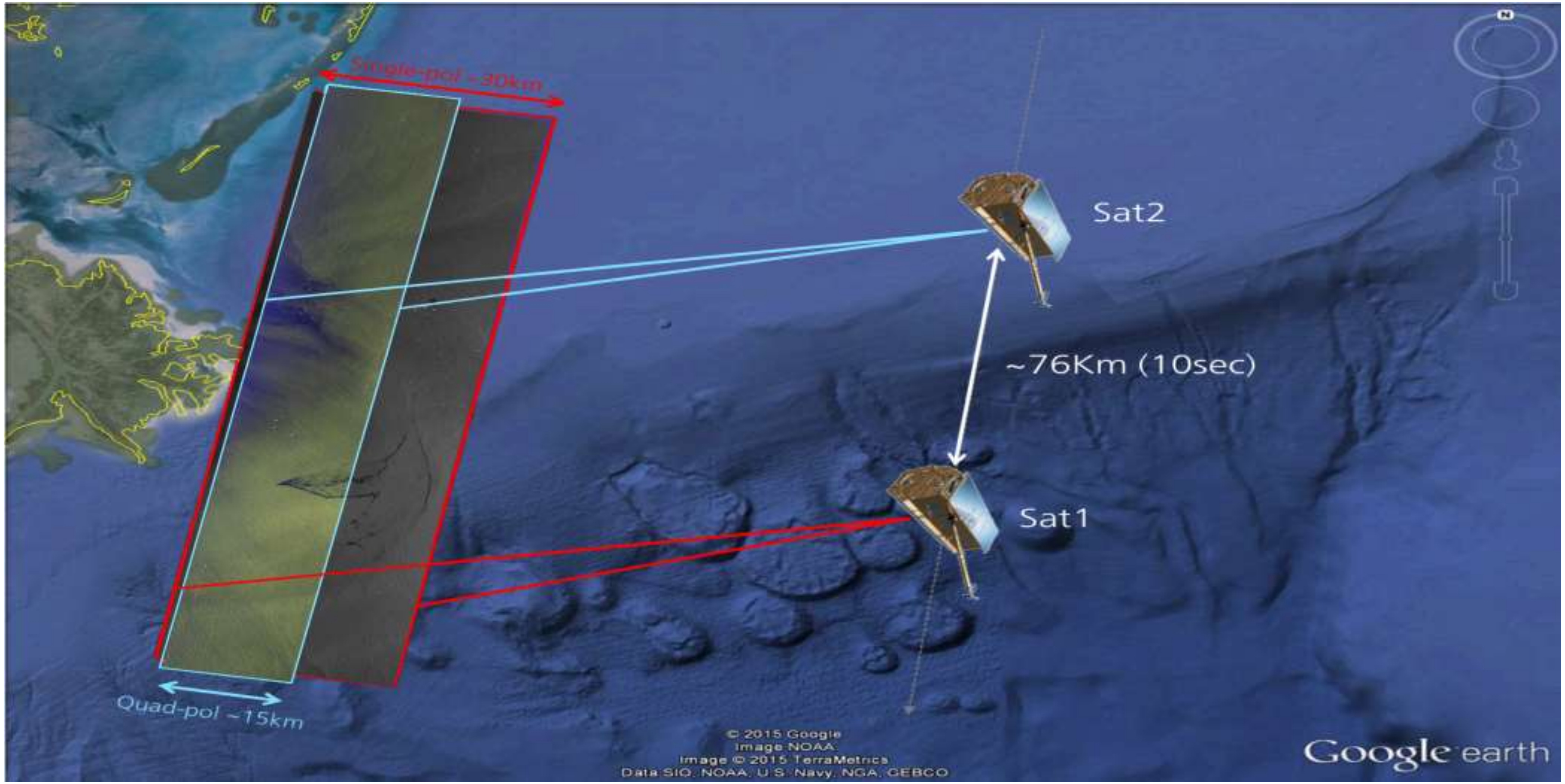

Effects of the PolSAR reduced spatial resolution for the ship detection

Single-pol HH polarization acquired by TS-X

Imaged ship
Length 67.0m
Width 14.6m

Quad-pol HH polarization acquired by TD-X

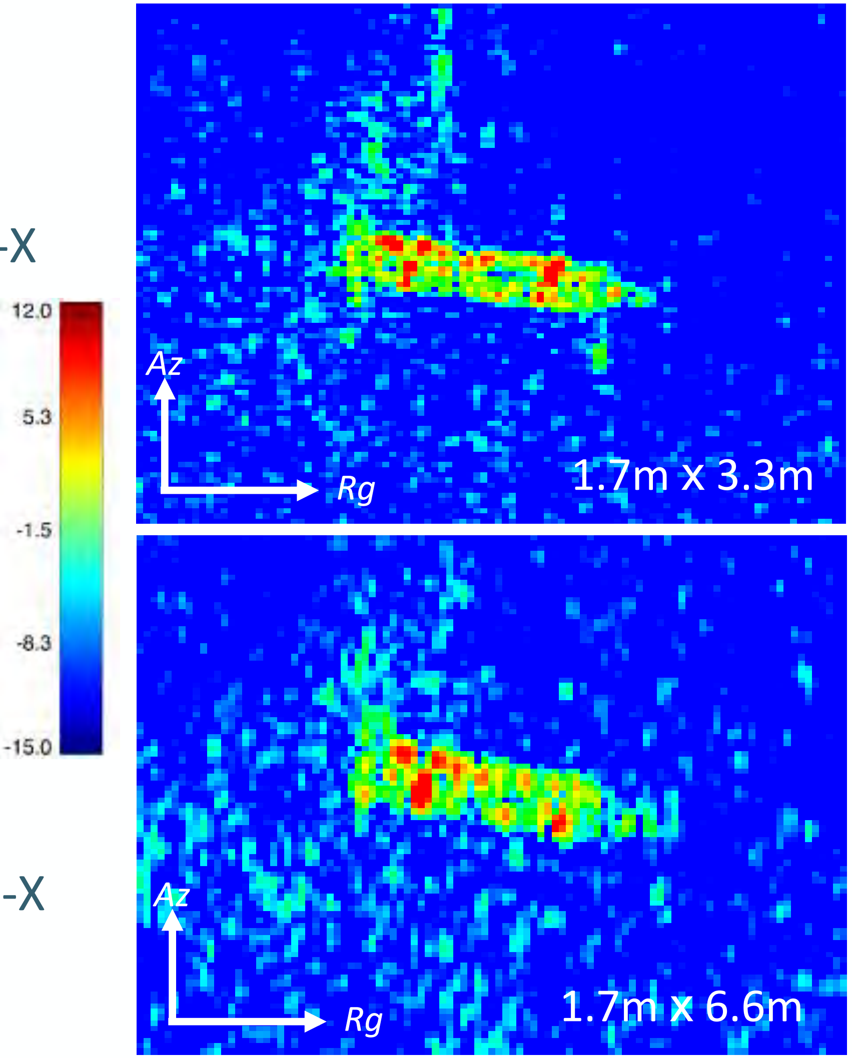

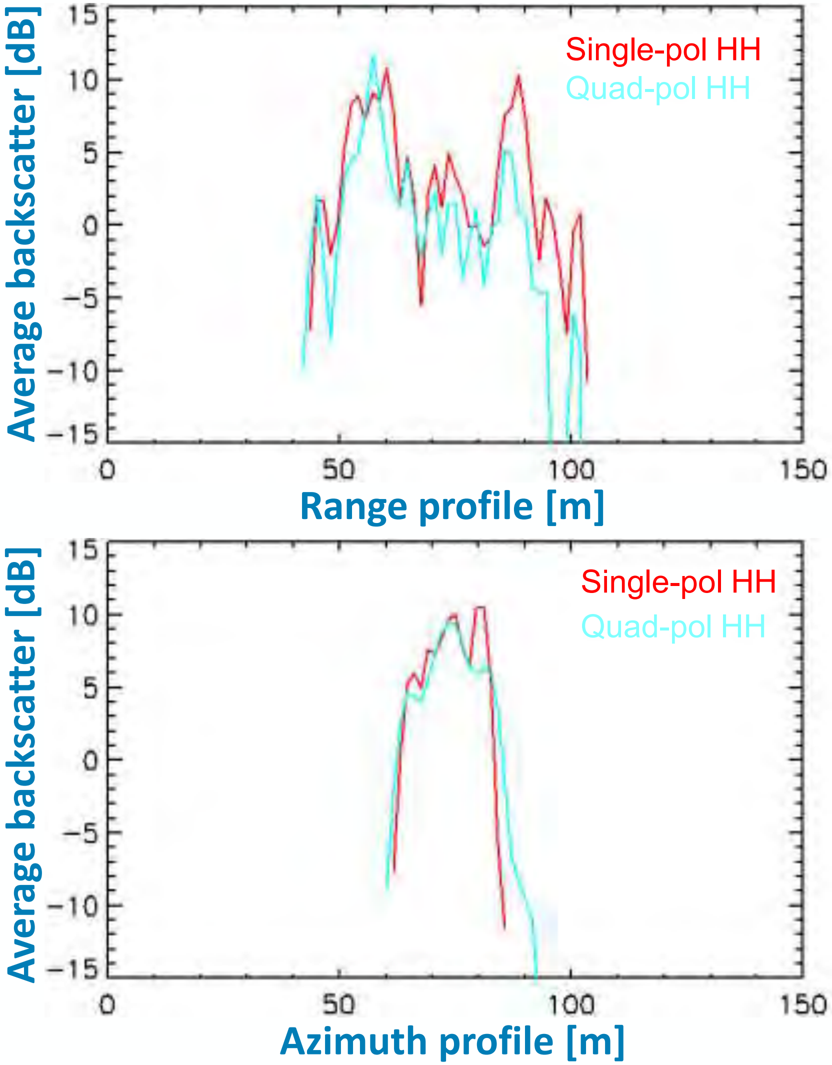

SAR imaging mode and TerraSAR-X PolSAR case example

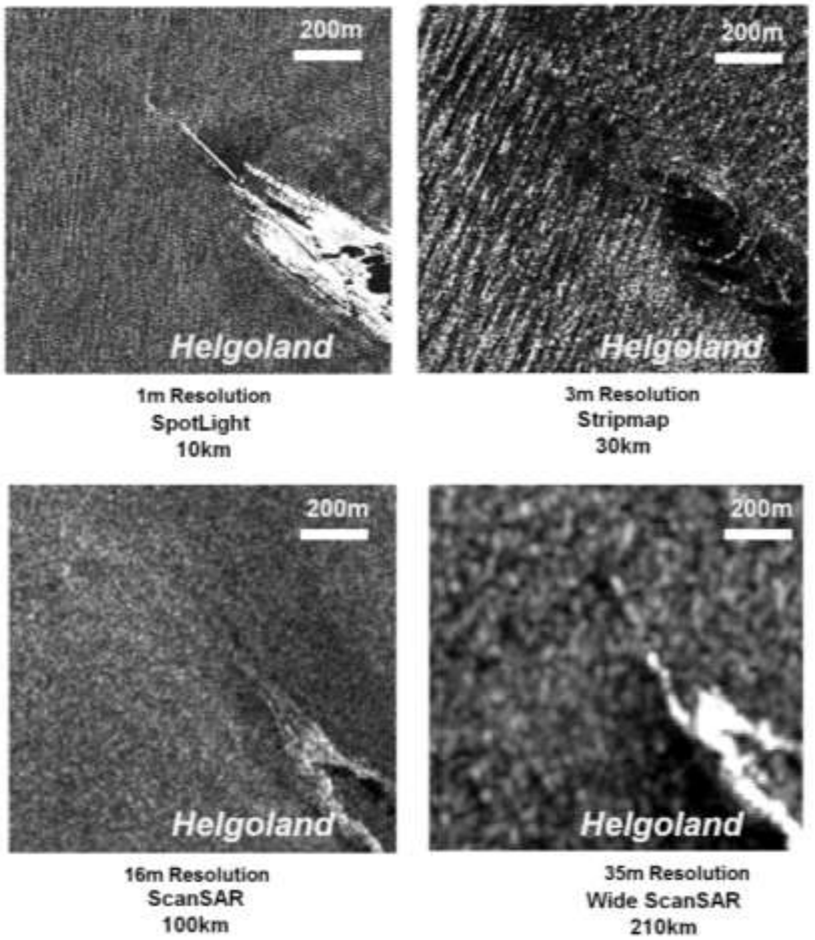

ScanSAR (Wide)

- Resolution [Rg x Az, m]: 18 x 18 (36 x 36)
- Coverage [Rg x Az, km]: 100 x 150 (200 x 150)
- Polarisation: only single-pol
- Applications: oil, ship, coastline, iceberg hurricane

StripMAP (Dual-pol)

- Resolution [Rg x Az, m]: 3 x 3 (6 x 6)
- Coverage [Rg x Az, km]: 30 x 50 (15 x 50)
- Polarisation: single-, dual-pol
- Applications: oil, ship, wake, iceberg, ice, wind, wave

SpotLight (Dual-pol)

- Resolution [Rg x Az, m]: 1.7 x 1.7 (3.4 x 3.4)
- Coverage [Rg x Az, km]: 10 x 10
- Polarisation: single-pol, only HH/VV
- Applications: ship, breaking wave, bathymetry

DRA Quad (ATI)

- Resolution [Rg x Az, m]: 6 x 6 (3 x3)
- Coverage [Rg x Az, km]: 15 x 50 (30 x 50)
- Polarisation: quad-pol (single-pol)
- Applications: oil, ship, current

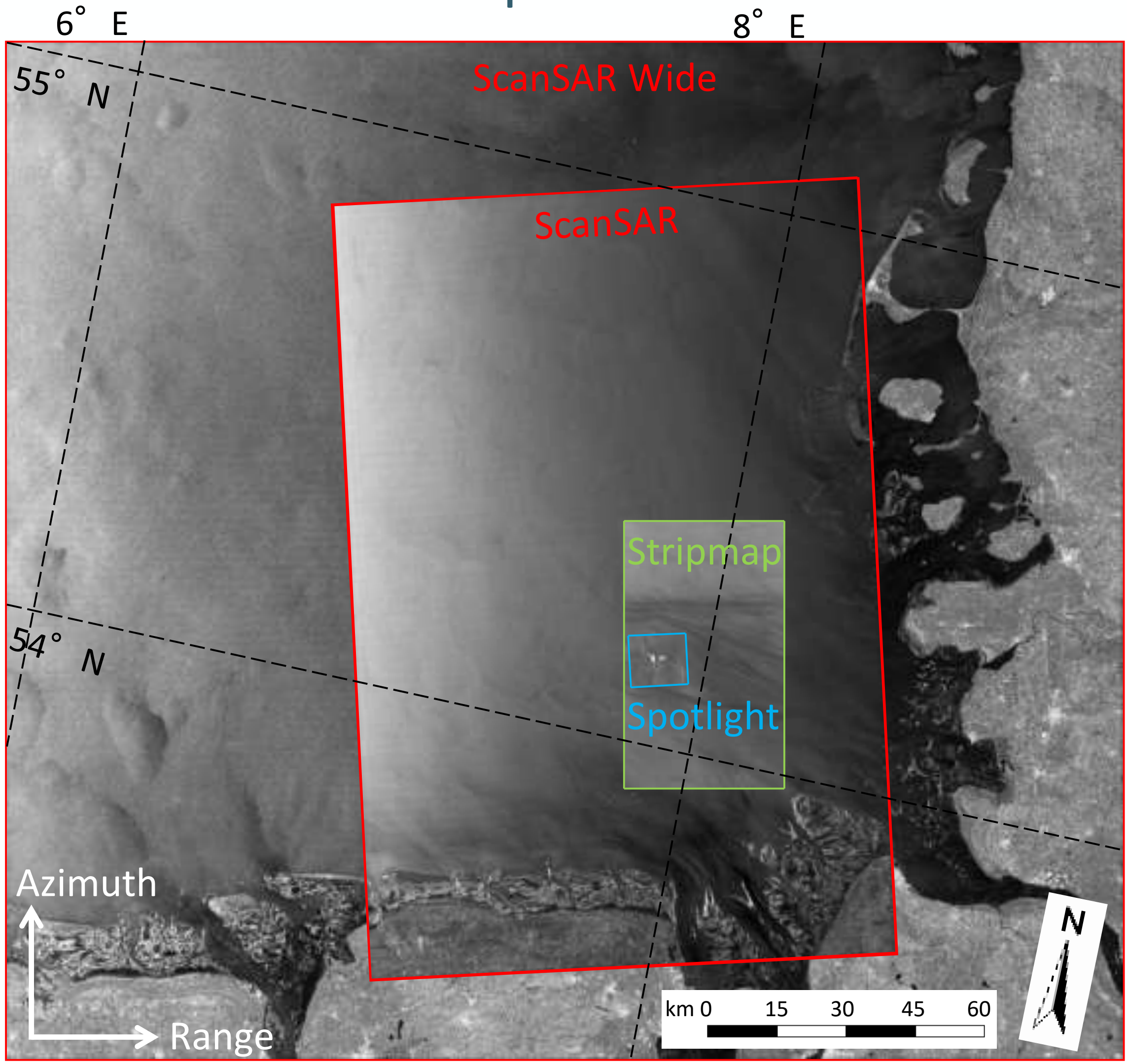

SAR MARINE APPLICATIONS

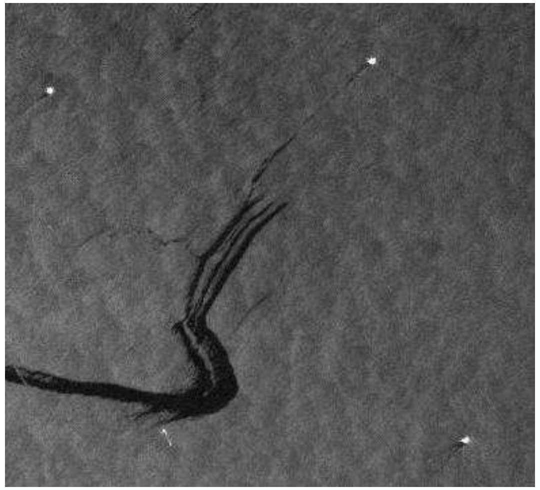

Oil spill, Seepage, Oil drift, Eddies

Ship detection, Wake

Land-Water line, Coastal erosion

Icebergs detection

Ice classification

Wind, Hurricane/Cyclone, Windfarm

Sea state, Wave breaking, Bathymetry

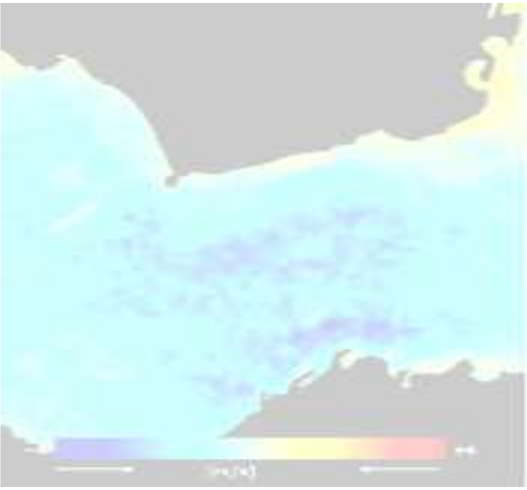

Surface current

DEFINITION OF OIL SPILL

- Oil is a general term used to denote petroleum products which mainly consist of liquid hydrocarbons.
- Crude oils are made up of a wide spectrum of hydrocarbons ranging from very volatile, light material such as propane and benzene to more complex heavy compounds such as bitumen, asphaltenes, resins and waxes.
- An oil spill is a violent spillage due to human activity that is concentrated in a specific area and surpassing the natural assimilation capacities of the surrounding environment.

SOURCE OF OIL SPILL

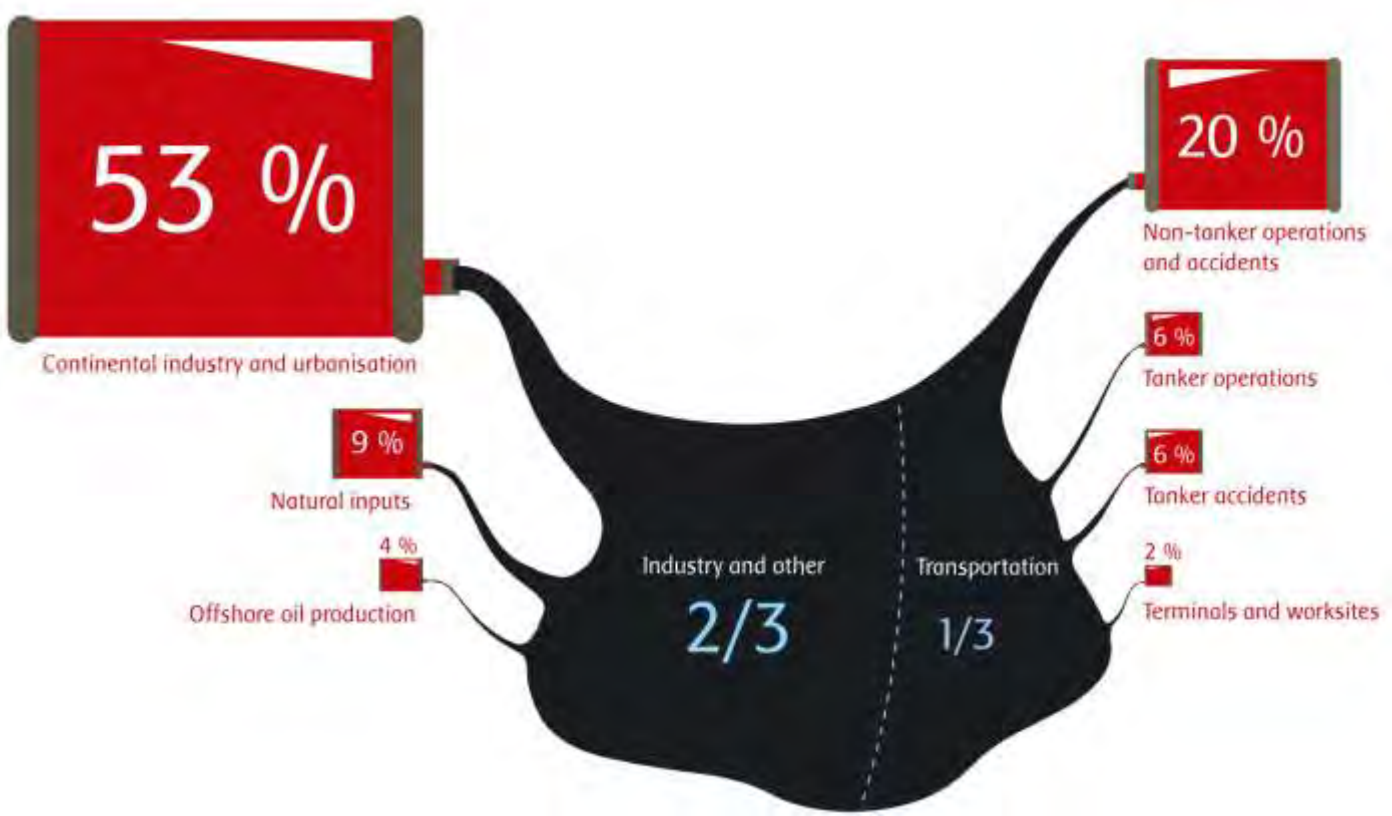

Selection of Largest oil spills			
Spill / Tanker	Location	Date	Tonnes of crude oil (thousands)
Kuwaiti Oil Fires	Kuwait	16.01.91 – 6.11.91	136,000
Kuwaiti Oil Lakes	Kuwait	01.91 – 11.91	3,409–6,818
Lakeview Gusher	California, USA	1910 – 1911	1,200
Gulf War oil spill	Kuwait, Iraq, and the Persian Gulf	1991	818–1,091
Deepwater Horizon	Gulf of Mexico, USA	20.04.2010 – 15.07.2010	560–585
Ixtoc I	Gulf of Mexico, Mexico	3.06.1979 – 23.03.1980	454–480
Atlantic Empress / Aegean Captain	Trinidad and Tobago	1979	287
Fergana Valley	Uzbekistan	2.03.1992	285
ABT Summer	Angola	28.05.1991	260
Nowruz Field Platform	Persian Gulf, Iran	4.02.1983	260
Castillo de Bellver	South Africa, Saldanha Bay	6.08.1983	252
Amoco Cadiz	France, Brittany	16.03.1978	223
Taylor Energy	Gulf of Mexico, USA	2004 – Present	210–490

SOURCE OF OIL SPILL

- Accidents involving tankers rank top in number but not in quantity (oil spills caused by war and wells blowout are larger)
- Some oil spill have marked history not for their size but for the combination geographical location, clean-up and compensations costs and political context, e.g. Exxon Valdez (Alaska), Erika (France), Deepwater Horizon (USA)

- There are 3 types of routine ship operations which pollute the sea:
  - Ballast water*
  - Tank washing residues*
  - Engine room effluent discharges

*Mainly tankers

Selection of Largest oil spills

Spill / Tanker	Location	Date	Tonnes of crude oil (thousands)
Kuwaiti Oil Fires	Kuwait	16.01.91 – 6.11.91	136,000
Kuwaiti Oil Lakes	Kuwait	01.91 – 11.91	3,409–6,818
Lakeview Gusher	California, USA	1910 – 1911	1,200
Gulf War oil spill	Kuwait, Iraq, and the Persian Gulf	1991	818–1,091
Deepwater Horizon	Gulf of Mexico, USA	20.04.2010 – 15.07.2010	560–585
Ixtoc I	Gulf of Mexico, Mexico	3.06.1979 – 23.03.1980	454–480
Atlantic Empress / Aegean Captain	Trinidad and Tobago	1979	287
Fergana Valley	Uzbekistan	2.03.1992	285
ABT Summer	Angola	28.05.1991	260
Nowruz Field Platform	Persian Gulf, Iran	4.02.1983	260
Castillo de Bellver	South Africa, Saldanha Bay	6.08.1983	252
Amoco Cadiz	France, Brittany	16.03.1978	223
Taylor Energy	Gulf of Mexico, USA	2004 – Present	210–490

© Info extracted from Wikipedia, 17.05.2022

OIL POLLUTION PREVENTION AND SURVEILLANCE

IMO MARPOL Annex I – Prevention of pollution by Oil

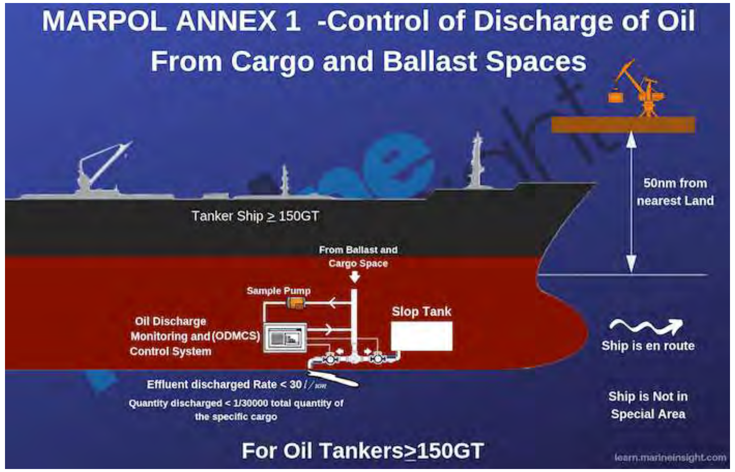

© marineinsight.com

- Special Areas Annex I: Mediterranean Sea, Baltic Sea, Black Sea, Red Sea, Gulf Area, Gulf of Aden, Antarctic area, North West European Waters, Oman area of the Arabian Sea, Southern South African waters
- Regional convention and community laws can be more restrictive: Bonn agreement, Helsinki convention, Directive 2005/35/EC

Monitoring and surveillance – The EMSA CleanSeaNet European satellite based oil spill monitoring and vessel detection service

© EMSA

REMOTE SENSING AND OIL SPILL

Overview table of remote sensing techniques used for oil spill monitoring

Type	Optical				Microwave	
Sensor	Visible	IR	UV	LFS	MWR	SAR/SLAR
Weather condition	No clouds	No clouds No fog	Clear atmosphere	No clouds No fog	All weather	All weather
24 h operation	No	Yes	No	Yes	Yes	Yes
Spatial Resolution	High	High	High	High (line profile)	Low	Very high-High
Spatial Coverage	Medium (airplane)	Small (airplane)	Small (airplane)	Small (airplane)	Small	High
Thickness Information	No	Rough Estimation	No	$<20\ \mu m$	$50\ \mu m$ – few mm	No
Oil classification	No	No	No	Yes	No	No
False Alarms	Algae, dark shoreline	Algae, shoreline	Algae, sun glint, wind sheen	No	No	Algae, low wind area, oceanic features

REMOTE SENSING AND OIL SPILL

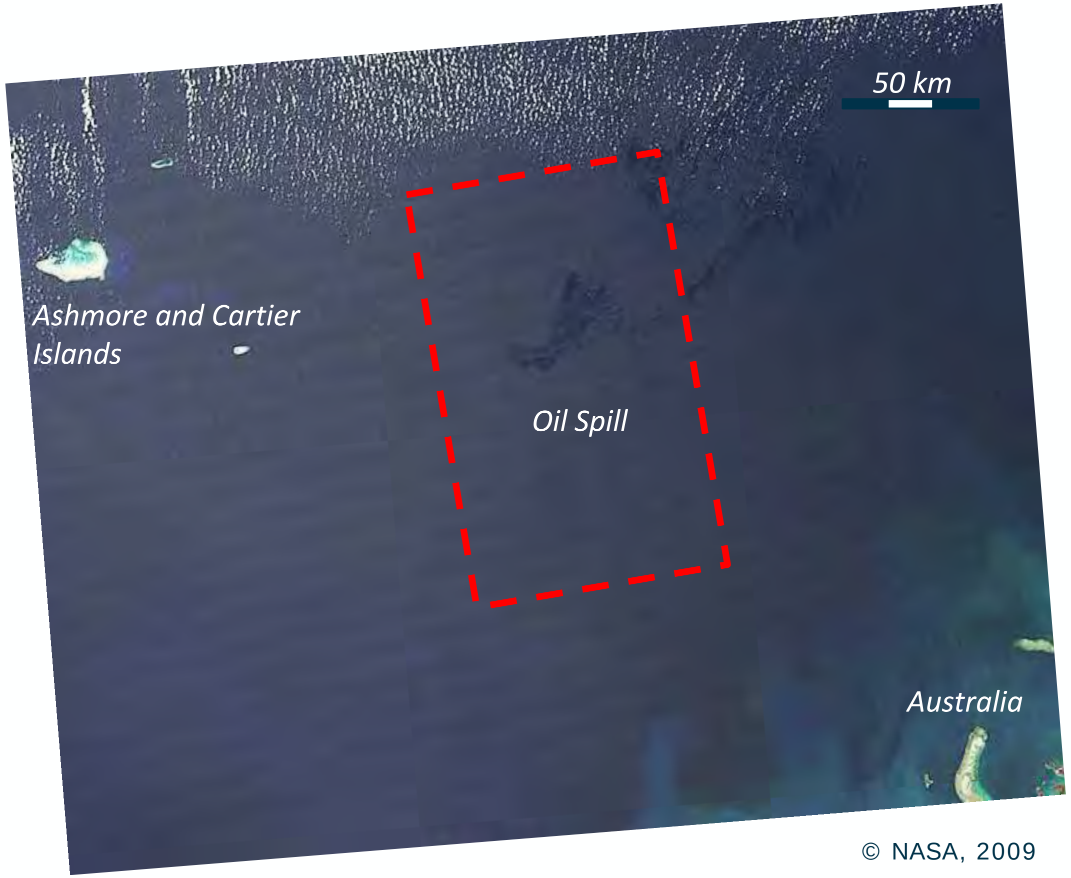

© NASA, 2009

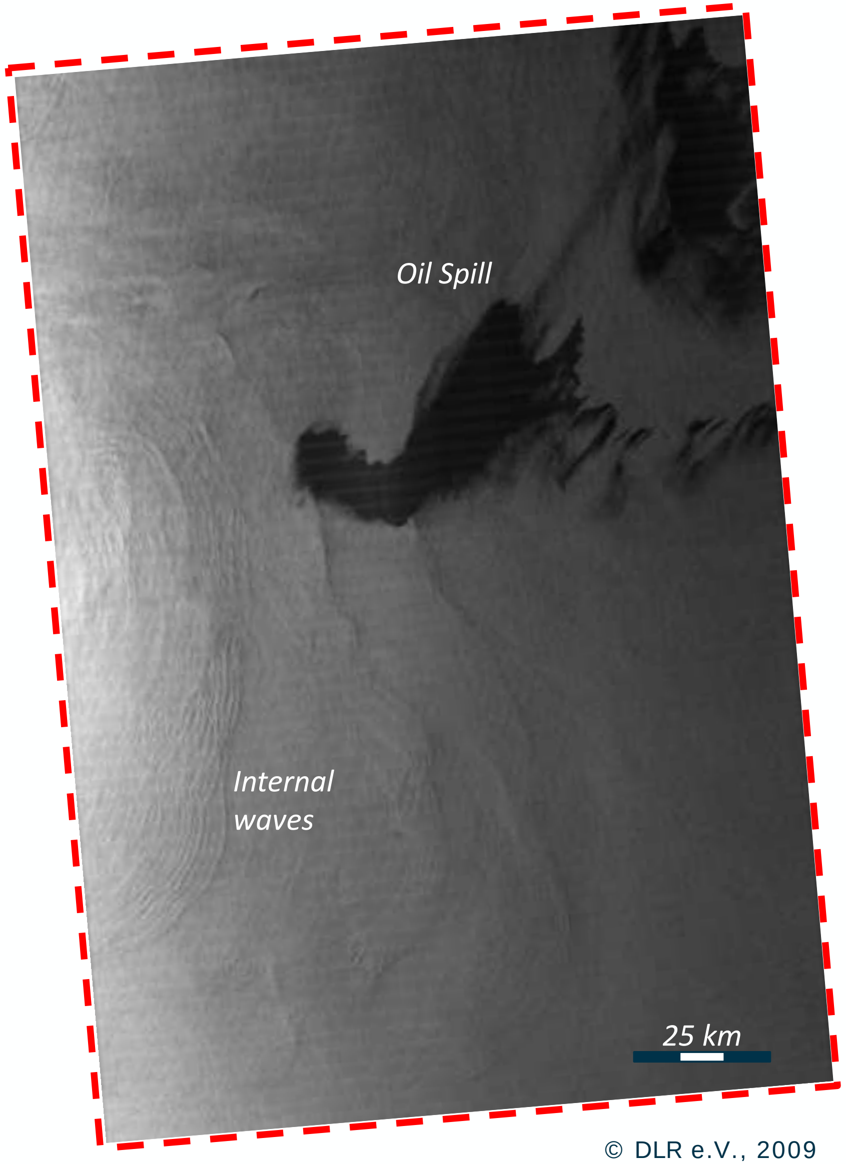

© DLR e.V., 2009

Left multispectral optical image acquired by the NASA satellite MODIS-AQUA on August 30, 2009 at 05:20 UTC during the Montara oil spill in Timor Sea

Right Synthetic Aperture Radar image acquired by the DLR satellite TerraSAR-X on August 30, 2009 at 09:58 UTC during the Montara oil spill in Timor Sea

REMOTE SENSING AND OIL SPILL

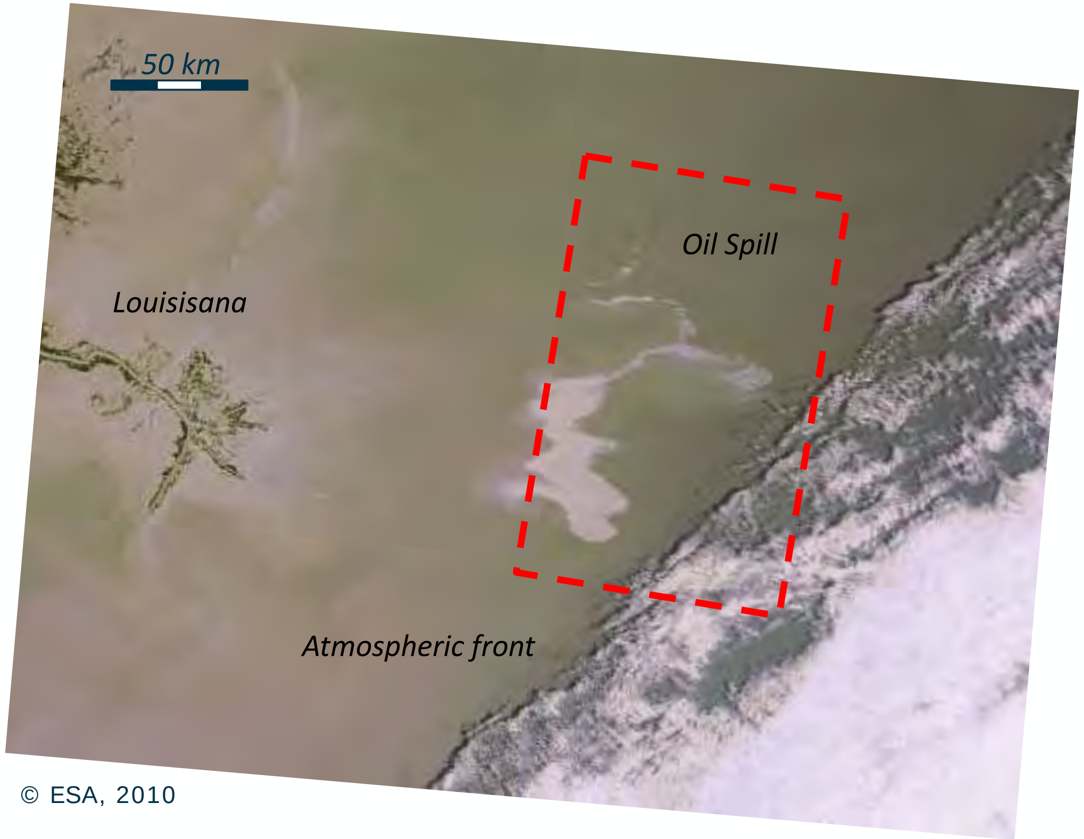

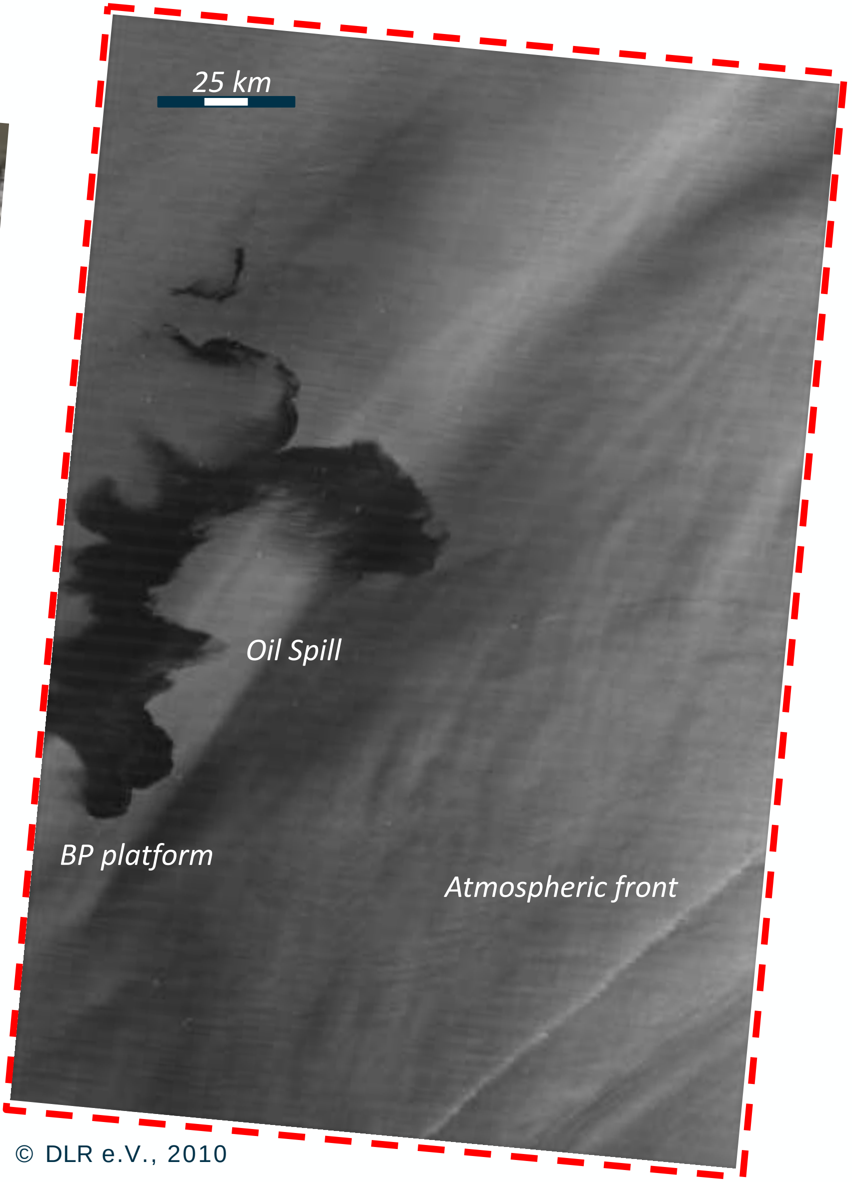

Left multispectral optical image acquired by the ESA satellite ENVISAT-MERIS on April 25, 2010 at 16:28 UTC during the DWH oil spill in the Gulf of Mexico

Right Synthetic Aperture Radar image acquired by the DLR satellite TerraSAR-X on April 25, 2010 at 11:50 UTC during the DWH oil spill in the Gulf of Mexico

REMOTE SENSING AND OIL SPILL

Satellite and aerial support during DWH clean-up procedure

Airplane equipped with thermal infrared, hyperspectral, camera, C-band microSAR

Aerial survey during clean-up procedure

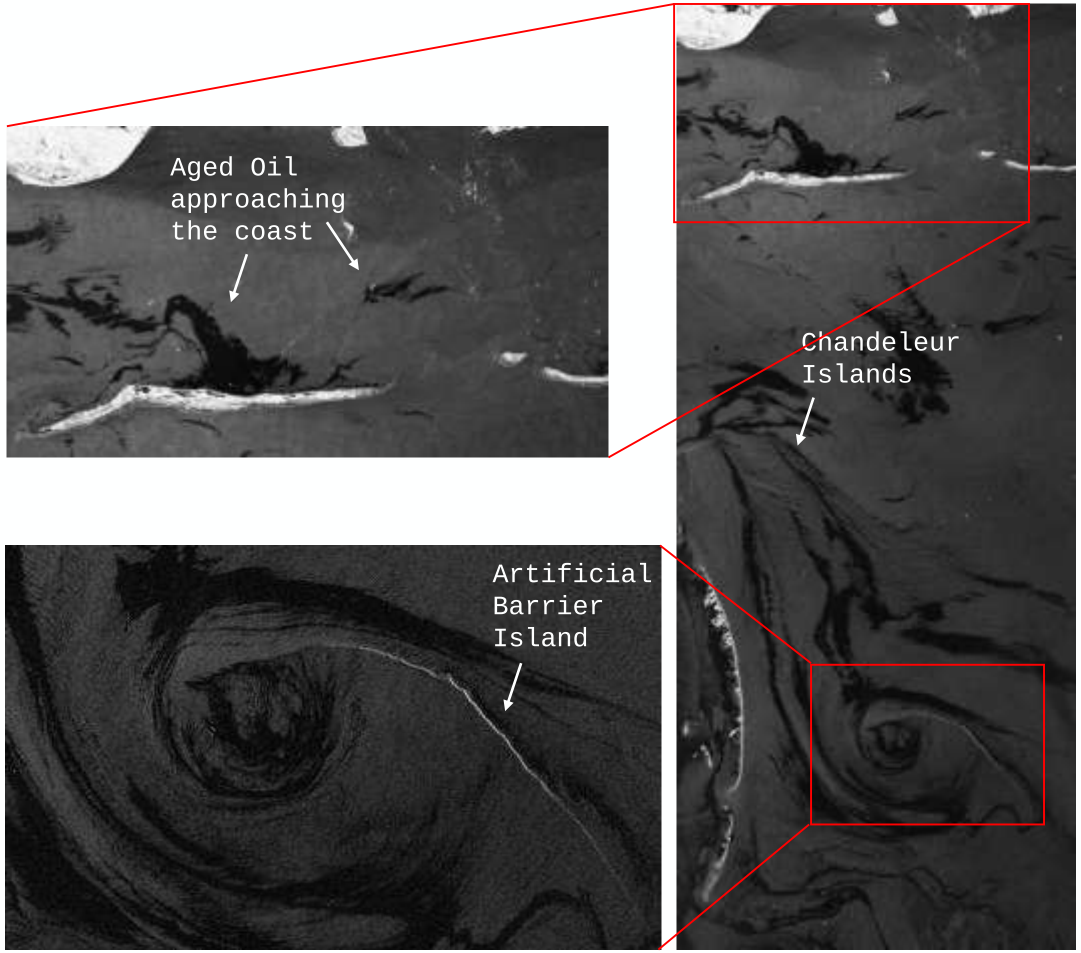

Several zoom-in of the satellite TerraSAR-X image acquired over the polluted area

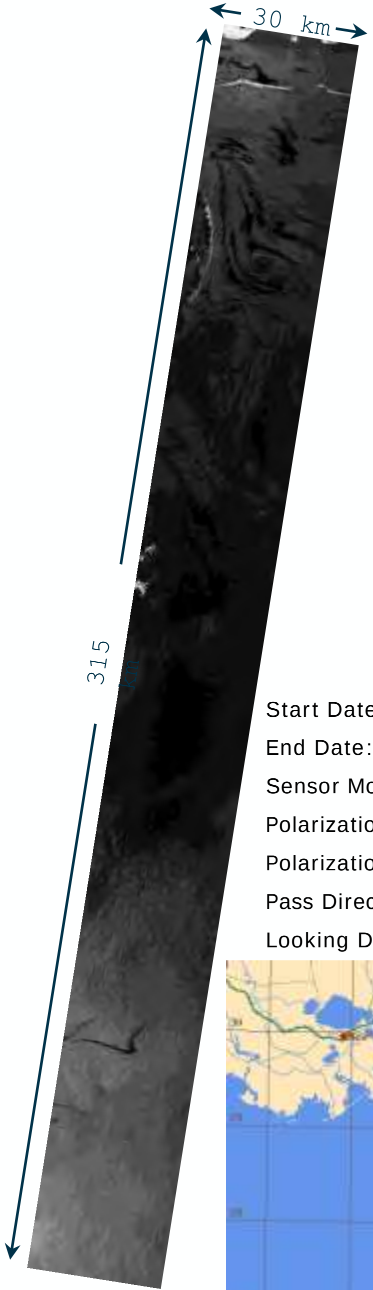

© DLR e.V., 2010

Start Date: 2010-07-09T12:24:52,131
End Date:2 010-07-09T12:25:36,628
Sensor Mode: StripMap
Polarization Mode: Single
Polarization Channels: VV
Pass Direction: Descending
Looking Direction: Left

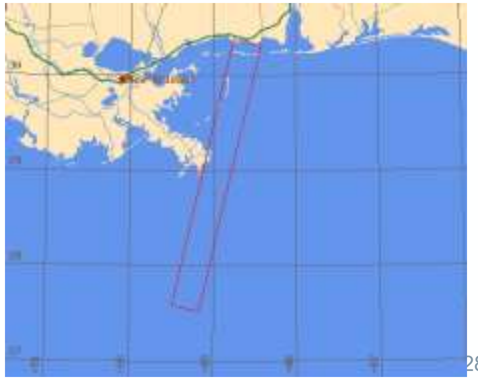

SAR OIL SPILL INTERPRETATION

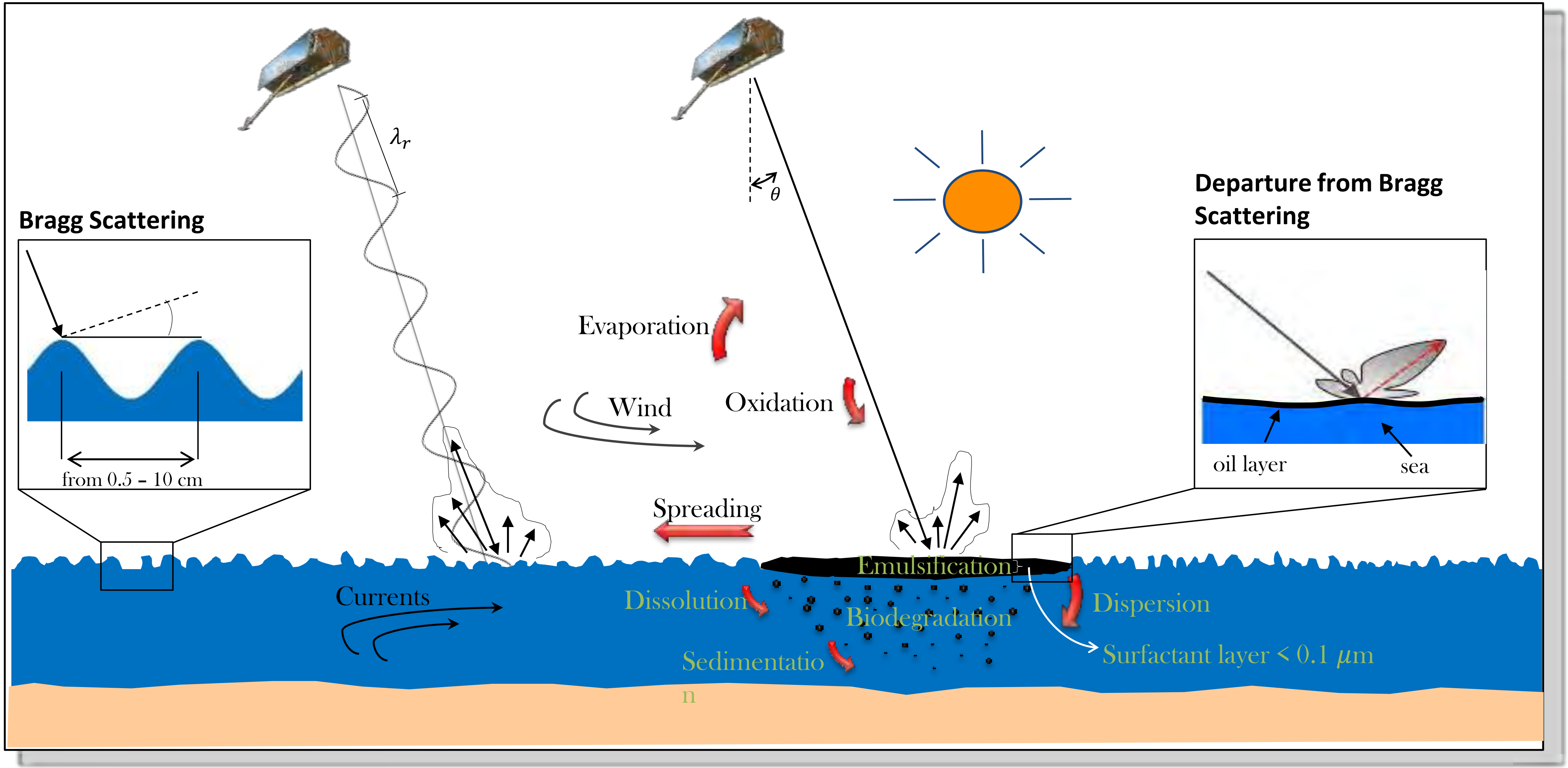

Bragg scattering $20 < \theta < 60$: $\lambda_B = \dfrac{\lambda_r}{2\sin\theta}$ $\Rightarrow$ $1.8 < \lambda_B < 4.5$ [cm] at X-band (9.65 GHz)

$3.2 < \lambda_B < 8.2$ at C-band (5.30 GHz)

SAR OIL SPILL INTERPRETATION – WIND SPEED

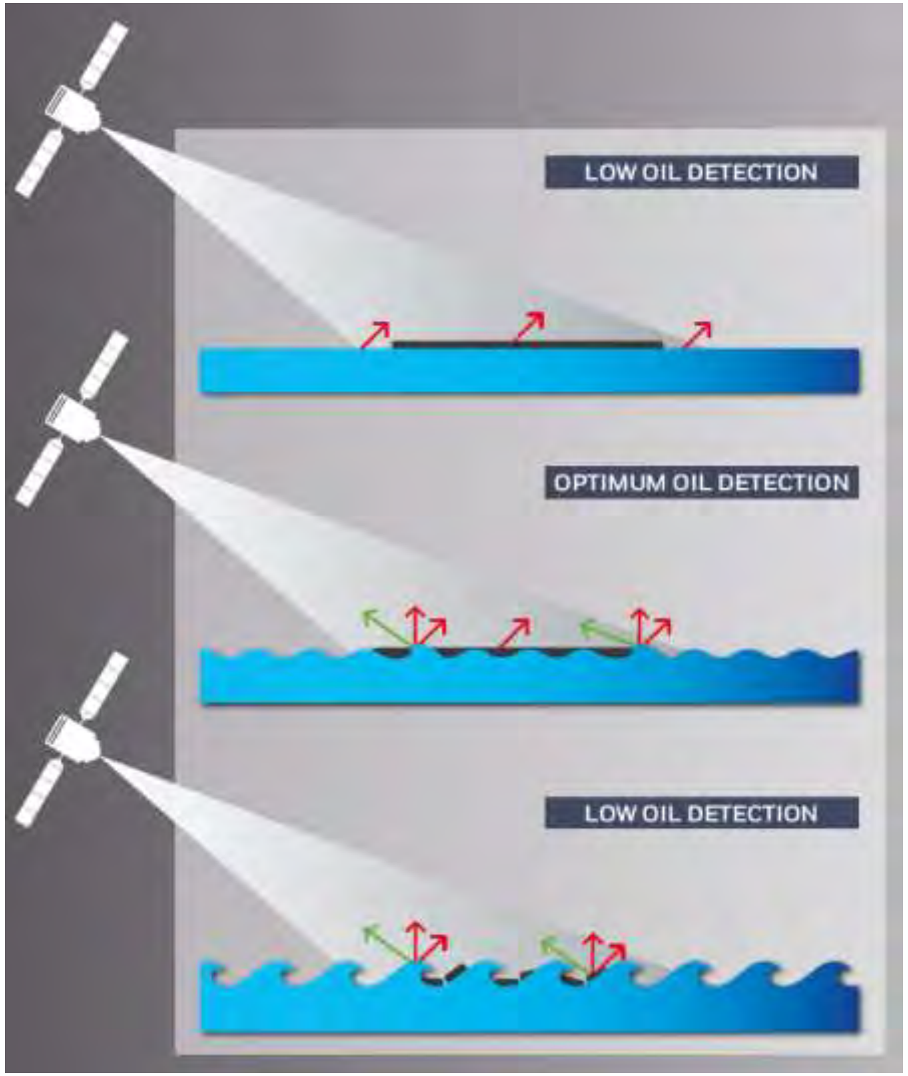

- Low wind speed → both oil and natural slicks
- Moderate wind speed → generation of natural slick impossible

  If detection -> pollution
- High wind speed → turbulence and waves, which drag slicks in the ocean sub-surface -> no detection

$$2 < U_{10} < 10 - 14\, m/s$$

SAR OIL SPILL INTERPRETATION

How man made oil spills looks like?

- ▶ Operational discharges
  - Straight linear
  - Curvilinear

Tank-washing procedure

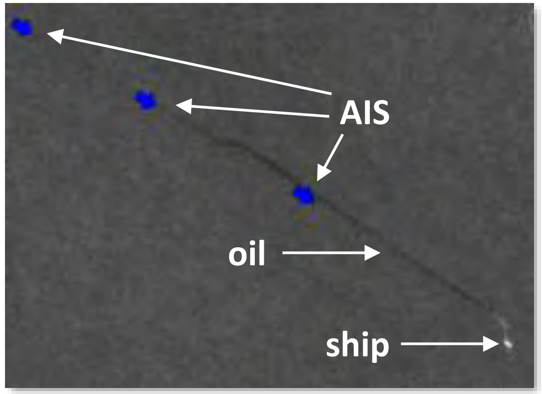

Platform-sourced pollution

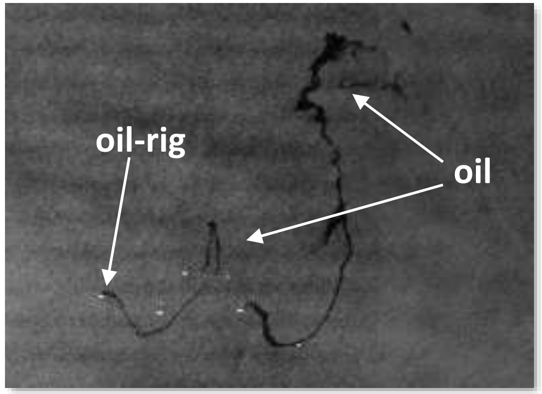

- ▶ Accidental discharges
  - Discontinuous patches
  - Rounded shape

Ship accident

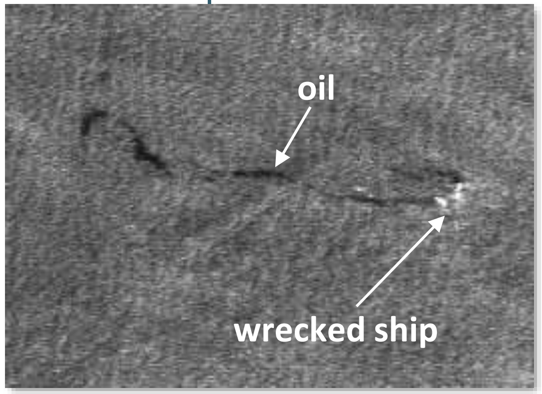

Platform accident

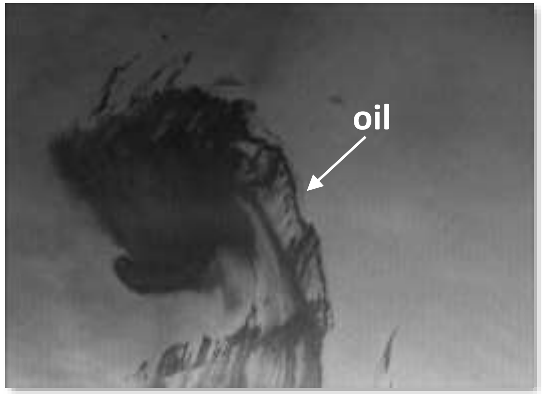

SAR OIL SPILL INTERPRETATION – OIL TYPE

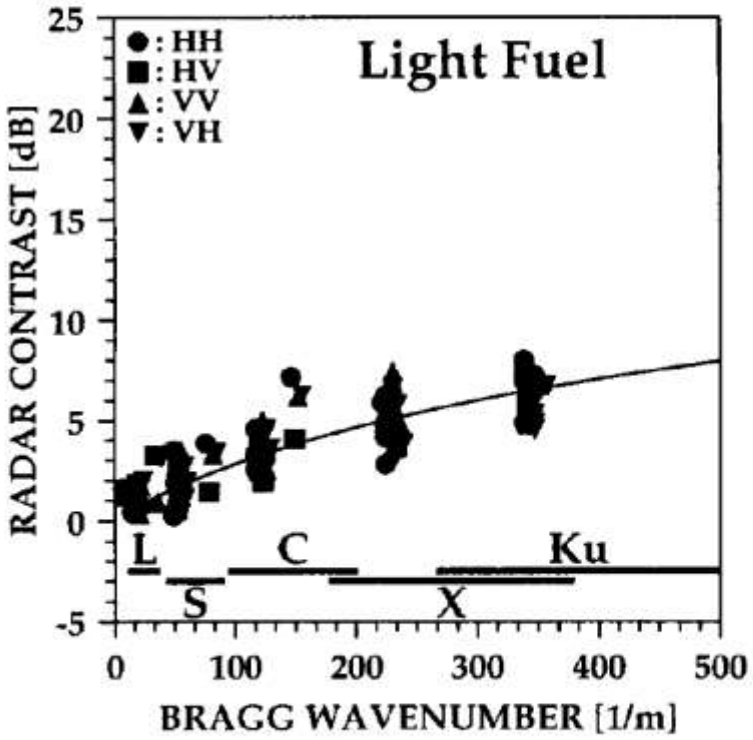

Figure 1: Radar contrast induced by the light fuel MARPOL spills as a function of the Bragg wavenumber k_B. The bars indicate how the Bragg wavenumbers are covered by the different radar bands. The solid line is computed from *Marangoni* wave damping theory [9]. © V. Wismann, 1993

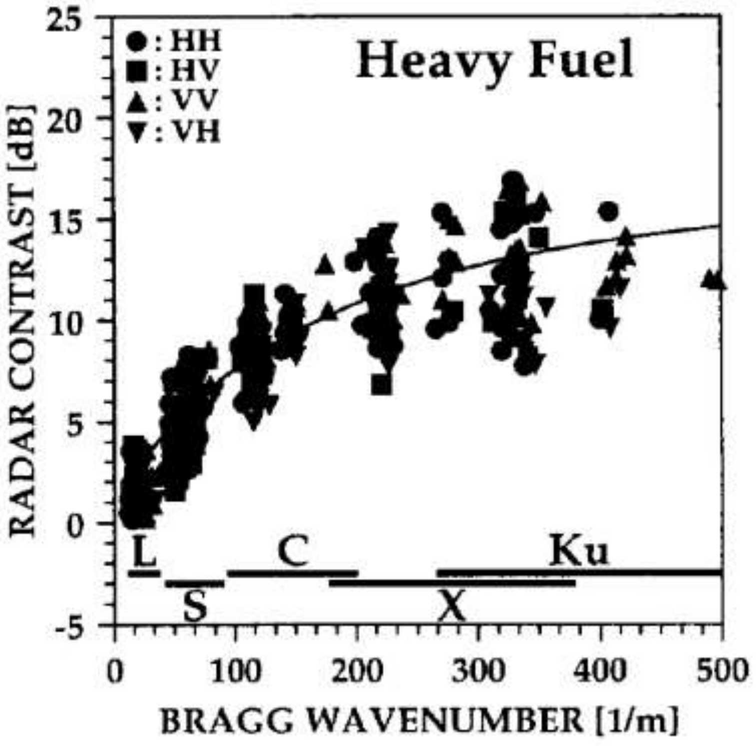

Figure 2: Same as Fig. 1, but for the heavy fuel spills. © V. Wismann, 1993

- Controlled oil spill experiment SAMPLEX
- Radar backscatter measurements done with HELISCAT at L- (1 GHz), S- (2.4 GHz), C- (5.3 GHz), X- (10 GHz) and Ku-band (15 GHz)
- Contrasts of light fuel spills well below those of heavy fuel spills

SAR OIL SPILL INTERPRETATION – WAVELENGTH

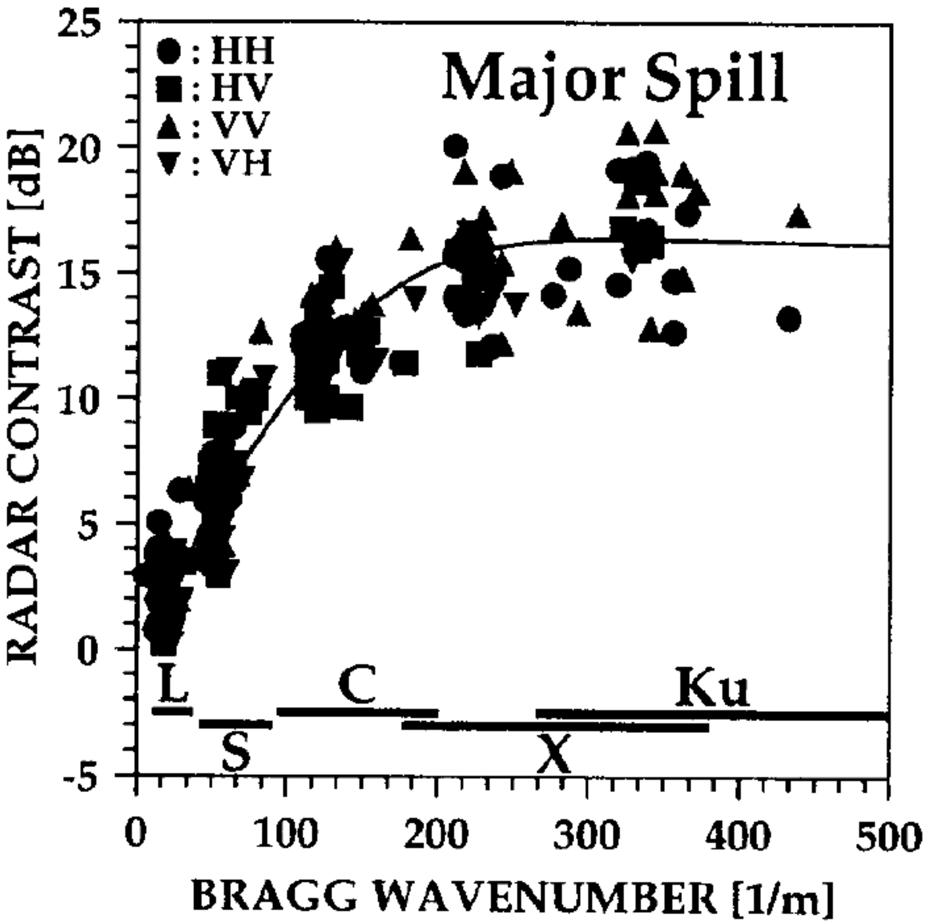

Figure 3: Same as Fig. 1, but for the thick part of the *Major-Spill*. © V. Wismann, 1993

- Controlled oil spill experiment SAMPLEX
- Radar backscatter measurements done with HELISCAT at L- (1 GHz), S- (2.4 GHz), C- (5.3 GHz), X- (10 GHz) and Ku-band (15 GHz)
- Major Spill made with heavy fuel discharged instantaneously
- Shorter wavelength higher radar contrast

SAR OIL SPILL INTERPRETATION – LOOK-ALIKES

Not all low backscatter area are related to oil spills. Man-made and natural phenomena damping the Bragg waves produce “dark areas” in SAR images are called look-alikes.

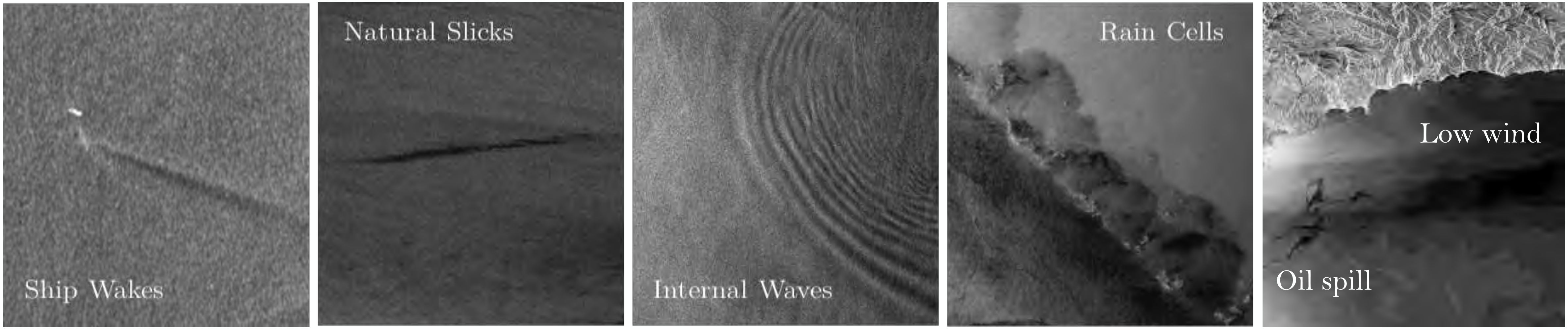

Look-alikes are therefore false alarms and should be reduced as much as possible. Unfortunately the discrimination is not an easy task either for trained operator than for automatic detection algorithm. Auxiliary information are generally needed, e.g. wind field, current, AIS, etc.

SAR OIL SPILL DETECTION WORKFLOW

- Image Product:
  - level-1 product
  - ScanSAR, StripMAP modes
  - (Multilooked) Ground Range Detected (GRD) type
- Ancillary Data:
  - product annotation metadata file
  - land mask dataset
  - weather information
- Final Product:
  - polygons of dark patches
  - oil spill/look-alike label

- Near-Real-Time: 20-30 mins from data downlink at base station

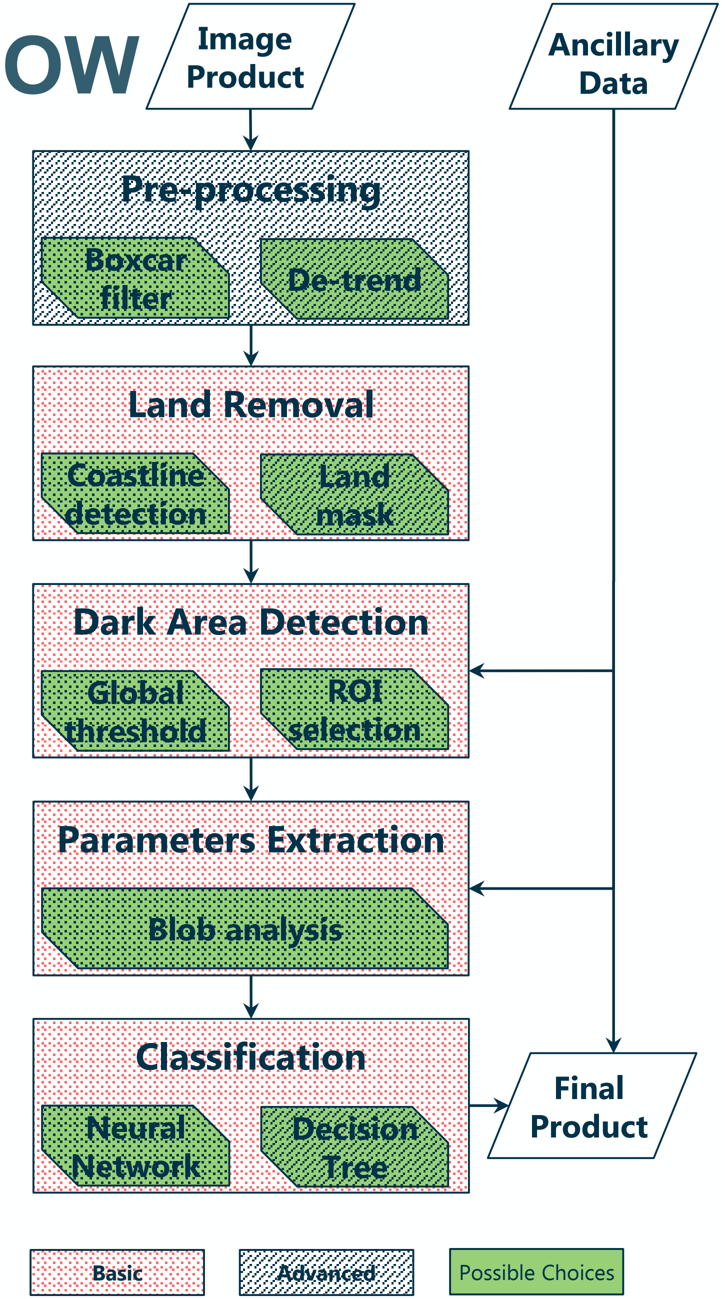

OFFSHORE PLATFORMS OIL SPILL DETECTION

Example of semi-automated oil spill detection for offshore monitoring

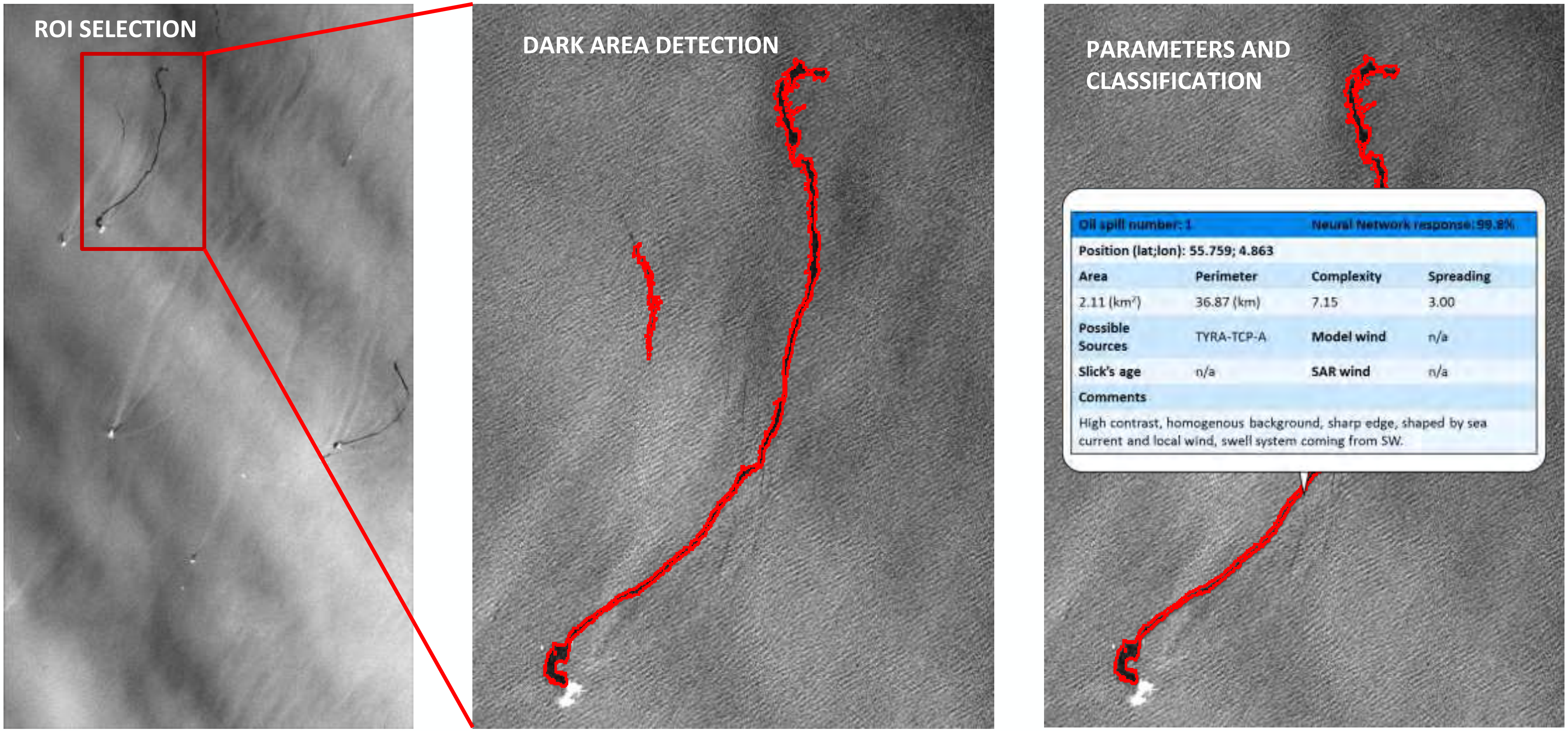

Oil spill number: 1		Neural Network response: 99.8%	
Position (lat;lon): 55.759; 4.863			
Area	**Perimeter**	**Complexity**	**Spreading**
2.11 (km^2)	36.87 (km)	7.15	3.00
Possible Sources	TYRA-TCP-A	**Model wind**	n/a
Slick's age	n/a	**SAR wind**	n/a
Comments			
High contrast, homogenous background, sharp edge, shaped by sea current and local wind, swell system coming from SW.			

OIL WELL LOCALIZATION

- Sea surface oil slick continuously reported in Gulf of Mexico
- Offshore structure destroyed by hurricane
- Leaks coming from the underwater oil wells once attached to the platform
- Multiple observation also in short revisit time

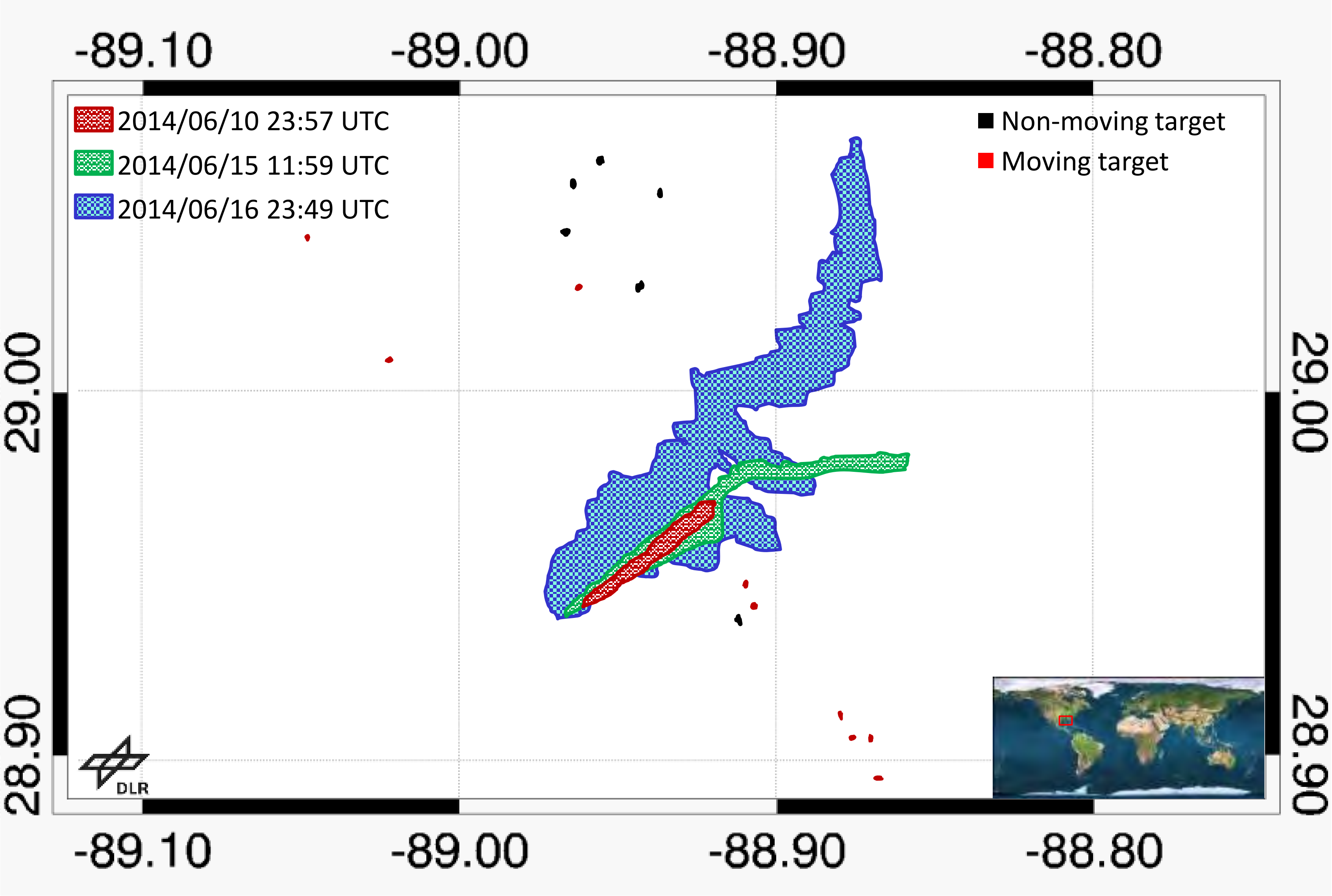

CLASSICAL VS POLSAR OIL SPILL

Classic approach

- Large number of false alarms (look-alikes)
- Reliability of final product depends on trained personnel
- Algorithms need to be developed for sensors specific acquisition mode and wavelength
- Mostly base on image processing with little physics involved
- Many images are needed for training
- Well accepted for routine operations

PolSAR approach

- Not so much used in operational context due to reduced coverage
- Some class of false alarms (weak damping look-alike) can be better discriminated already with dual-pol
- Based on electromagnetic modelling of the sea surface scattering
- Robust and effective across wavelength and SAR missions
- Quad-pol approaches can't be employed when only dual-pol are available

POLARIMETRIC SCATTERING MODEL

The oil spill detection using PolSAR data is based on a polarimetric model developed by Prof. M. Migliaccio to understand the sea surface scattering with and without surface slicks in terms of some polarimetric features

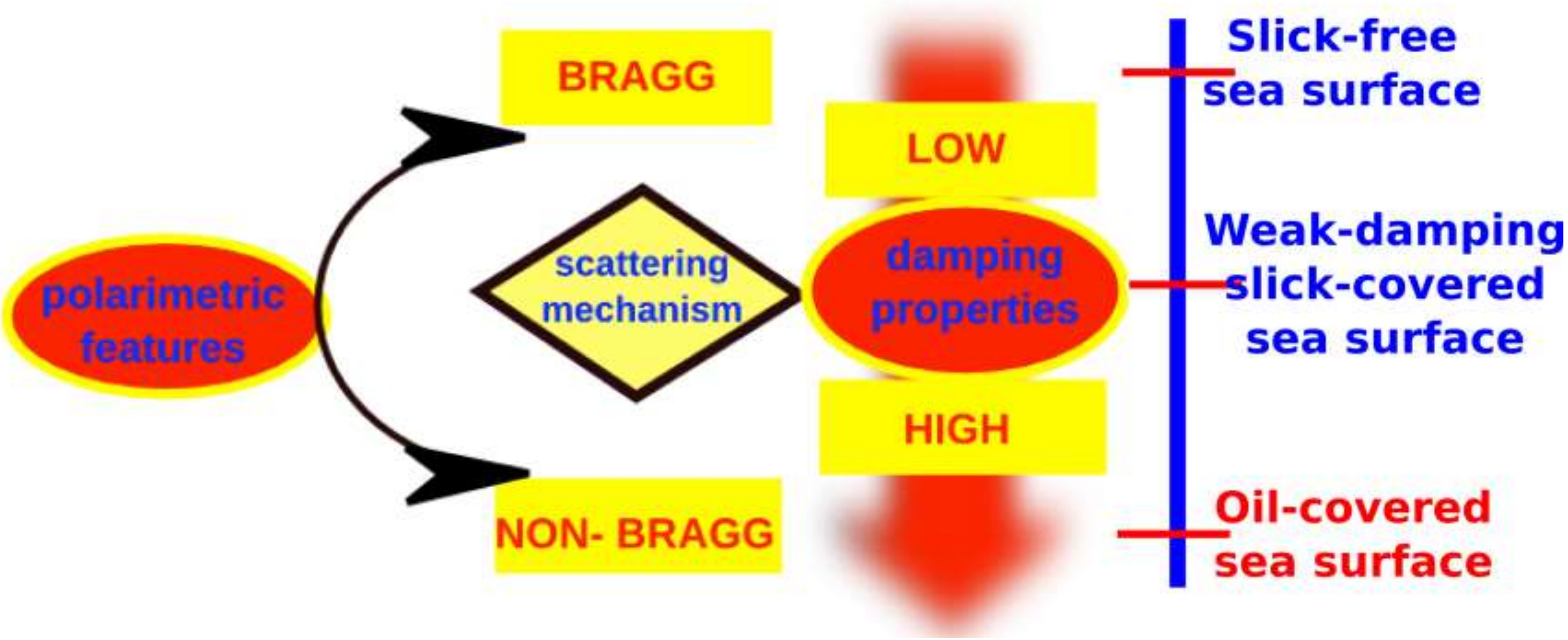

© Prof. M. Migliaccio

QUAD- AND DUAL-POL FEATURES OIL SPILL

Extraction of PolSAR techniques for oil spill detection available in literature

- **Quad-pol measurements**
  - Mueller filter
  - Polarimetric entropy
  - Degree of polarization
  - Unpolarized backscattered energy
  - Conformity coefficient
- **Dual-pol measurements**
  - Co-polarized Phase Difference
  - Co-pol coherence
  - Geometric intensity
  - Dual-pol degree of polarization

THE OIL SPILL CPD ON X-, C- AND L-BAND

Co-pol channels
$\{\dot{S}_{hh} \quad \dot{S}_{vv}\}$

$$CPD = \angle \dot{S}_{hh}\dot{S}_{vv}^*$$

Polarimetric features

$$\eta = \langle |\dot{S}_{vv}|^2 \rangle \qquad \gamma = \frac{\langle |\dot{S}_{hh}|^2 \rangle}{\langle |\dot{S}_{vv}|^2 \rangle} \qquad \rho = \frac{\langle \dot{S}_{hh}\dot{S}_{vv}^* \rangle}{\sqrt{\langle |\dot{S}_{hh}|^2 \rangle \langle |\dot{S}_{vv}|^2 \rangle}}$$

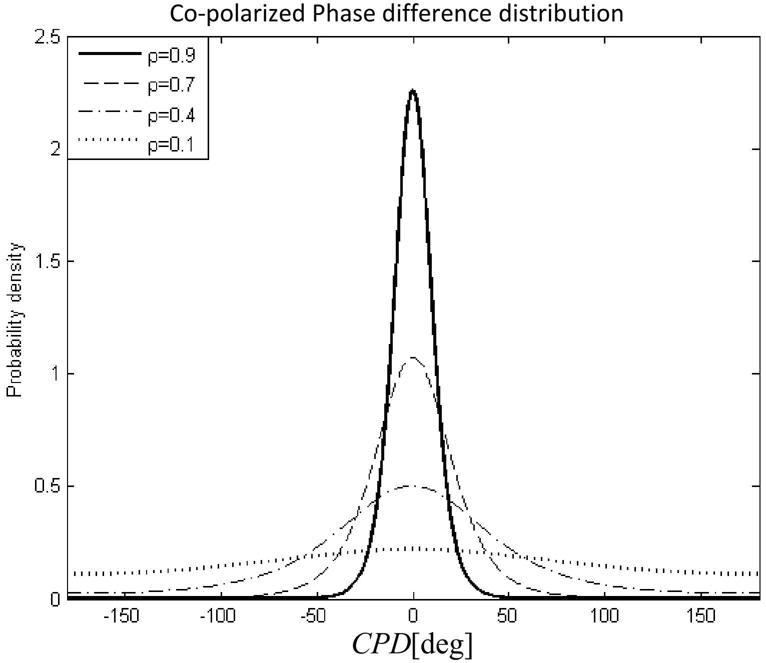

$$\hat{\rho} = \frac{\left|\sum_{n=1}^{L} \dot{S}_{hh}[n]\dot{S}_{vv}^*[n]\right|}{\sqrt{\sum_{n=1}^{L} |\dot{S}_{hh}[n]|^2 \sum_{n=1}^{L} |\dot{S}_{vv}[n]|^2}}$$

$$CPDstd = \sqrt{\left(\frac{1}{L}\sum_{n=1}^{L} \left(\angle \dot{S}_{hh}[n]\dot{S}_{vv}^*[n]\right)^2\right) - \left(\frac{1}{L}\sum_{n=1}^{L} \left(\angle \dot{S}_{hh}[n]\dot{S}_{vv}^*[n]\right)\right)^2}$$

Ocean-surface and weak-damping slicks (Bragg):

- **High** $\hat{\rho}$
- Narrow CPD pdf $\rightarrow$ **low** $CPDstd$

Oil-covered sea surface (departure from Bragg):

- **Low** $\hat{\rho}$
- Broaden CPD pdf $\rightarrow$ **high** $CPDstd$

THE CPD IN X-BAND – TANKER ACCIDENT

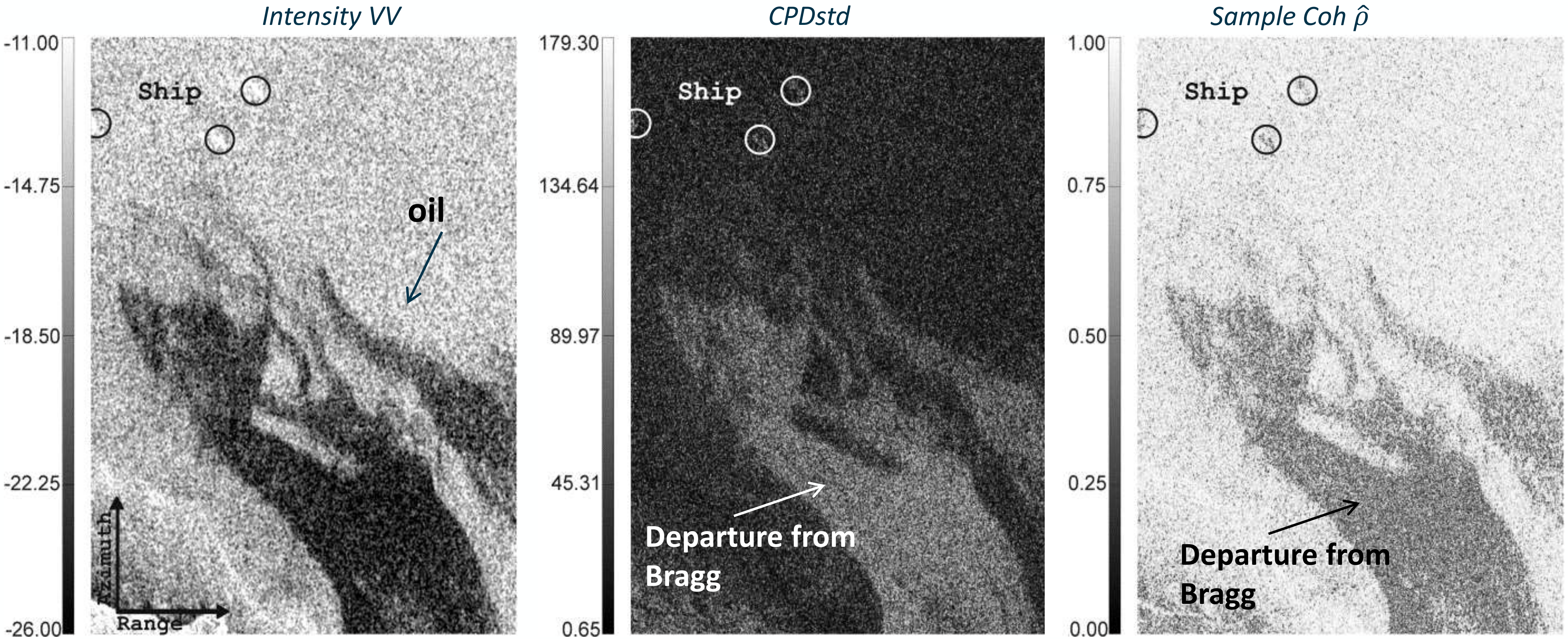

THE CPD IN X-BAND - OPERATIONAL SPILLAGE

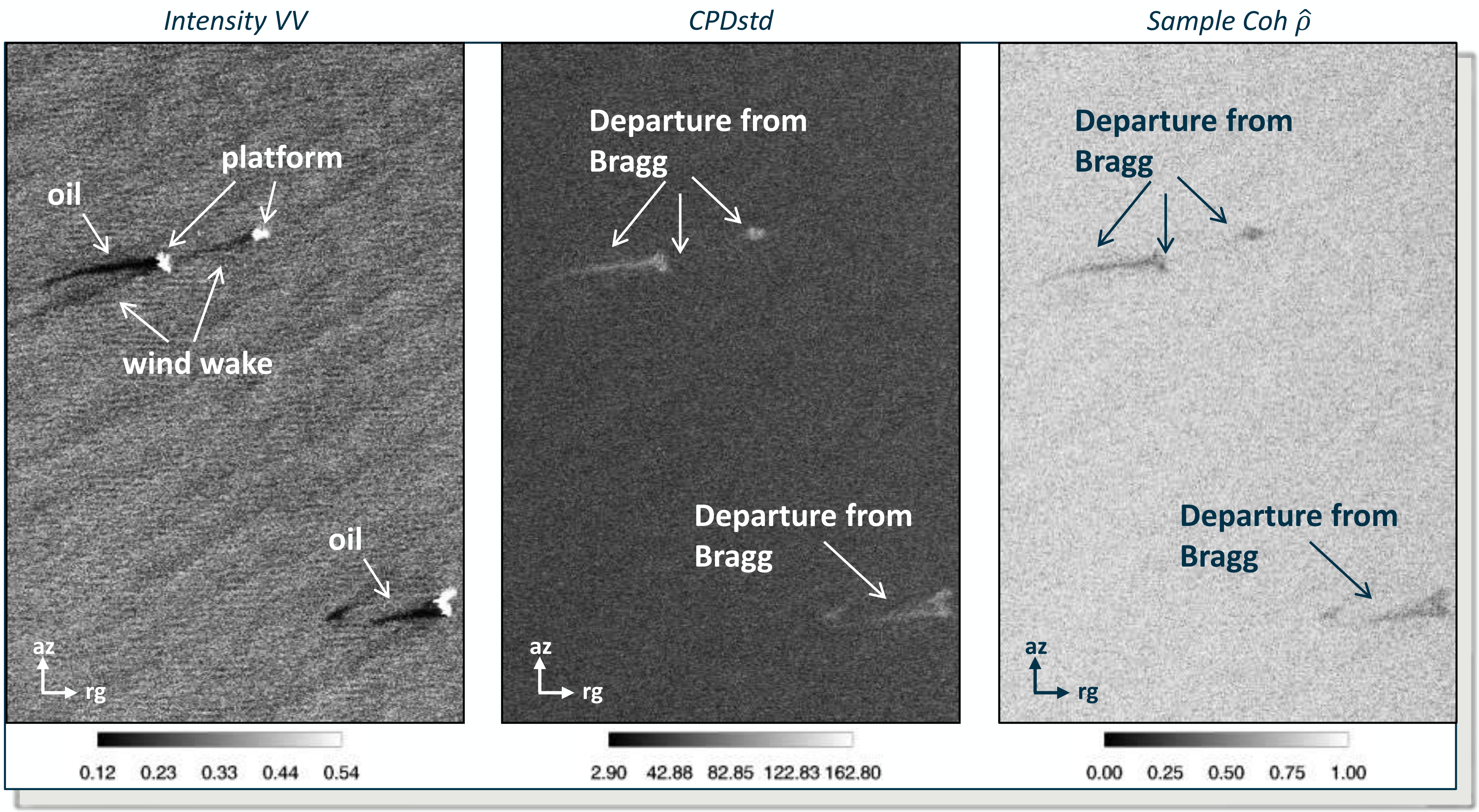

THE CPD IN X-BAND - NATURAL SLICKS

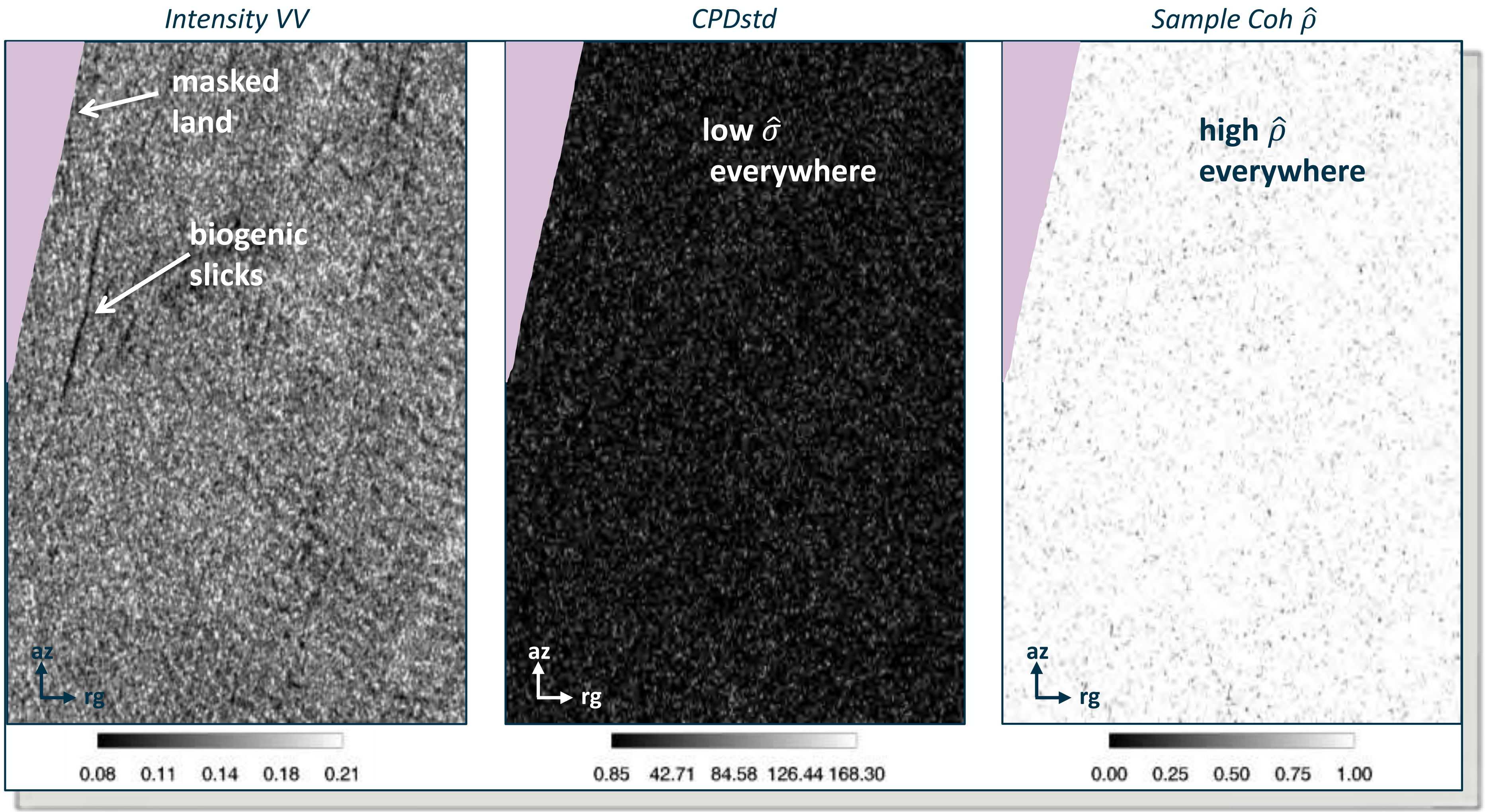

VERIFICATION OF THE CPD IN X-BAND

The probability density functions of the CPD retrieved from the data confirm the soundness of the polarimetric modelling of the sea surface scattering with and without oil

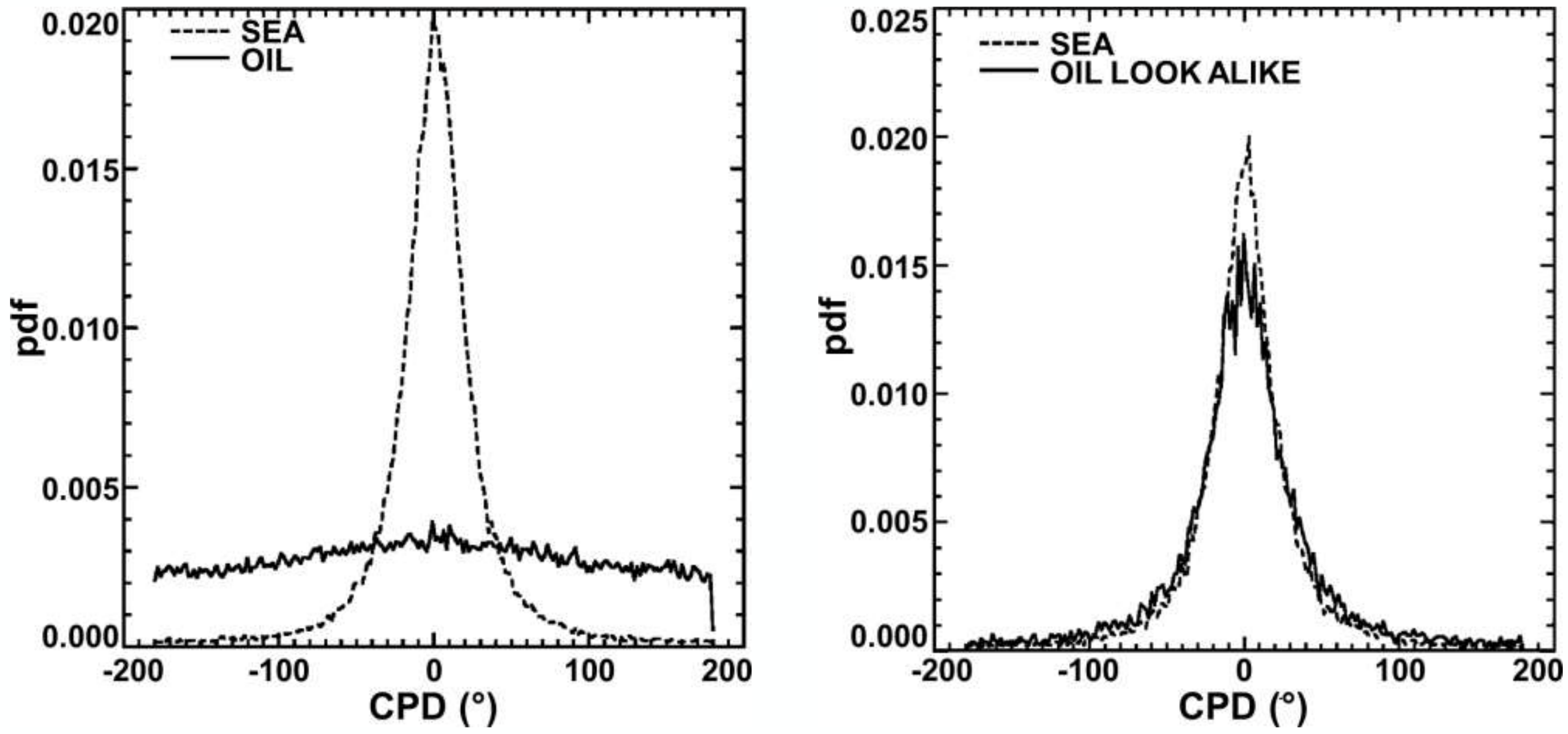

THE CPD IN C-BAND – DWH SPILL

Intensity HH

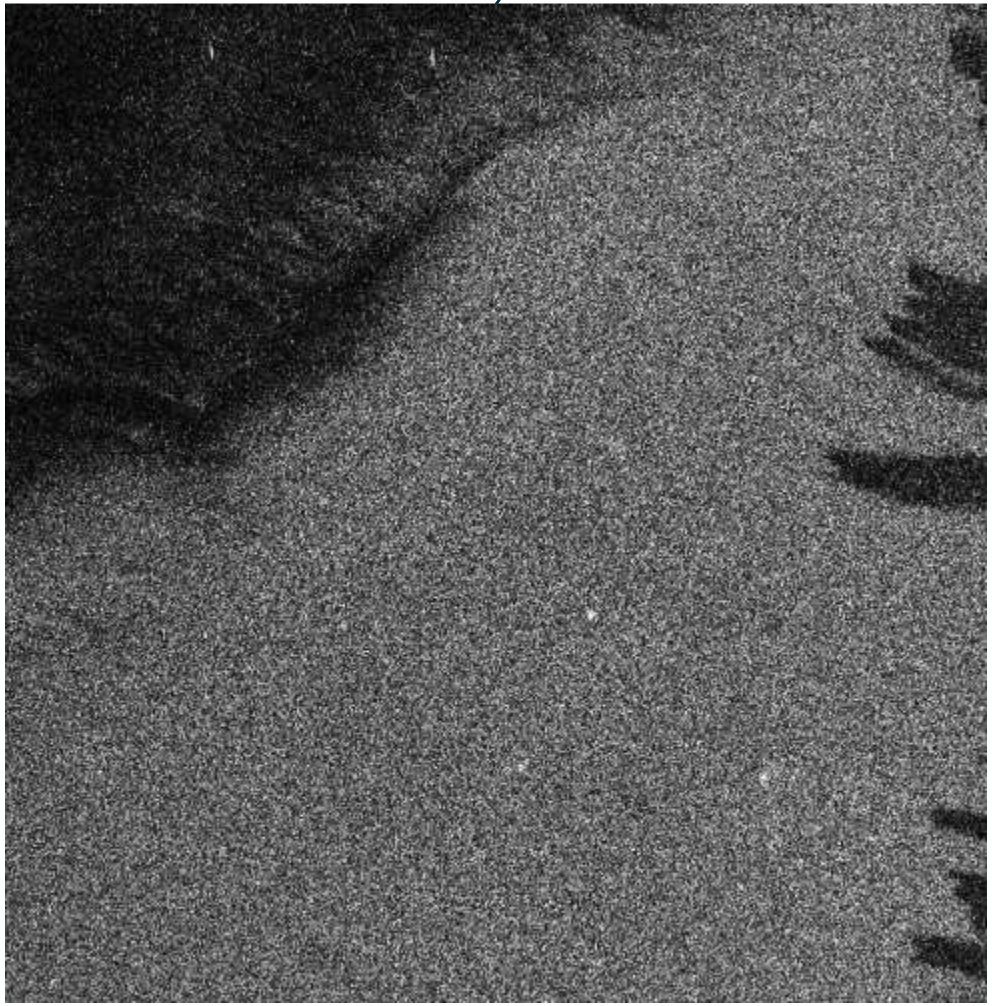

CPDfilter

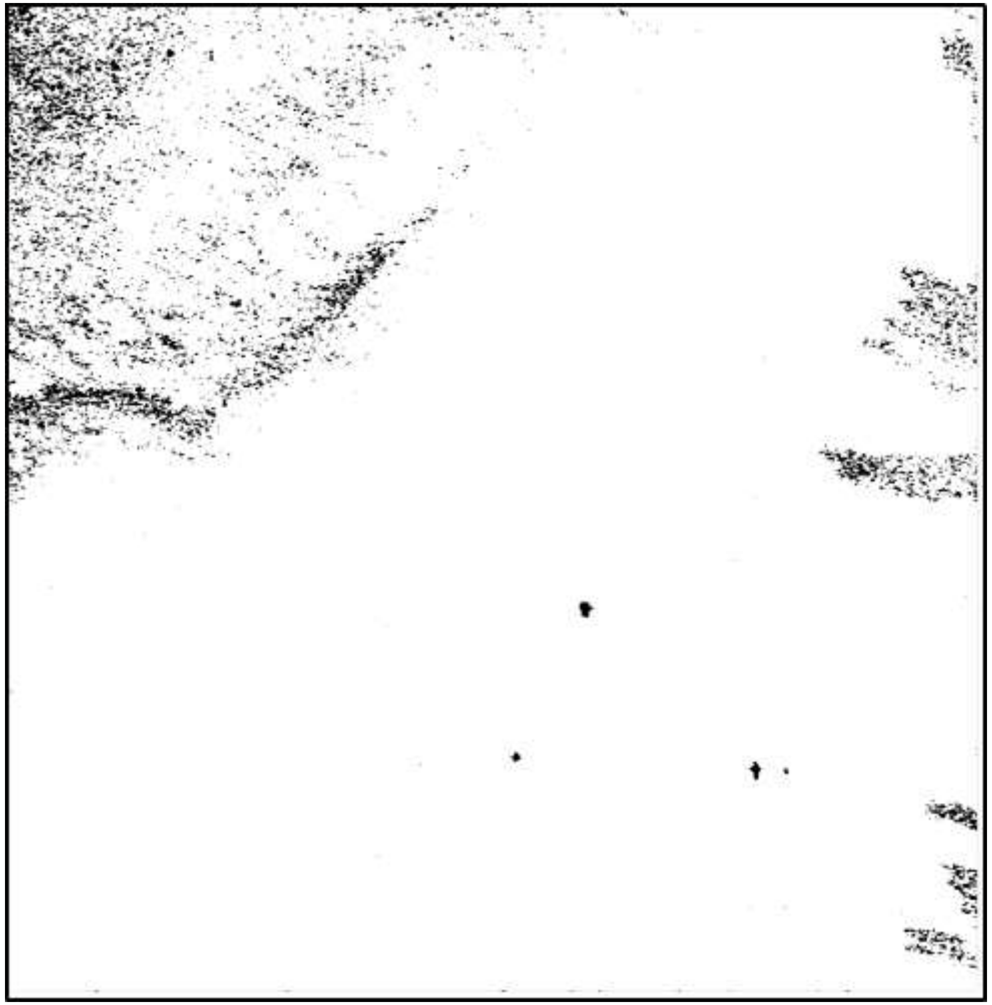

THE CPD IN L-BAND – VIETMAN OIL SLICK

Intensity HH

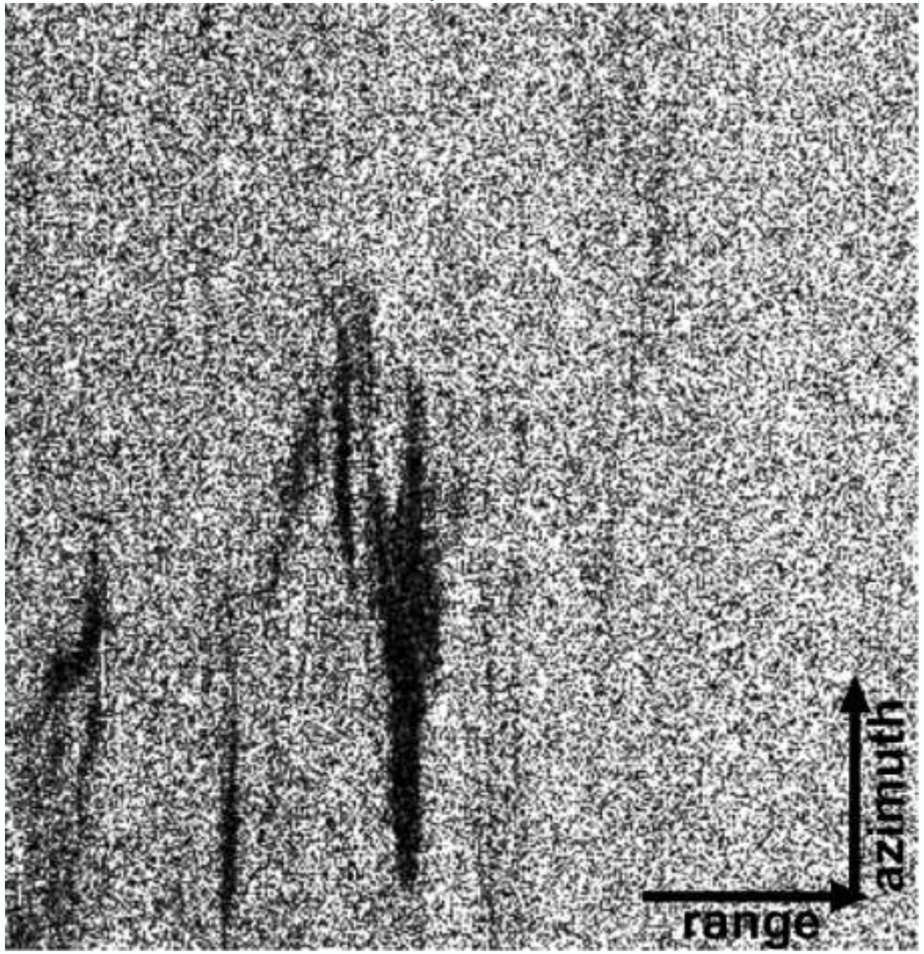

CPDstd

DUAL-POL OIL SEEP CPD ANALYSIS

- Time-series of dual-pol HH/VV TerraSAR-X acquired over a known source of oil spill
- Dataset partitioned in three groups based on the acquisitions angle of incidence 26° ,34° ,43°

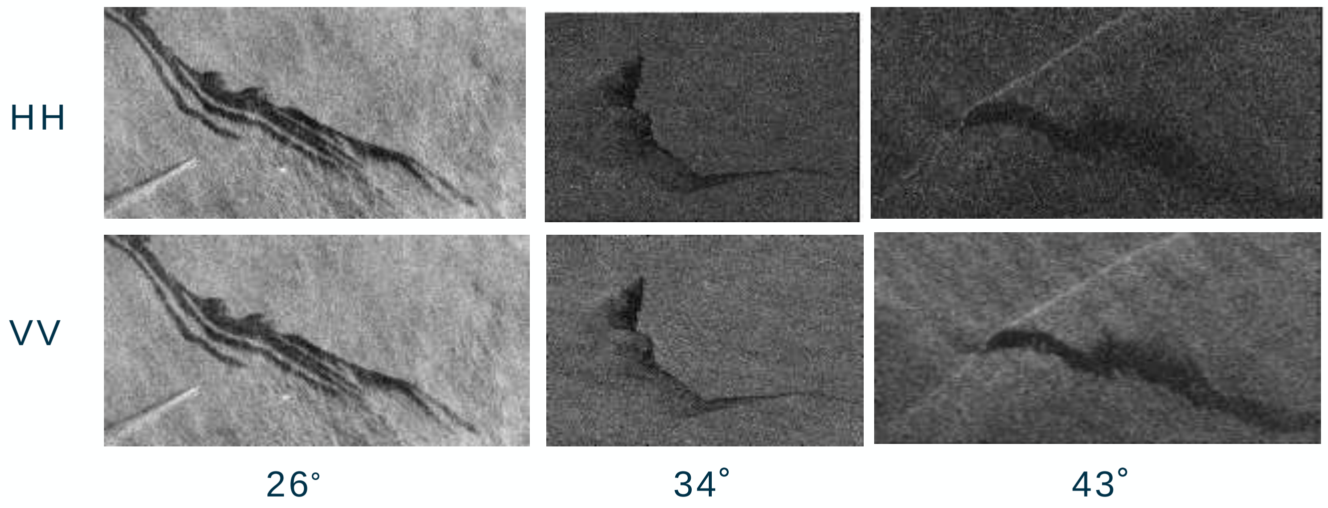

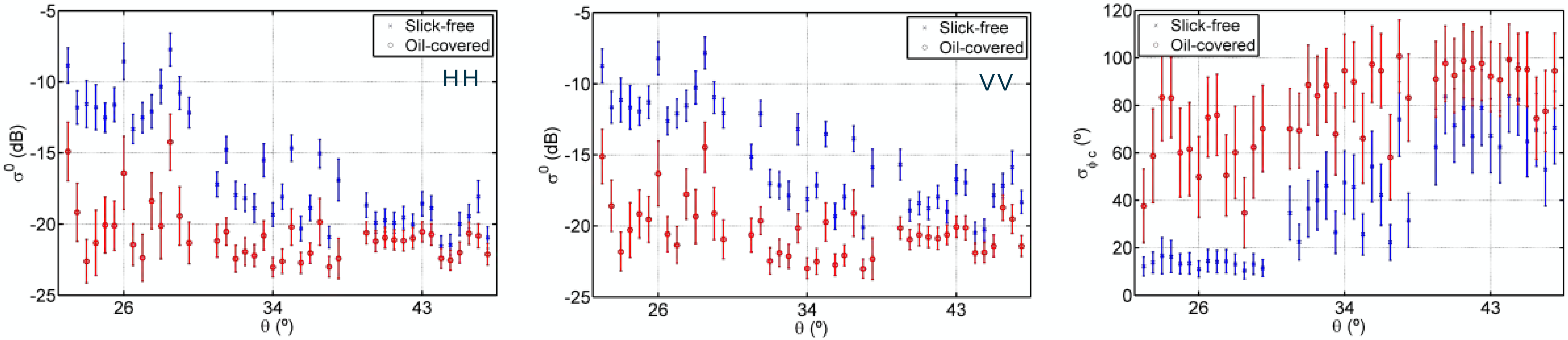

DUAL-POL OIL SPILL DETECTION

TerraSAR-X dual-pol HH-VV data during the annual NOFO oil-on-water (OOW) exercise 2011 in the North Sea

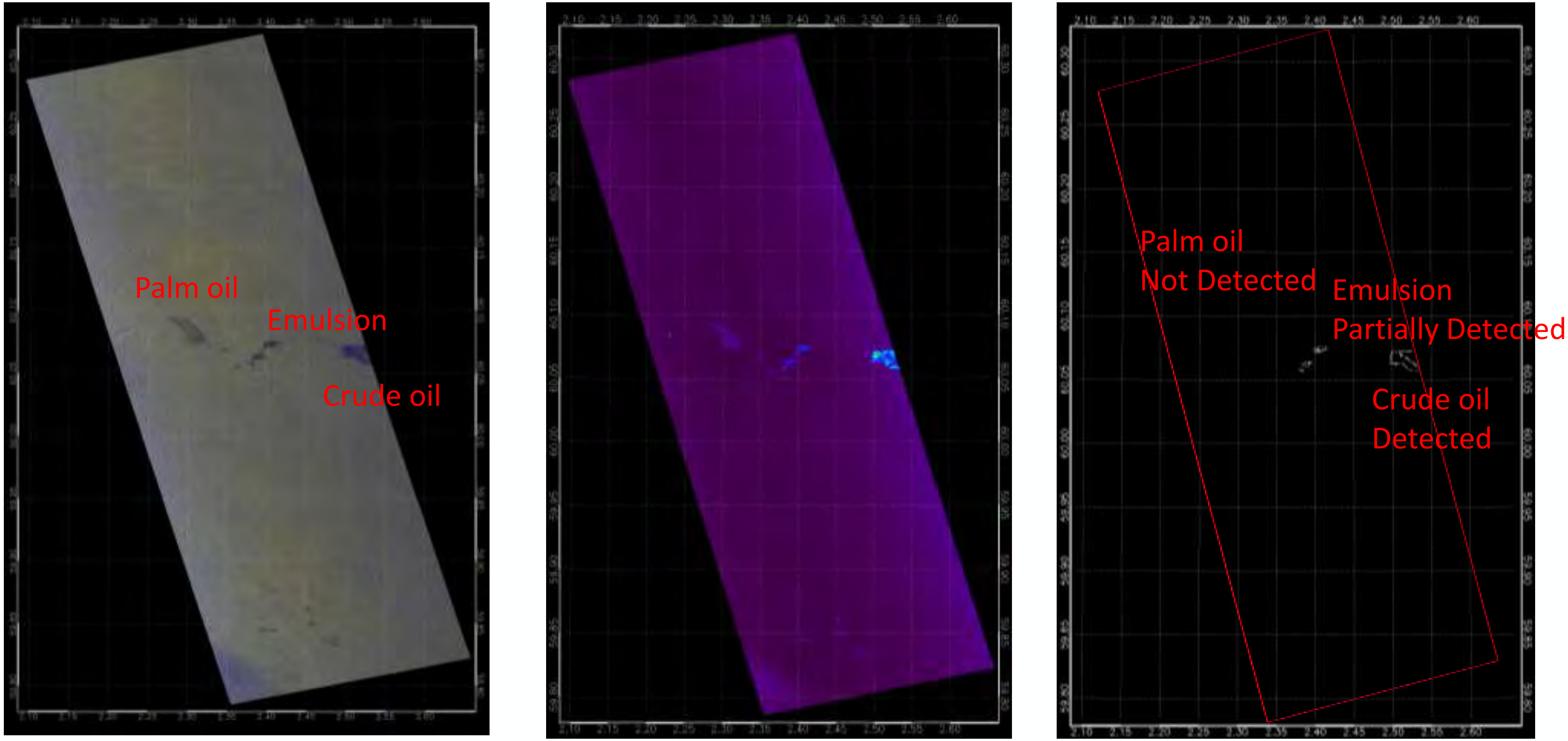

DUAL-POL OIL SPILL DETECTION

TerraSAR-X dual-pol HH-VV data during the annual NOFO oil-on-water (OOW) exercise 2011 in the North Sea. Dual-pol polarimetric features

Entropy H | Anisotropy A | alpha $\bar{\alpha}$ | Geometric intensity | Correlation ρ

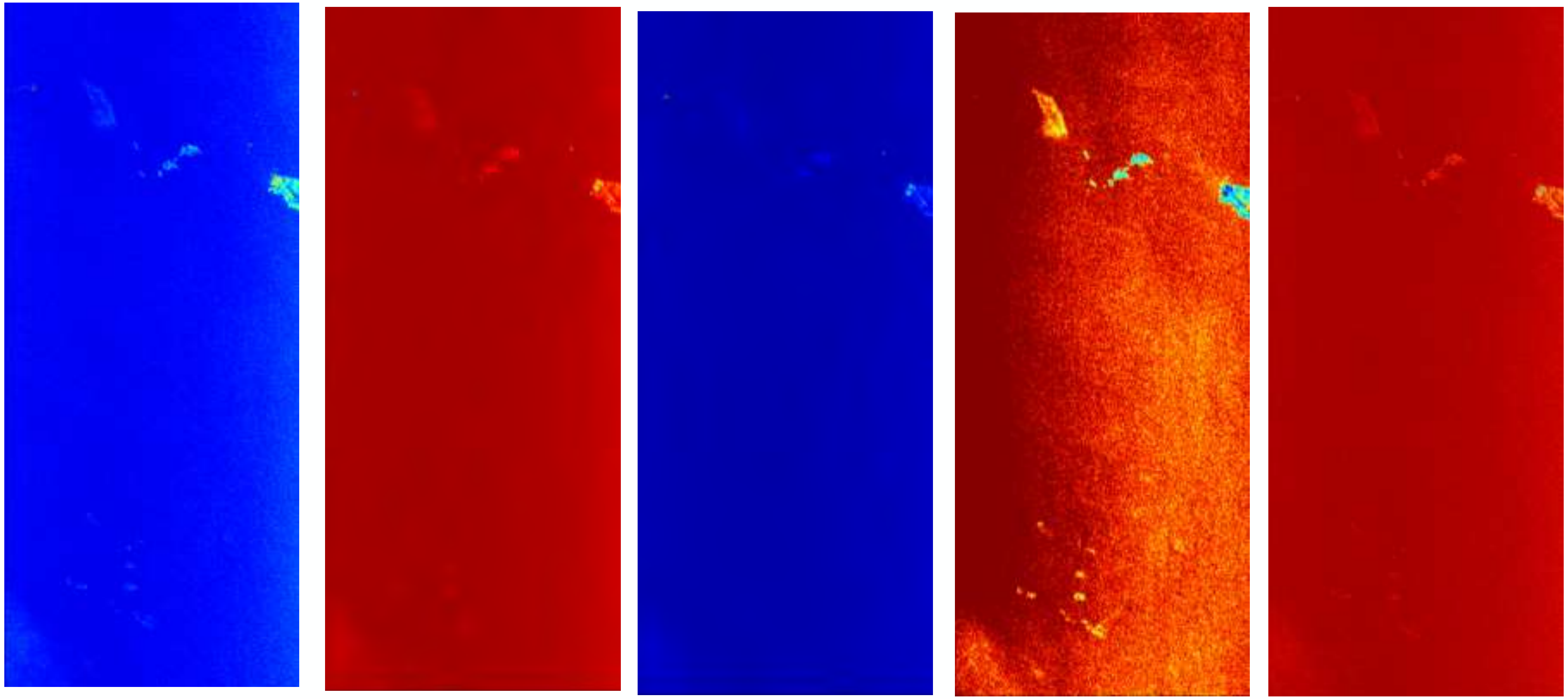

TRADITIONAL AND DUAL-POL FEATURES

Histogram-based discrimination power of X-band dual-pol features. For each feature the contrast is evaluated:

$$Contrast = \langle PF_{\text{darkarea}} \rangle / \langle PF_{\text{sea}} \rangle$$

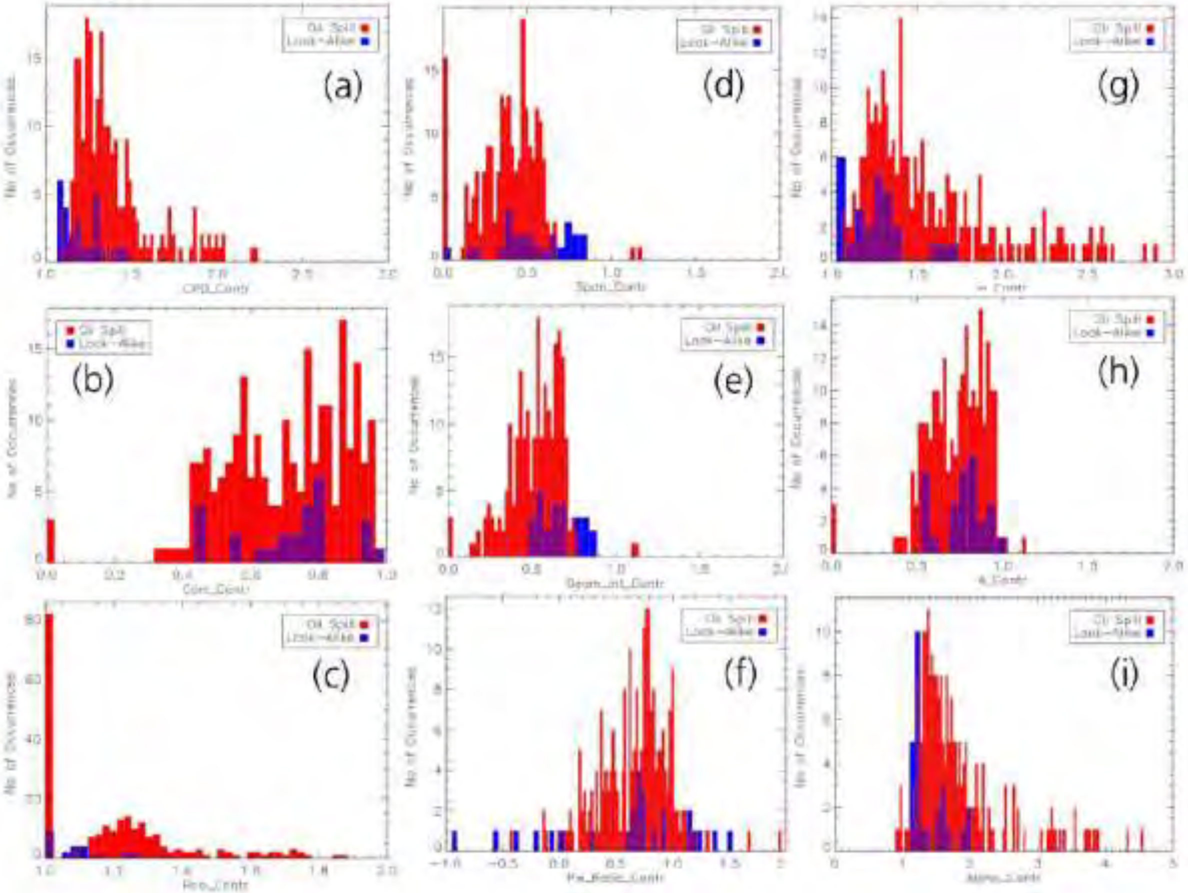

(a) CPDstd, (b) sample coh, (c) Real co-pol product, (d) span, (e) Geometric intensity, (f) co-pol power ratio, (g) entropy, (h) Anisotropy, (i) mean alpha angle

Mutual information analysis of X-band traditional and polarimetric features (225 oil class, 26 look-alike class)

$$\mathcal{I}(X/Y) = \sum_{y \in Y} \sum_{x \in X} p(x,y) \log(p(x,y)/p(x)p(y))$$

Feature Y_i	$\mathcal{I}(Y_i; Class)$
Y_1 =Geom_Int_Contr	0.43435536
Y_2 =Pw_Ratio_Contr	0.43030952
Y_3 =Span_Contr	0.41153182
Y_4 = Pw_Ratio_Obj	0.39556791
Y_5 = A_Contr	0.38074514
Y_6 = Max_Contr	0.37435768
Y_7 =StdDev_Obj	0.37396138
Y_8 = Alpha_Obj	0.37385888
Y_9 = CPD_Contr	0.36981304
Y_{10} = Corr_Contr	0.36836651
Y_{11} =Mean_Contr	0.36487212
Y_{12} = Complexity	0.36091791
Y_{13} =H_contr	0.35548907
Y_{14} = H_Obj	0.34583747
Y_{15} = Corr_Obj	0.34455698
Y_{16} = Alpha_Contr	0.33402118
Y_{17} = CPD_Obj	0.31725307
Y_{18} = A_Obj	0.31501395
Y_{19} = Geom_Int_Obj	0.28707119
Y_{20} =Rco_Contr	0.28407560
Y_{21} =Perimeter	0.26252907
Y_{22} =Area	0.24698244
Y_{23} =Span_Obj	0.24439306
Y_{24} = Rco_Obj	0.21920133
Y_{25} =Spreading	0.14384433

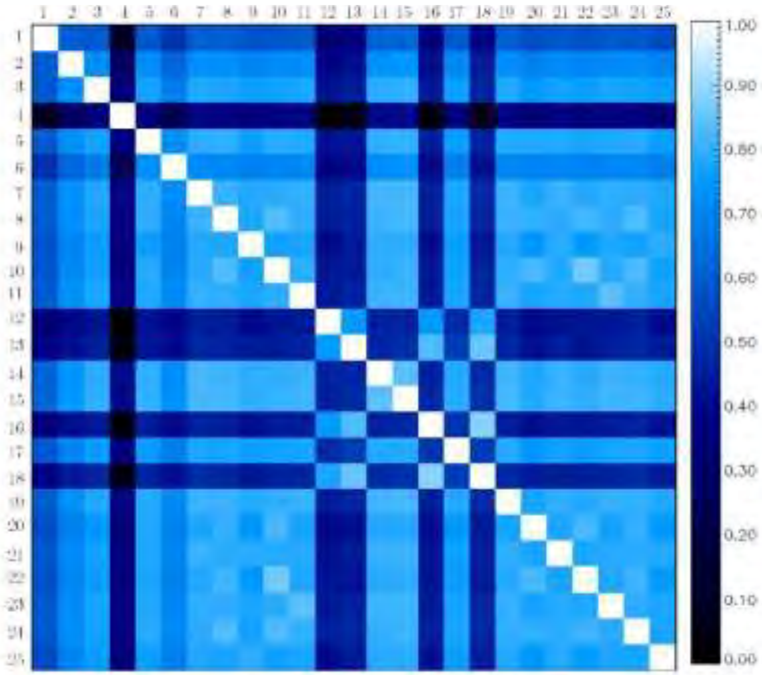

(left) Ranking of traditional and dual-pol features based on mutual information (right) matrix of normalized mutual information values

SAR MARINE APPLICATIONS

Oil spill, Seepage, Oil drift, Eddies

Ship detection, Wake

Land-Water line, Coastal erosion

Icebergs detection

Ice classification

Wind, Hurricane/Cyclone, Windfarm

Sea state, Wave breaking, Bathymetry

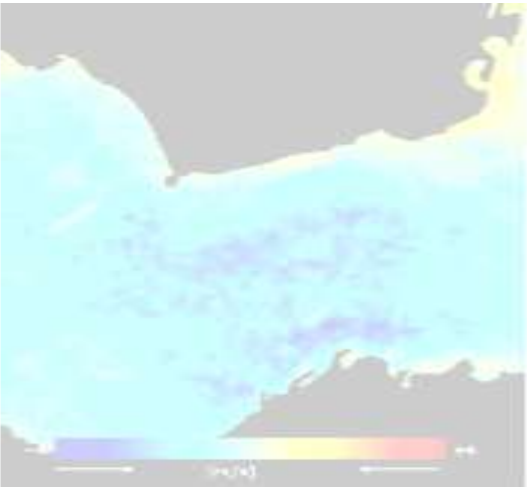

Surface current

SHIP TRAFFIC

- About **90%** of the worldwide good traffic goes by ship.
- **Human activities** at sea:
  - Transport (Safety)
  - Pleasure (Safety)
  - Waste dumping (Security)
  - Illegal trafficking (Security)
  - Piracy (Security)
  - Etc.

Worldwide ship density map based on AIS data in 2021

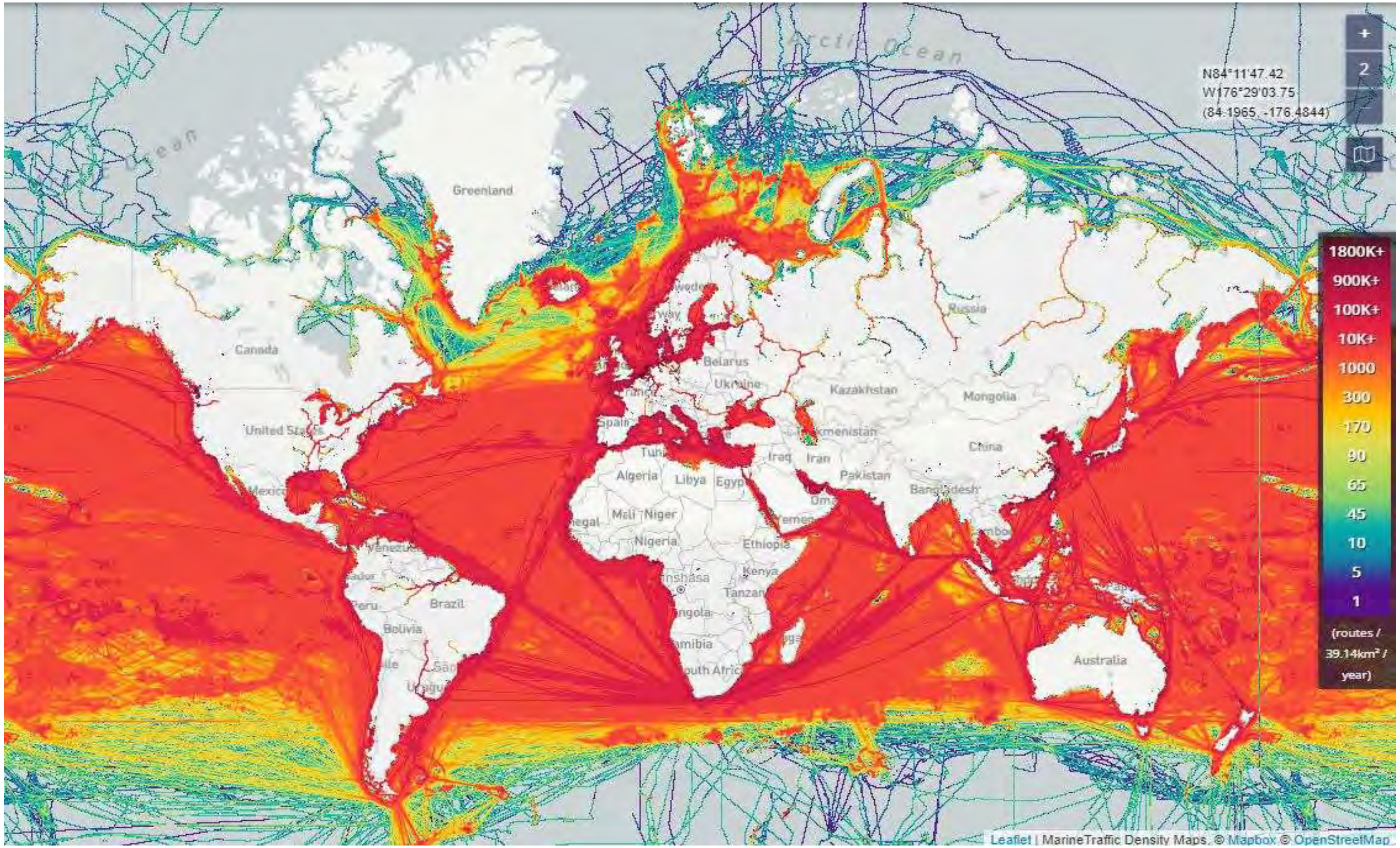

© marinetraffic.com

WHAT IS AIS

The **Automatic Identification System** (AIS) is a vessel collision avoidance/tracking system designed for autonomous information exchange between ship-ship and ship-shore base station.

Short messages are sent and received by the transceiver using radio waves in two dedicated VHF (very high frequency) channels: AIS 1 161.975 MHz, marine channel 87B and AIS 2 162.025 MHz, marine channel 88B

Autonomous and continuously operation is ensured by the transmission protocol:

- Self Organized Time Division Multiple Access (SOTDMA) for Class A (large vessels)
- Carrier Sense Time Division Multiple Access (CSTDMA) for Class B (small vessels)
- Fixed Access Time Division Multiple Access FATDMA for base station and Aids to Navigation (AtoN)
- Pre Announced Time Division Multiple Access PATDMA for Search and Rescue Radar Transponder (SART)

WHAT IS AIS

Each minute of time is divided in 2250 timeslots. Having two channels it makes 4500 time slots available. 1 timeslot is 256 Bits.

There are 27 message types currently in use out of the 64 possible. The most relevant are:

- Position messages: 1, 2, 3, 4, 18 and 27
- Static and voyage messages: 5 and 24

Updates of position messages happen at intervals from 2 secs to 3 mins depending on ship status and AIS class. Static and voyage message at 6 mins interval.

Position messages (MMSI, latitude, longitude, timestamp, speed and course, heading, etc.) are compiled using other navigation instruments (GPS, long-range nav system, gyrocompass, rate of turn indicator). Static and voyage messages (MMSI, name, type, dimension, IMO number, ETA, etc.) are manually compiled during installation.

WHAT IS AIS

Ships that must be equipped with an AIS according to SOLAS:

- All passenger ships
- All ships > 300 gross tonnage engaged on international voyages
- Cargo ship > 500 gross tonnage not engaged on international voyages

Additional regional agreements:

- EU flagged fishing ships > 15m length
- US commercial flagged fishing ship > 65 ft length

The AIS horizontal range is limited by the line-of-sight propagation of VHF radio wave, e.g. a receiving station at 100m ASL receive with a range of 35-40 km

AIS messages can be received by satellite (S-AIS) in Low Earth Orbit (LEO). Dense ship areas might create message collision. Refresh rate depends on the number of satellite in the constellation.

WHAT IS AIS

AIS are used in practice beyond collision avoidance in several applications:

- Vessel Traffic Services (VTS). Provides additional information on the type of vessels and their movement among other useful vessel specific data
- Aids to Navigation. Ability to broadcast positions and names of objects, such as lighthouse, buoys, and markers
- Search and Rescue. Status information of vessel in the vicinity of a vessel or person in distress
- Accident investigation. Provide accurate navigation data history of the vessels involved in an accident.
- Binary messaging. Use of binary data for broadcasting communication, for example meteorological conditions
- Surveillance and security. Border control, counter piracy, fishing regulation compliance.
- **Add-on for SAR oil spill and ship detection**

SAR SHIP DETECTION INTERPRETATION

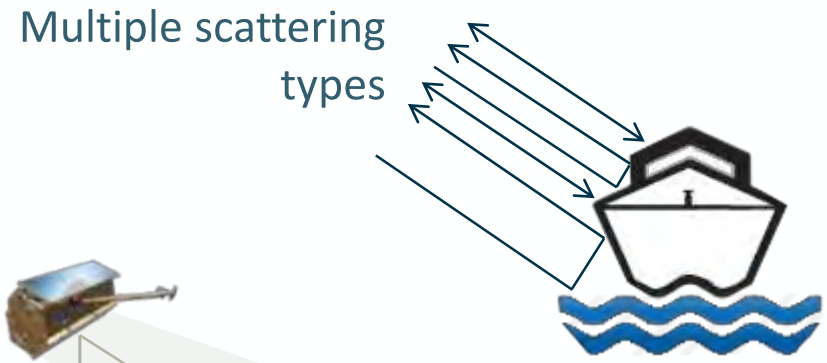

Target scattering

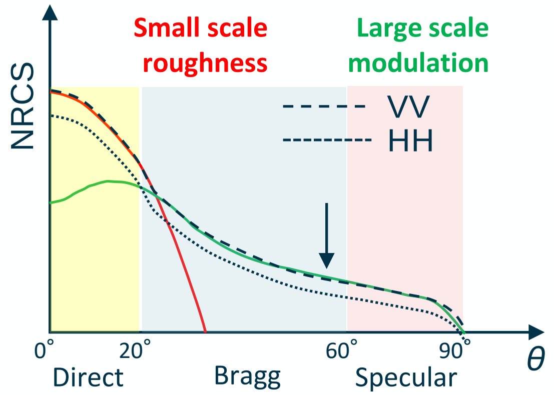

Ocean scattering

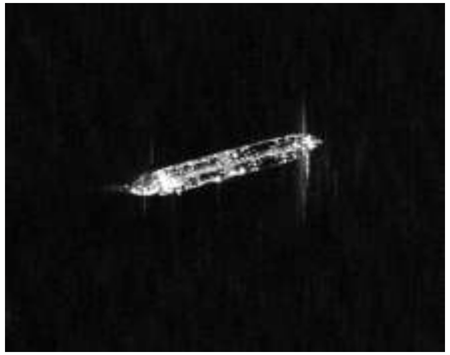

Ship and ocean signature on SAR

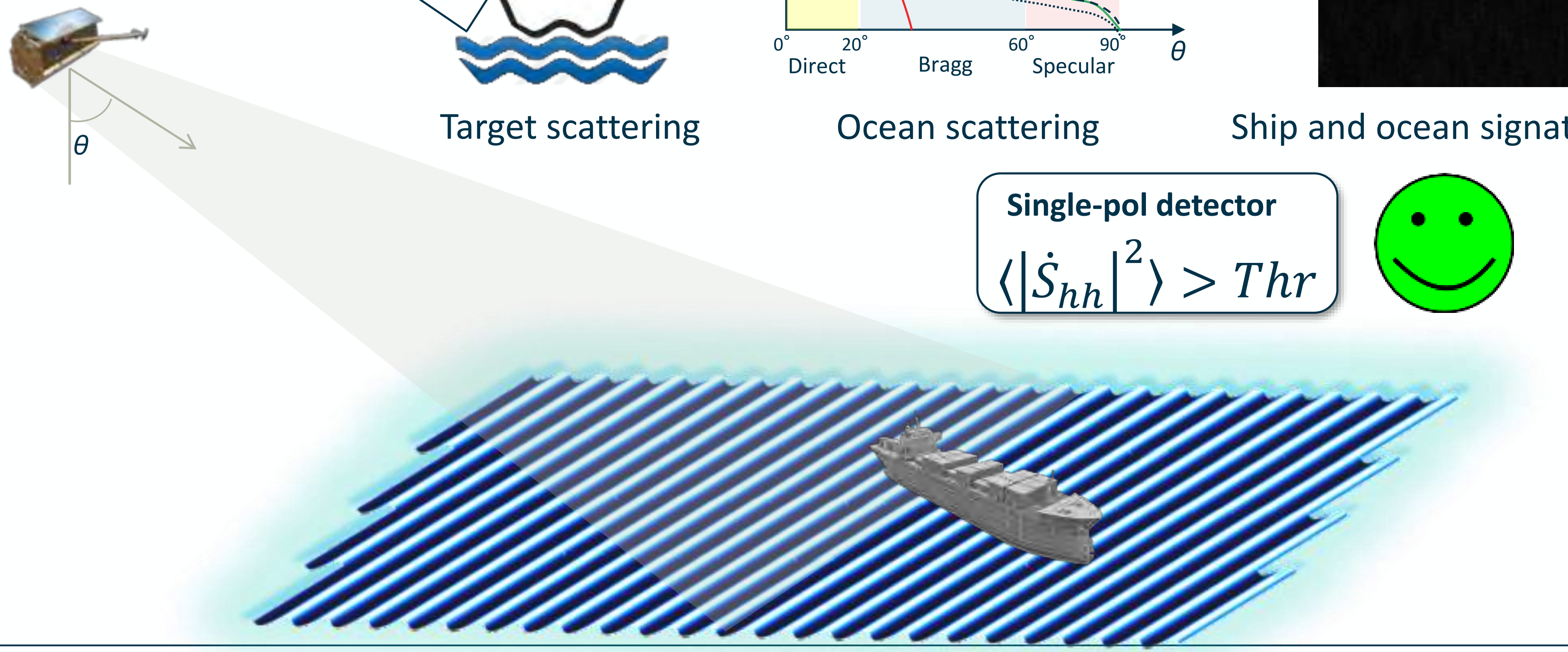

Single-pol detector

$$\langle |\dot{S}_{hh}|^2 \rangle > Thr$$

SAR SHIP DETECTION INTERPRETATION

Multiple scattering types

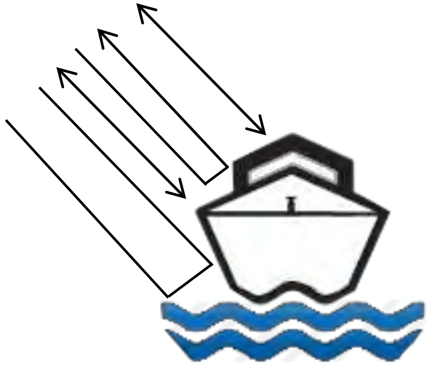

Target scattering

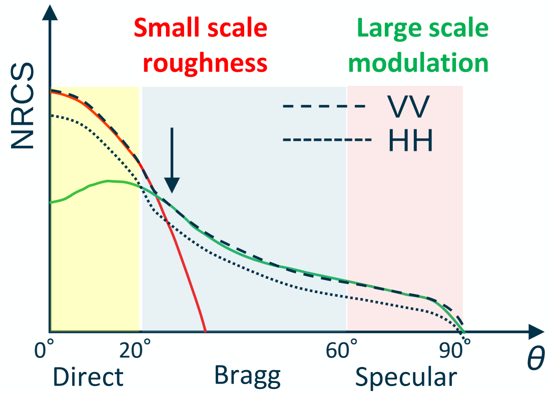

Ocean scattering

Ship and ocean signature on SAR

Single-pol detector

$$\langle |\dot{S}_{hh}|^2 \rangle > Thr$$

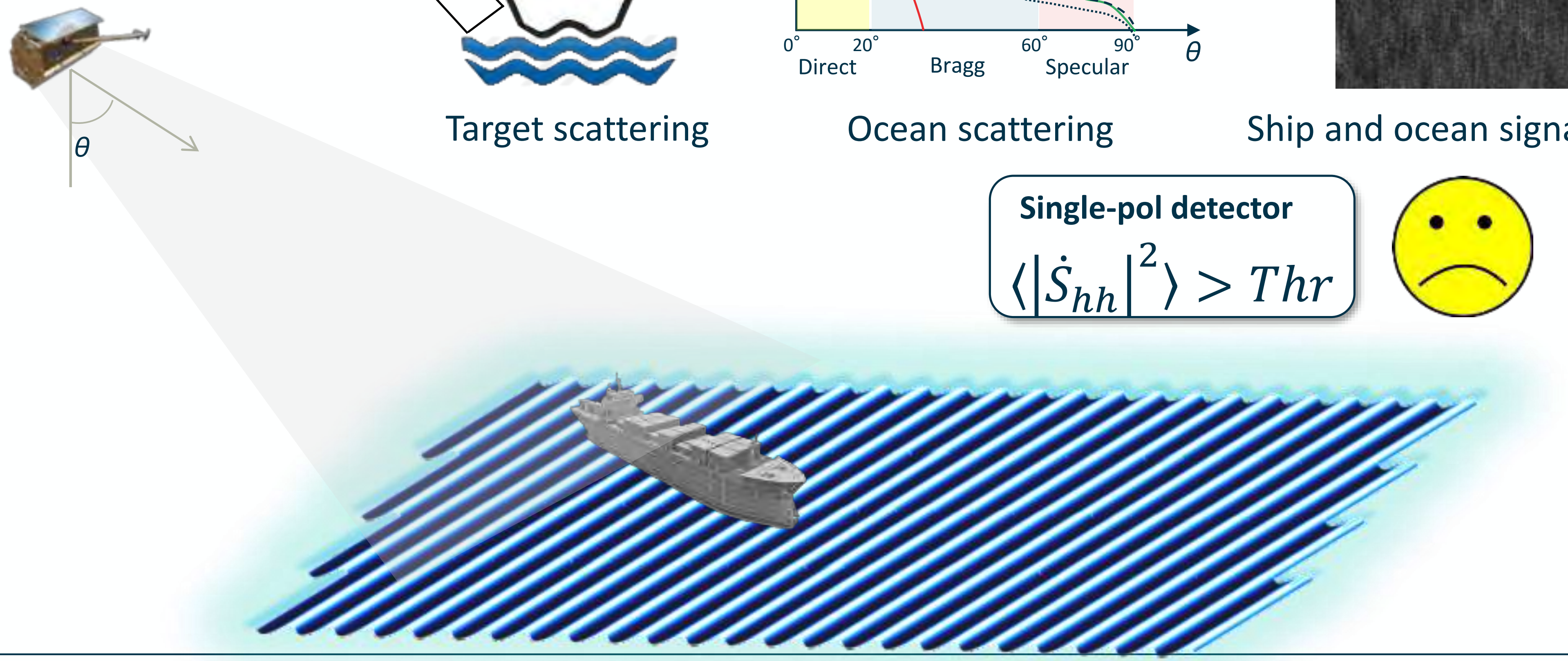

SAR SHIP DETECTION INTERPRETATION

How ships looks like in SAR image?

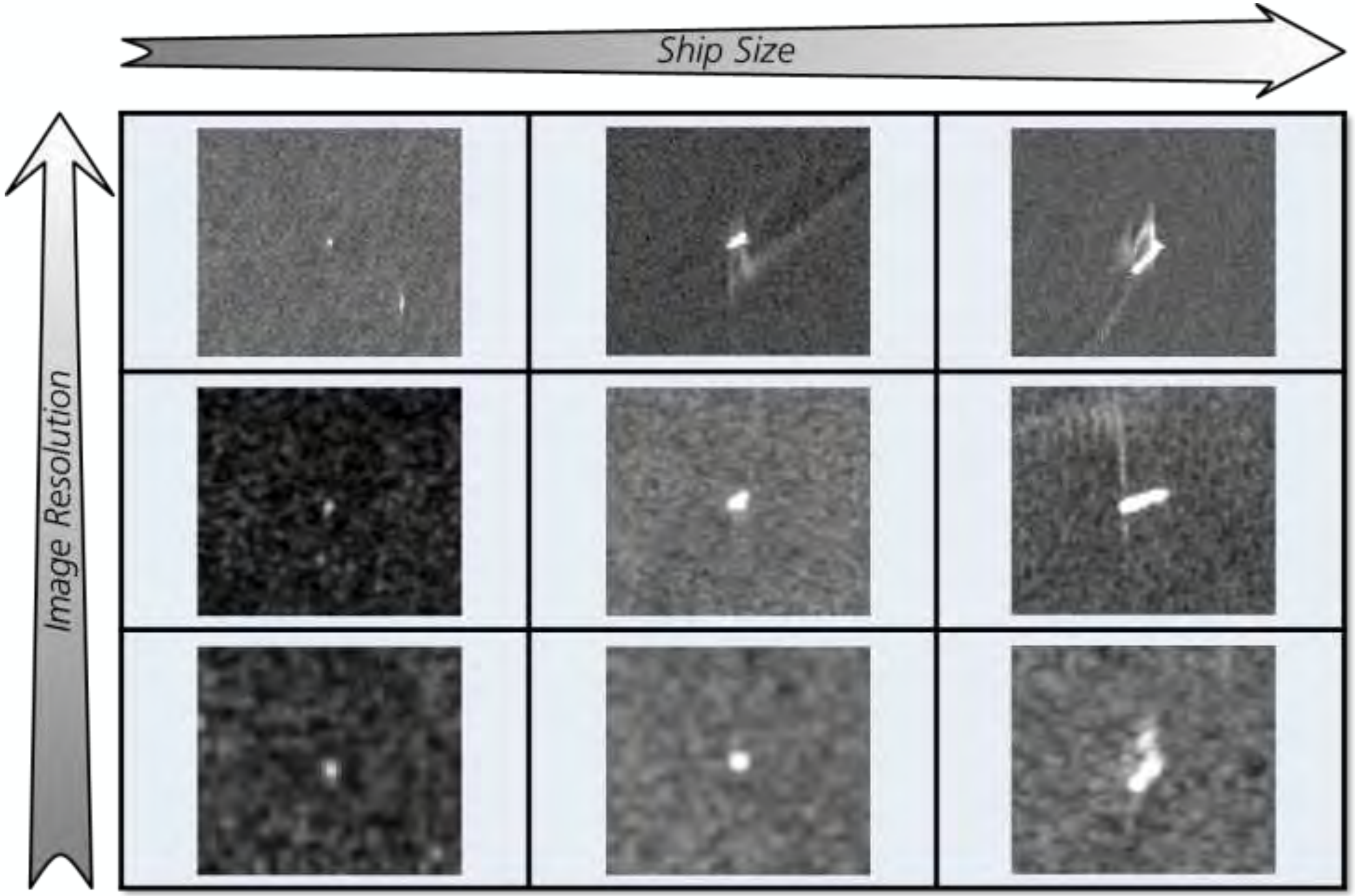

SAR SHIP DETECTION INTERPRETATION

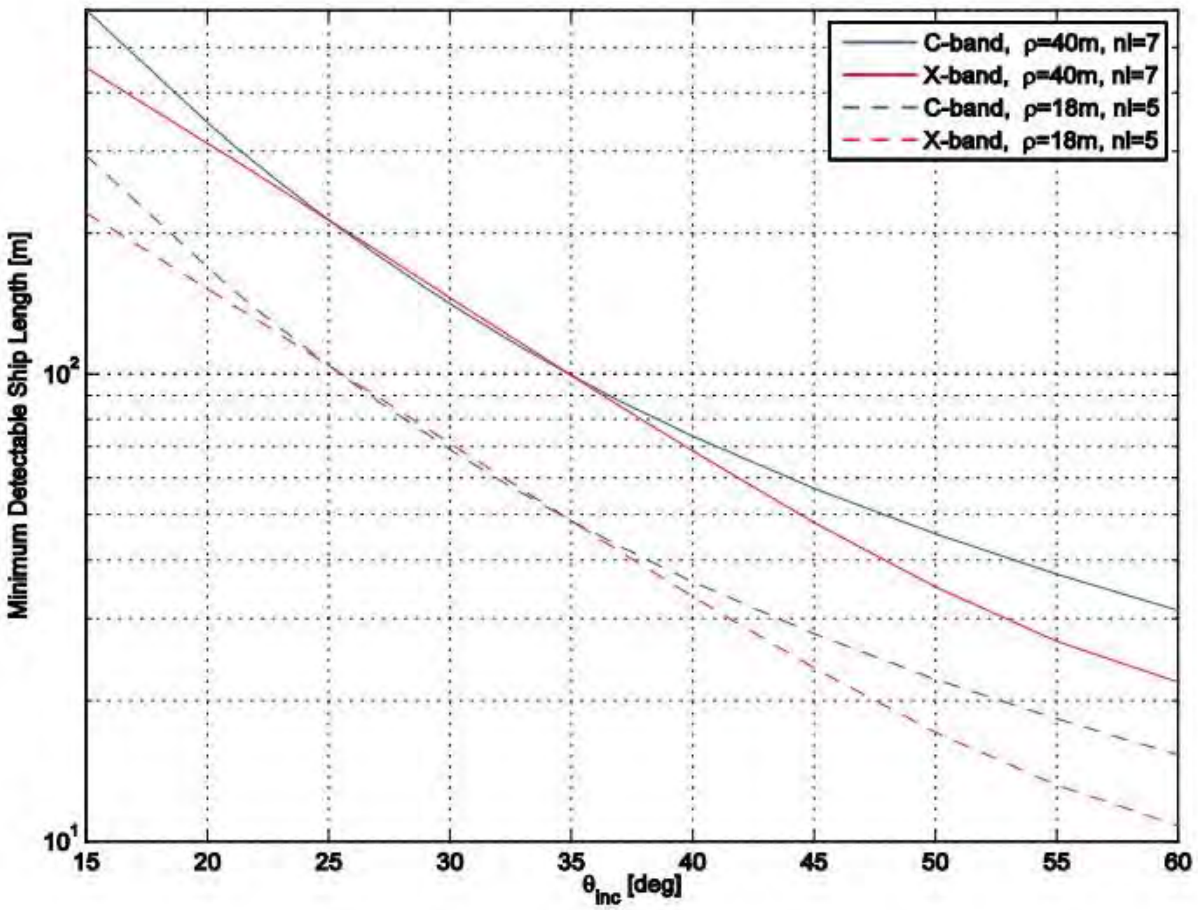

- Paris W. Vachon (DRDC Canada) has developed a performance tool to predict the ship detectability in C-band SAR
- The tool is based on modelling the ship RCS as function of the ship's length and the ocean RCS as function of wind speed/direction (CMOD and XMOD) and following a K-distribution
- The tool has been extended to X-band and can give an indication of ship detectability at different wavelength (HH, PFA=$2.5(10)^{-9}$, PD=0.9, margin=3dB

SAR SHIP DETECTION INTERPRETATION

Data-driven probability of detection map based on X-band high resolution (better than 6m) SAR data, under moderate sea state conditions, as function of wind speed, incidence angle and ship size classes, small, medium and large.

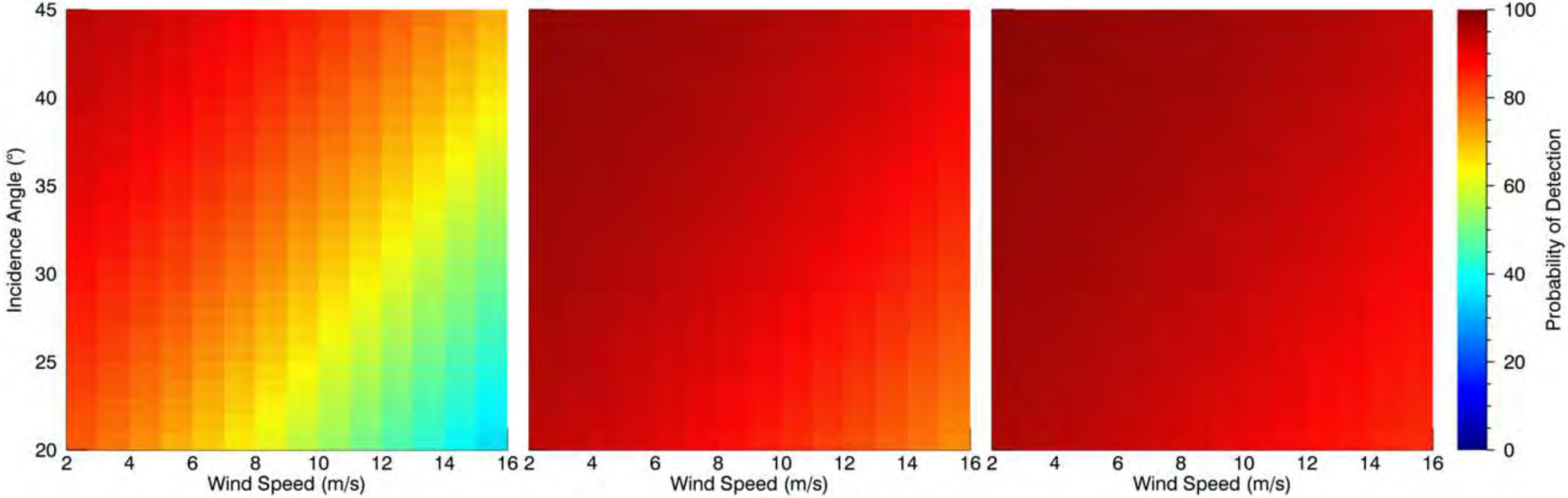

Small ship
$1 < l[m] \leq 25$

Medium ship
$25 < l[m] \leq 150$

Medium ship
$l[m] > 150$

SAR SHIP DETECTION INTERPRETATION

- Comparison of SAR single-pol and PolSAR mode for the detection of small metallic target at sea

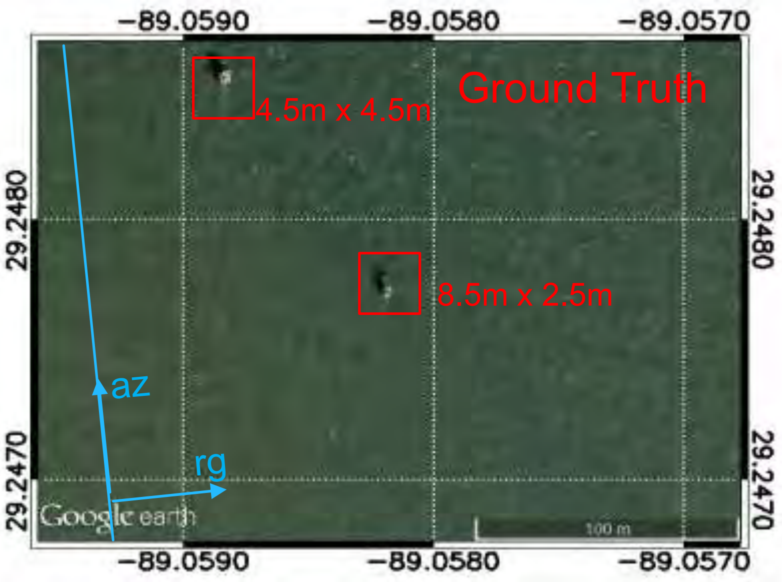

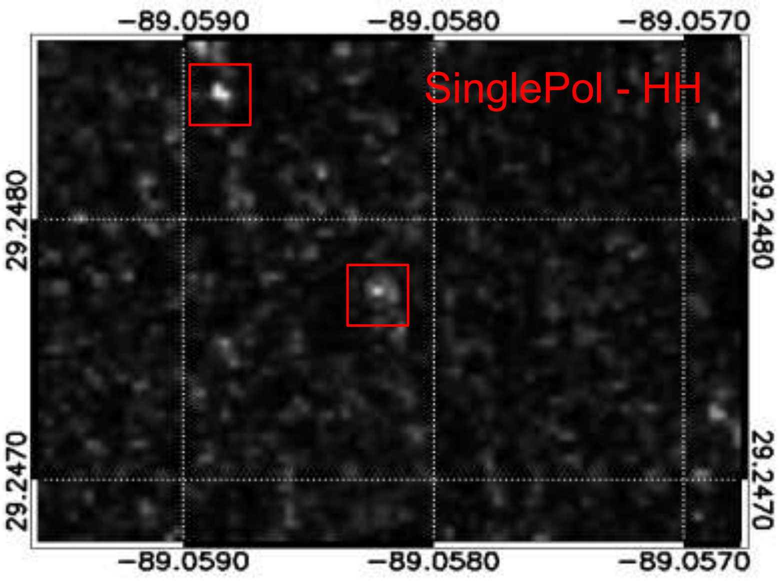

SAR SHIP DETECTION INTERPRETATION

- Comparison of SAR single-pol and PolSAR mode for the detection of small metallic target at sea
- The resolution loss of the PolSAR mode might end-up in losing some targets, but this drawback is compensated by the different polarization available

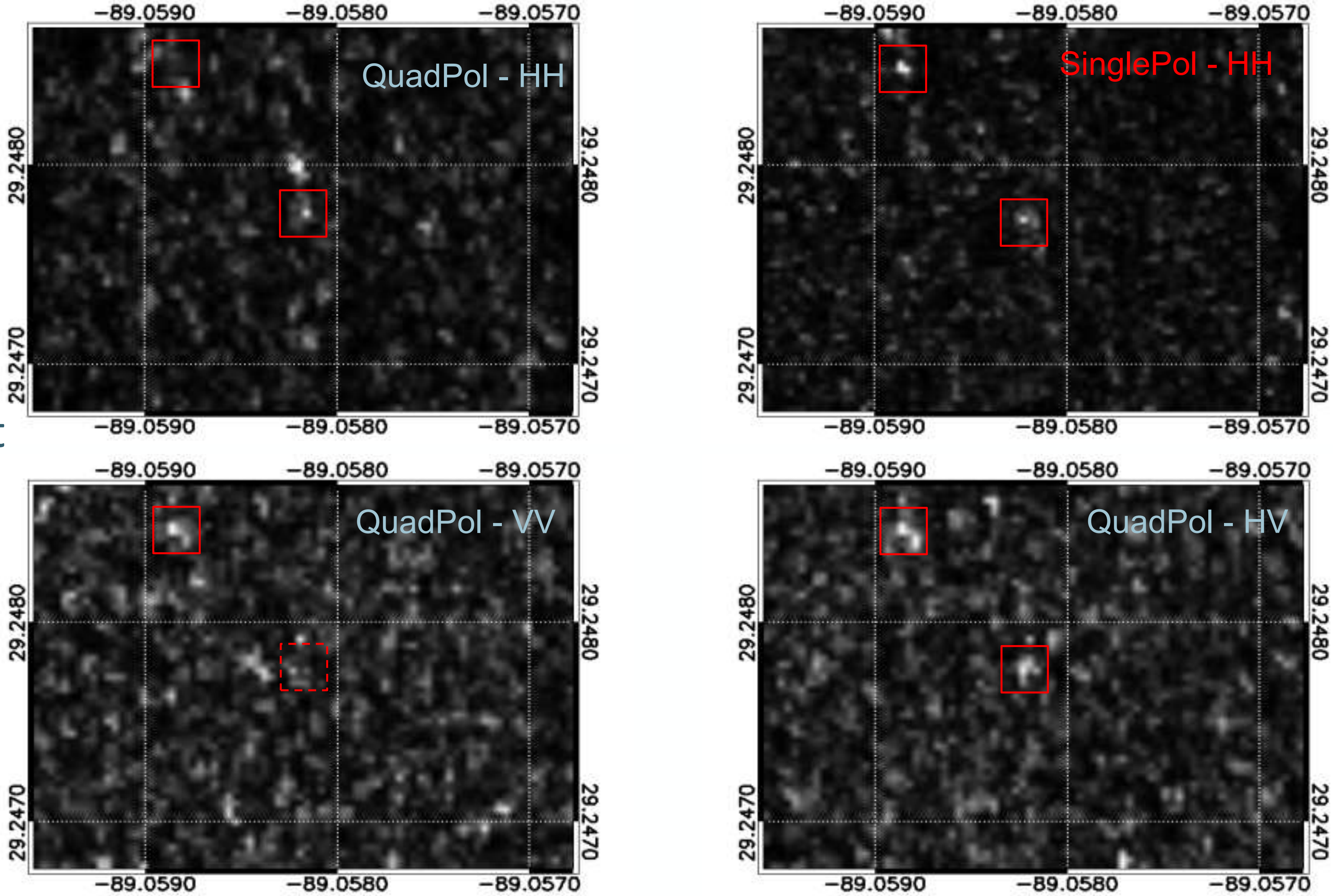

SAR SHIP DETECTION CHALLENGES

- Ship's velocity radial component produces a Doppler shift which results in the ship to be located at displaced position in azimuth "train off the track effect".
- This impacts the geo-location estimation of the detected ships

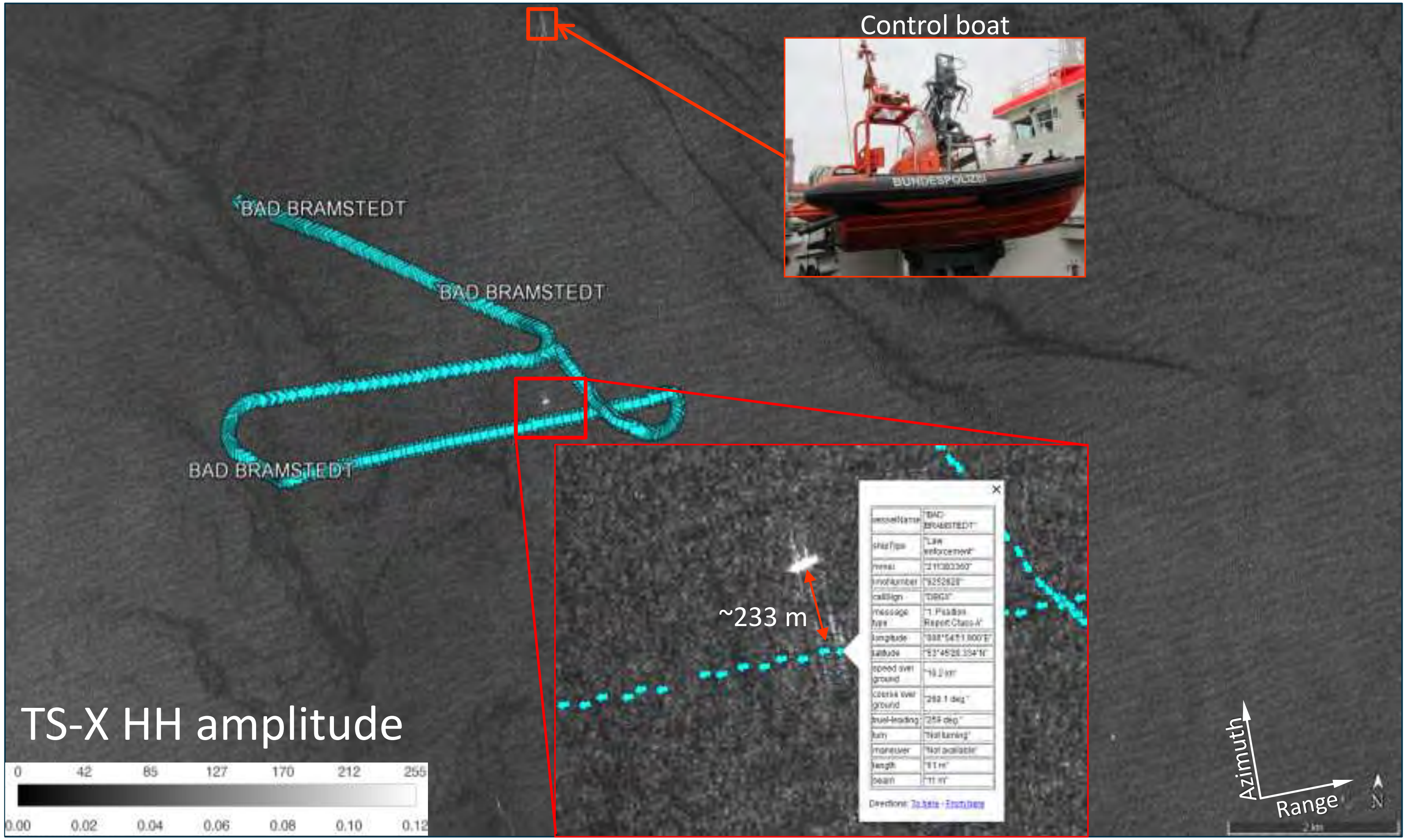

SAR SHIP DETECTION CHALLENGES

- Ship's velocity along track component, i.e. azimuth, change the Doppler slope which results in a defocusing of the impulse response with a consequent "smearing" of the ship.
- This impacts the detection and ship's length estimation

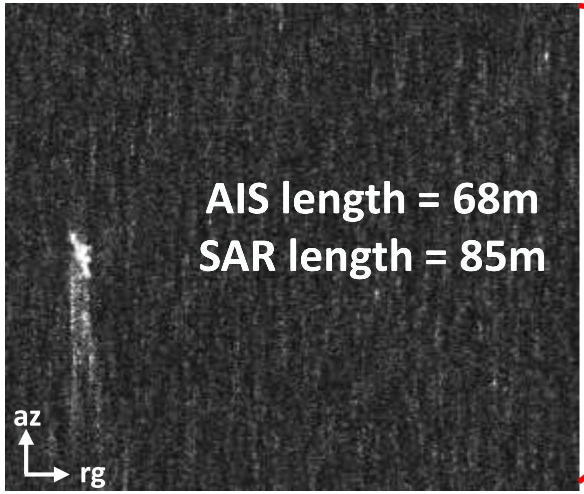

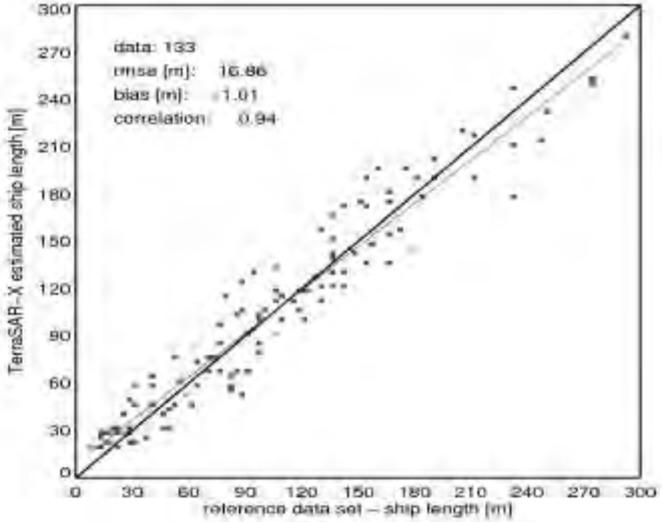

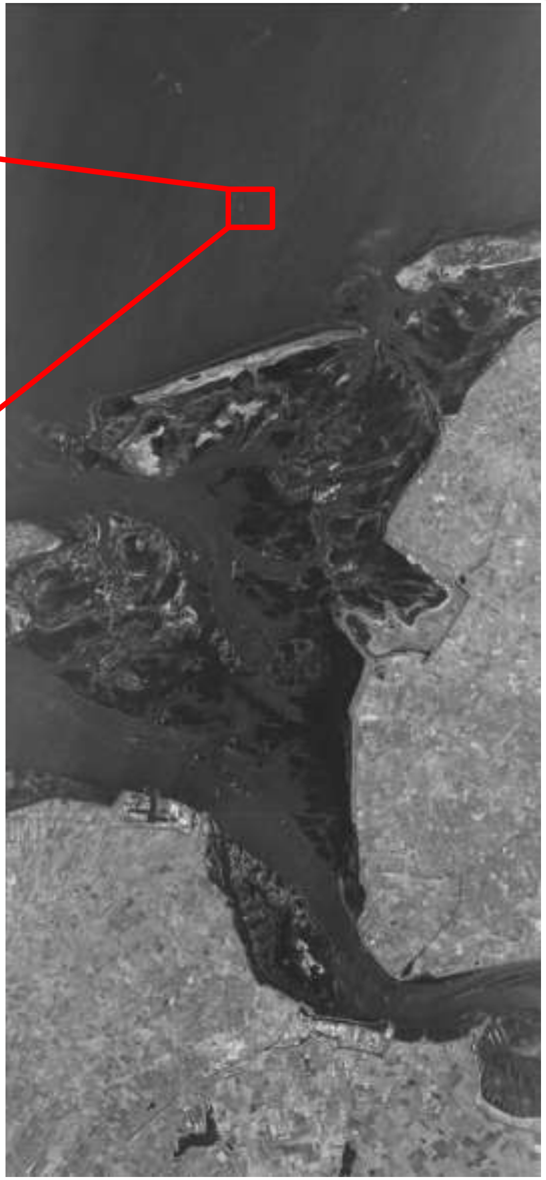

SAR SHIP DETECTION CHALLENGES

- Ship's dihedral structures, e.g. bridge-deck, produce a "cross-like" radar signature
- This impacts the estimation of the ship's width.

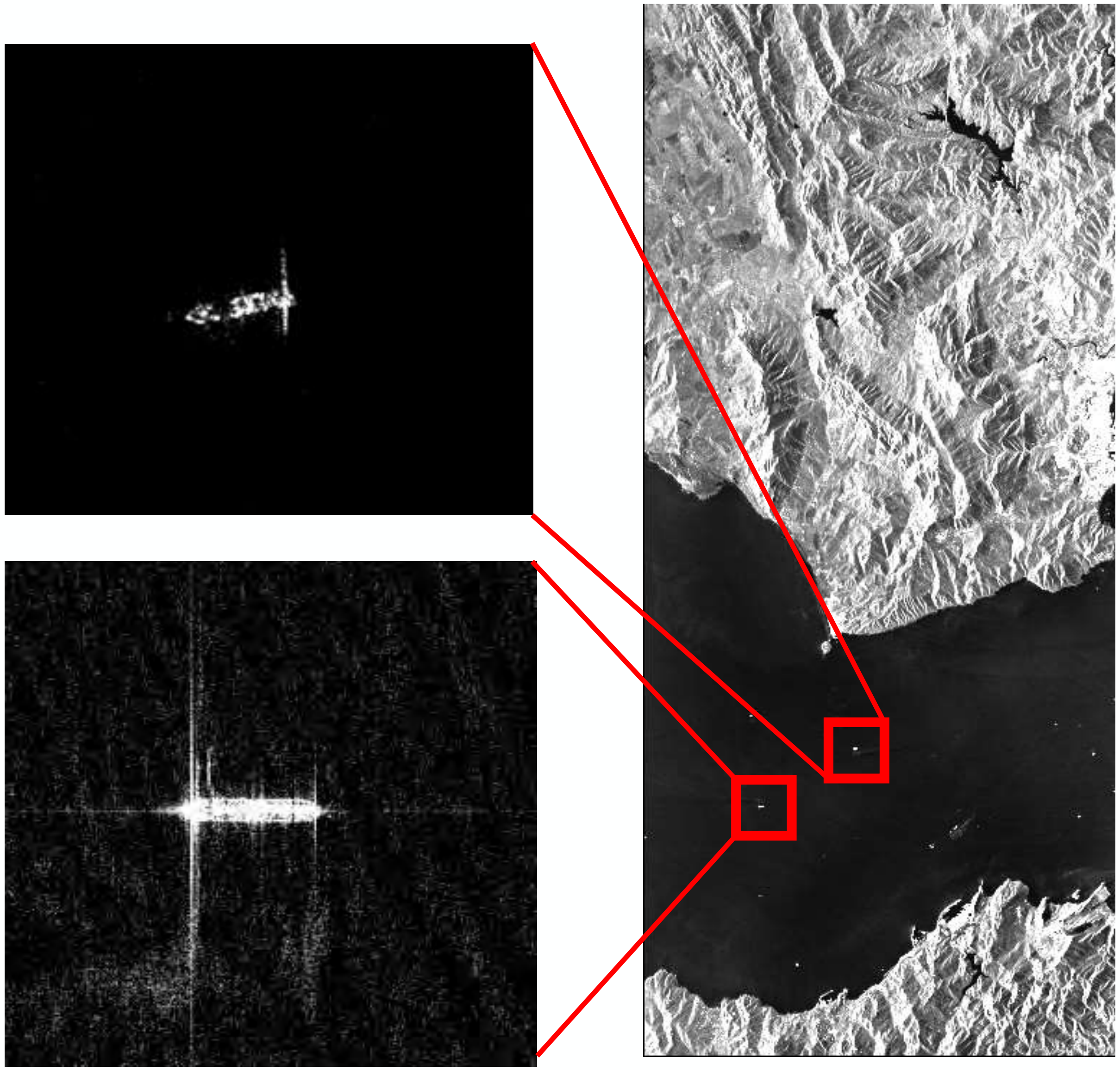

© source SAR data: DLR e.V., 2011.

SAR SHIP DETECTION CHALLENGES

- The SAR finite sampling of the Doppler spectrum at PRF produce signal components outside the processed bandwidth to fold back and generate the ghost replicas “azimuth ambiguity”.
- This impacts the detection performance increasing the false alarms

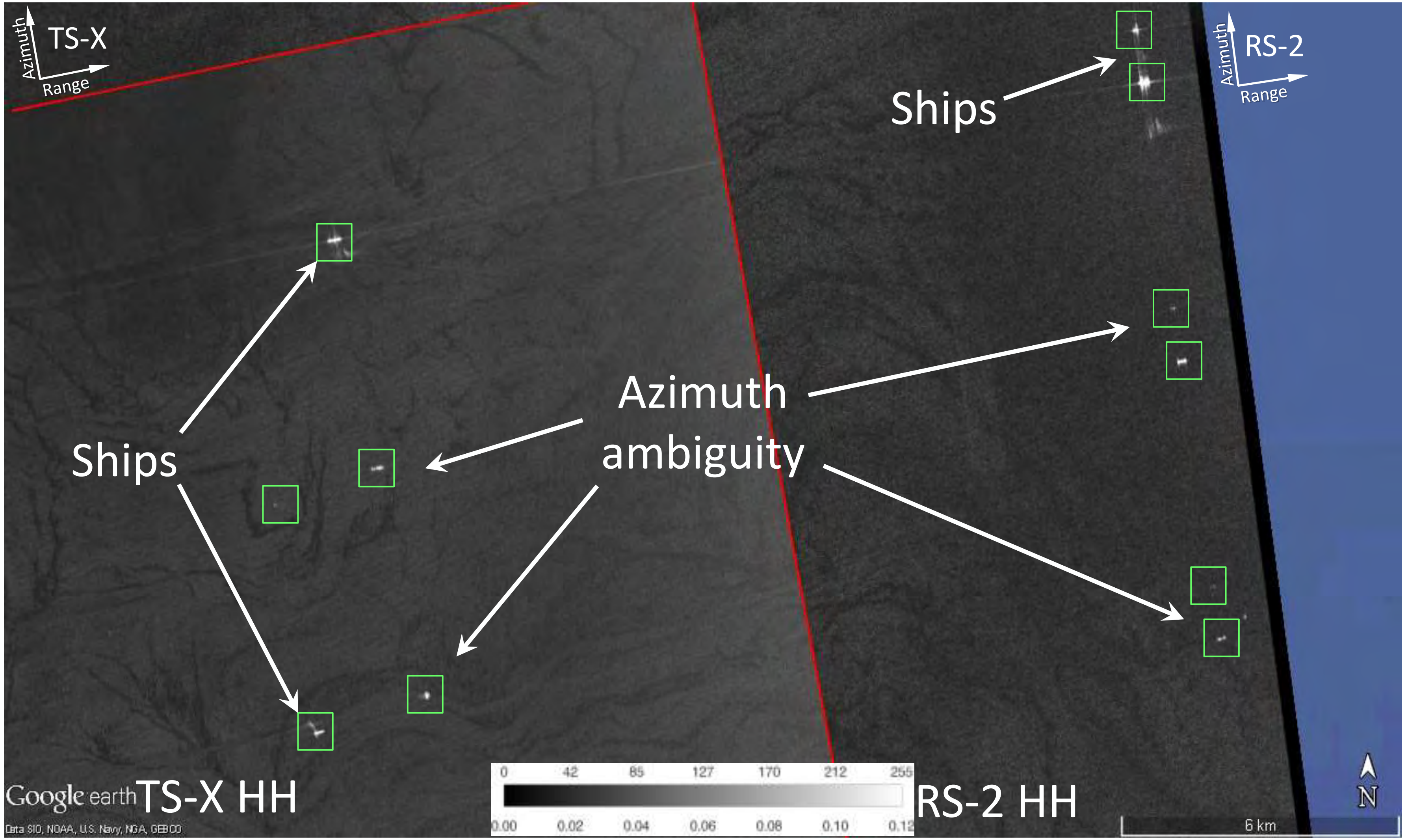

SAR SHIP DETECTION CHALLENGES

- The SAR finite sampling of the Doppler spectrum at PRF produce signal components outside the processed bandwidth to fold back and generate the ghost replicas “azimuth ambiguity”.
- This impacts the detection performance increasing the false alarms

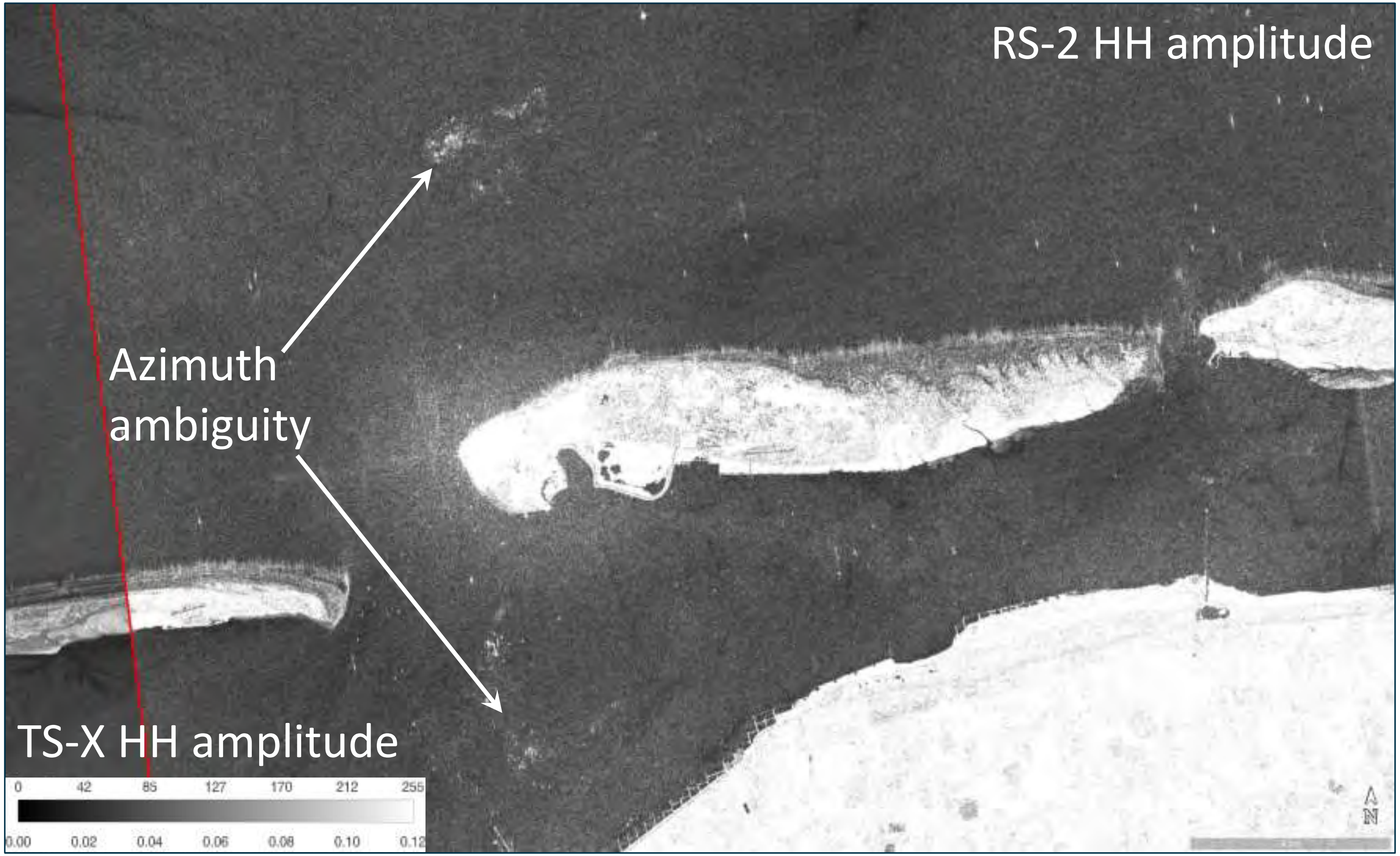

NRT SAR SHIP DETECTION WORKFLOW

- Image Product:
  - Level-1 product
  - ScanSAR, StripMAP, SpotLigth modes
  - (Multilooked) Ground Range Detected (GRD) type
- Ancillary Data:
  - product annotation metadata file
  - land mask dataset
  - AIS data stream
- Final Product:
  - detected targets and parameters list
  - match with AIS and ship identification
- Near-Real-Time: 20-30 mins from data downlink at base station

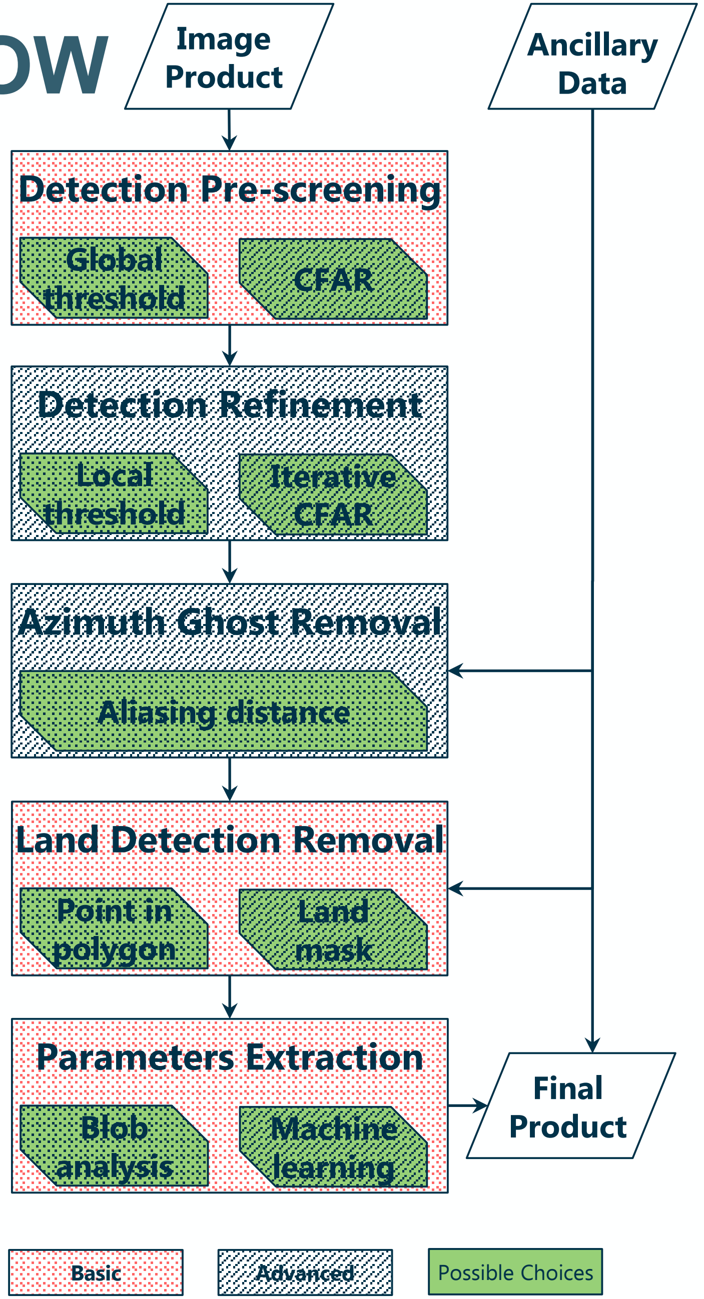

SHIP DETECTION – CFAR

Basic concept of Constant False Alarm Rate: identify pixels that do not fit to the statistical properties of sea clutter keeping constant the probability of false alarms along the input image

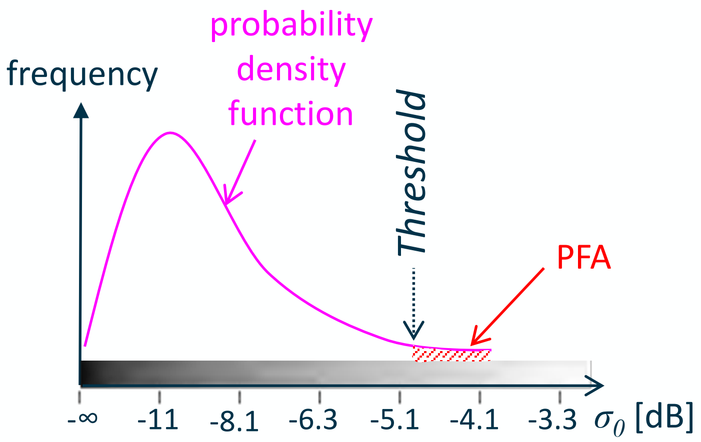

$$PFA = \int_{Thr}^{\infty} p(x)dx$$

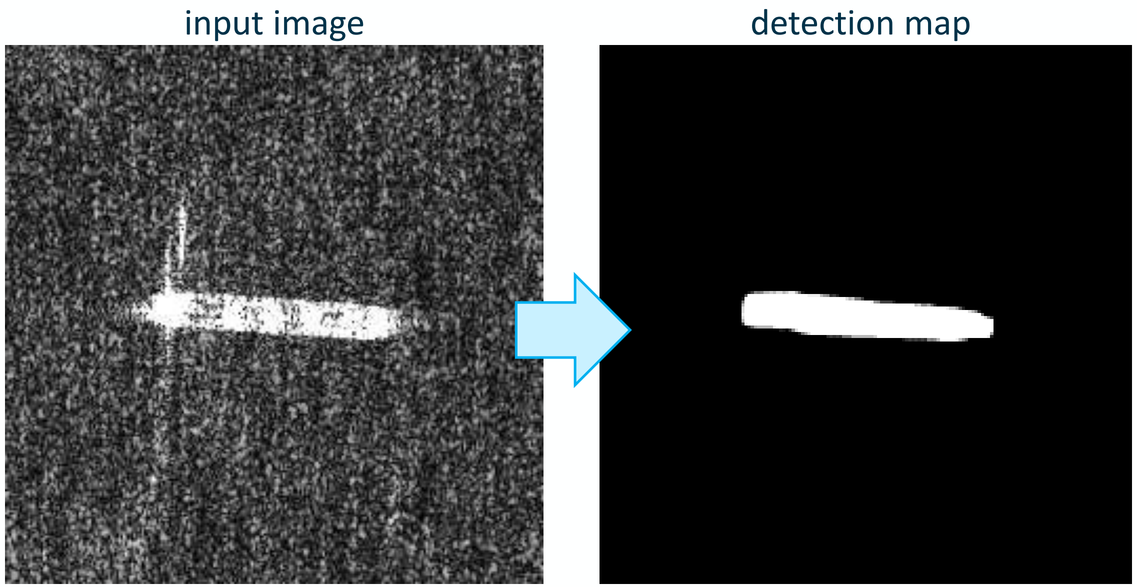

The threshold changes adaptively and the detector is usually applied on pixel-bases. 30 x 50 km^2 VHR SAR image @1.5m pixel spacing is ~660 * 10^6 pixels

SHIP DETECTION – CFAR

Nested sliding moving window concept and ocean clutter parameters

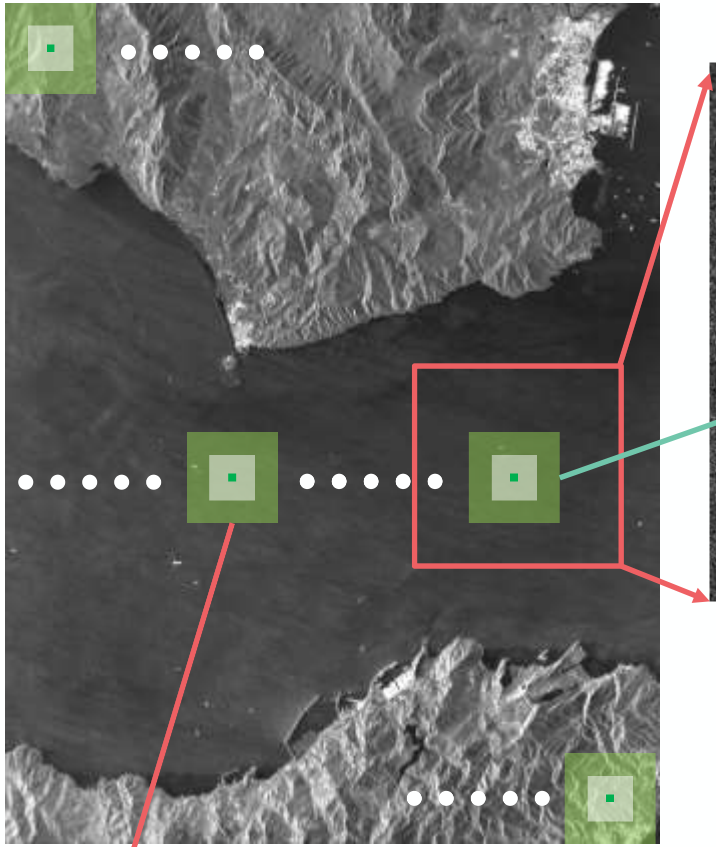

input image

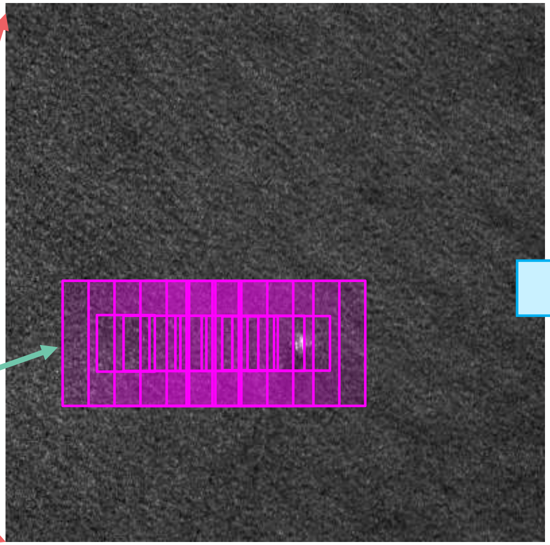

detection map

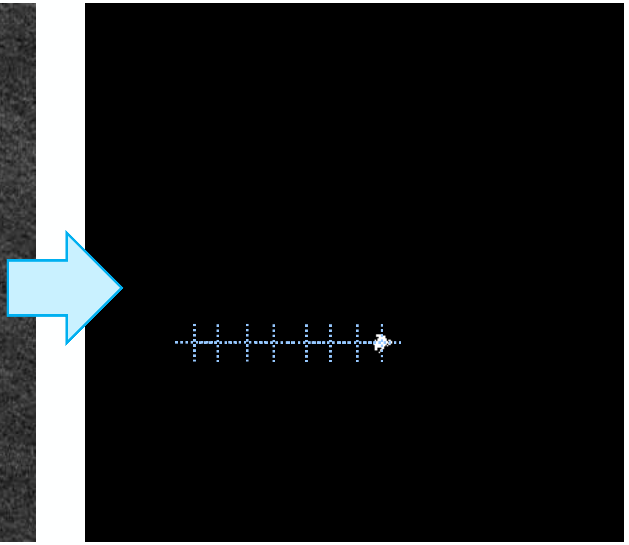

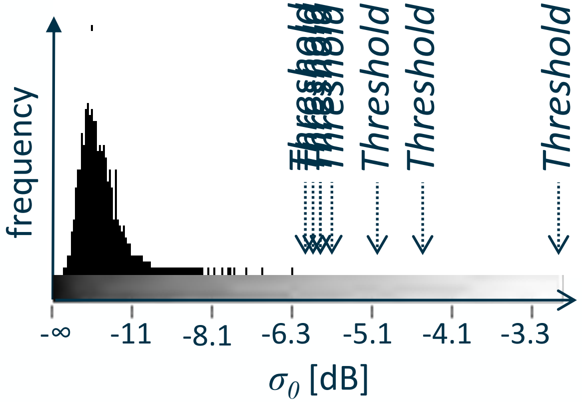

CA-CFAR: pixel is target if $mean(w_T) > t_{CFAR} * mean(w_B)$

2P-CFAR: pixel is target if $mean(w_T) > mean(w_B) + \ t_{CFAR} * stddev(w_B)$

The background w_B, guard w_G and target w_T window sizes are detector design parameters. t_{CFAR} governs the PFA

SHIP DETECTION – CFAR ITERATIONS

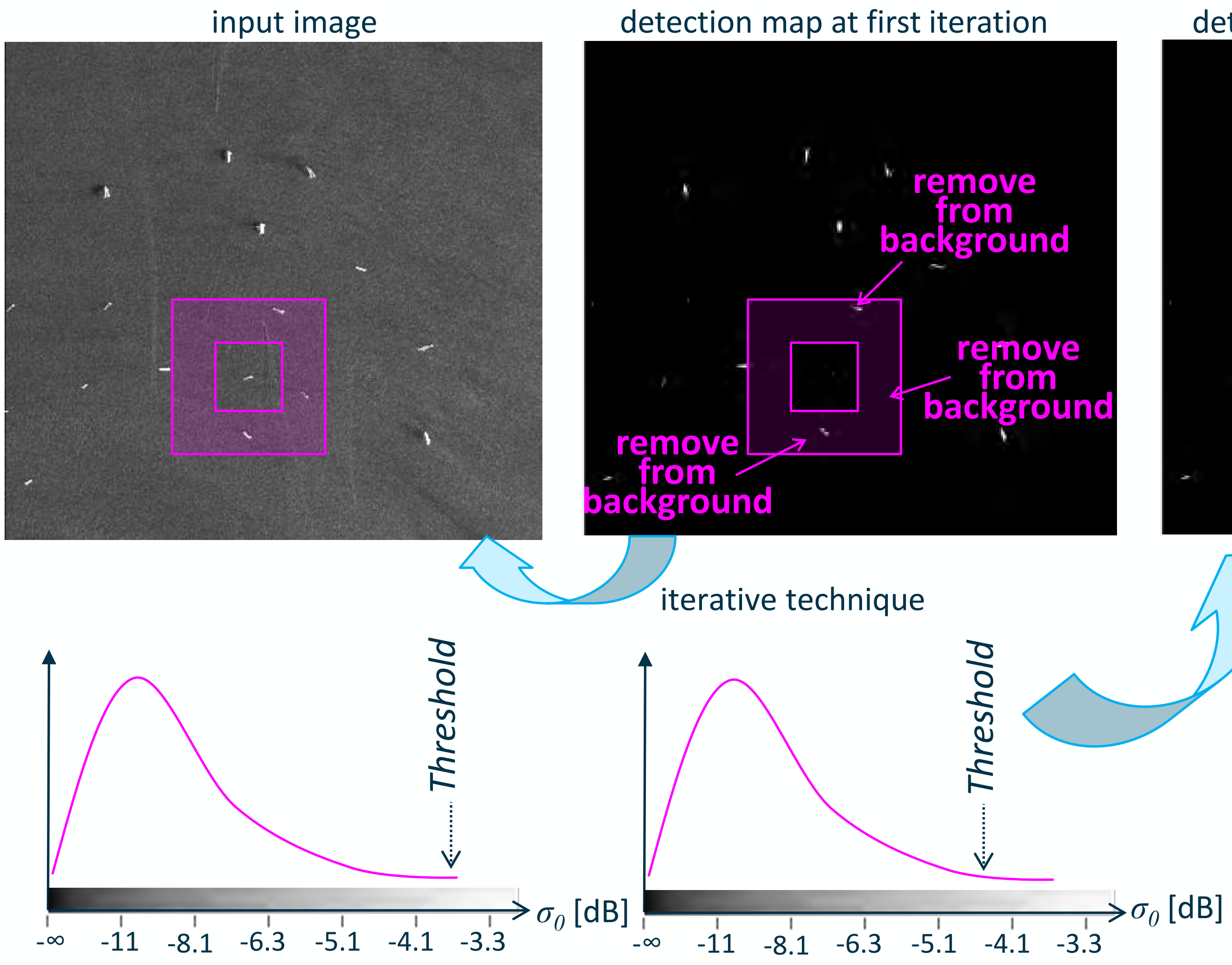

- Detection fails as the background statistics are corrupted by surrounding ships
- Making use of the first detection map, background statistics is less corrupted

SHIP DETECTION IN SLC DATA

- The detection step can take advantages of the Time-Frequency (TF) decomposition of Single Look Complex SAR data
- Several variations of the TF have been proposed for ship detection based on:
  1) Single, dual- or quad-pol
  2) Fourier in range, azimuth or both
  3) Partitioning strategy: only time, only frequency and TF
  4) Number of partitions
  5) With and without overlap between partitions
  6) Yes/No re-oversample and tapering function
  7) How n complex signals are combined

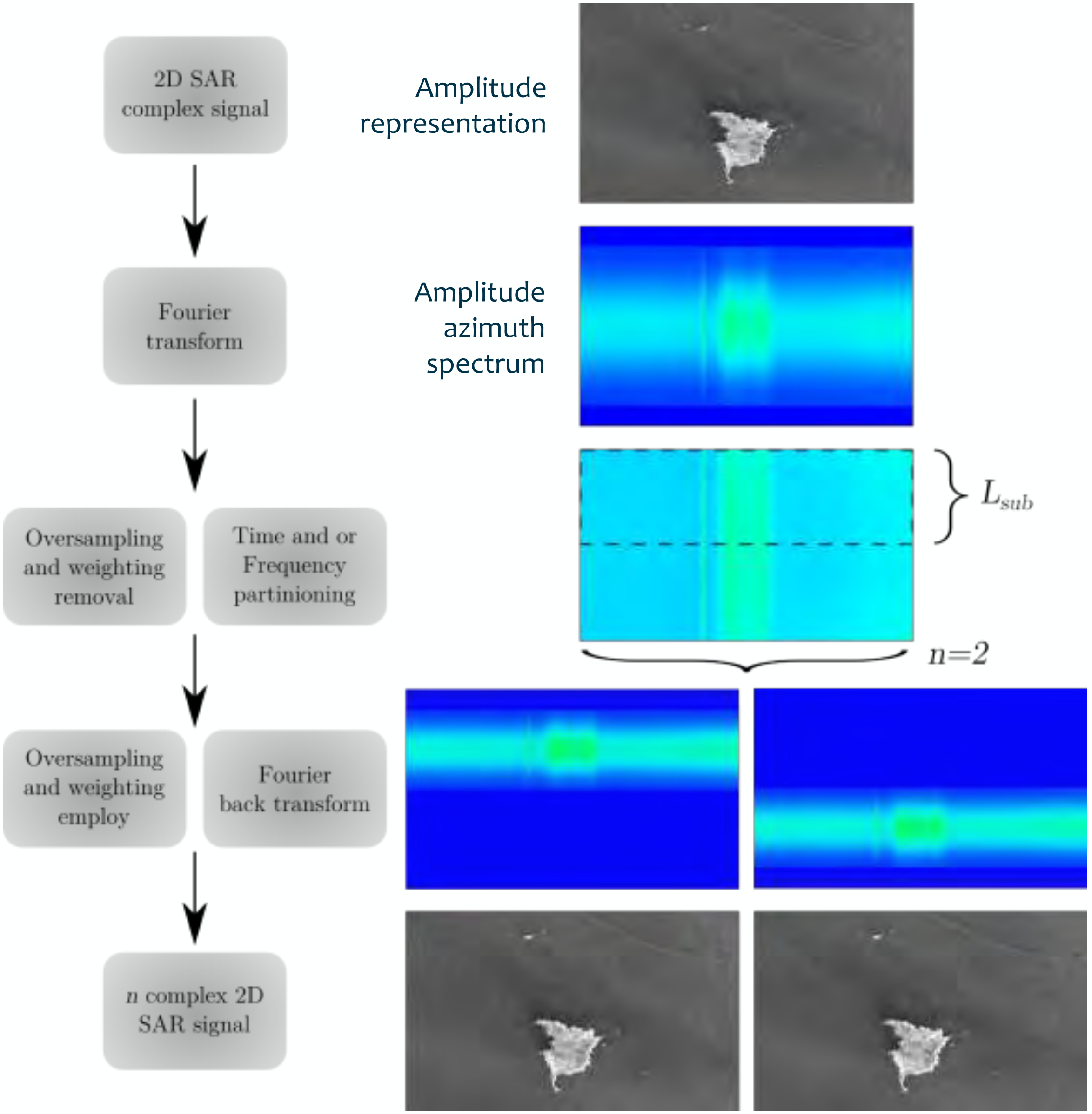

SHIP DETECTION IN SLC DATA

- Arnaud ’99, Ouchi et. al. ‘04:

  single-pol input, azimuth direction and partitioning, 2 non-overlapping frequency band (halved $B_{Doppler}$), magnitude normalized coherence ρ. Higher TCR, sea decorrelation, clutter suppression. Limited data, no info on data oversampling, Doppler centroid correction and data weighting function.

- Souyris et. al. ‘03:

  single-pol input, range and azimuth direction and partitioning, oversampling only in range, Doppler centroid correction, 2 non-overlapping (halved $B_{Doppler}$ and B_{chirp}) resulting in 4 complex signal output, complex correlation ρ_{herm}^{azi}, ρ_{herm}^{rge} and their incoherent sum. Polarimetric extension. ρ_{herm} better than ρ, decomposition in range investigated. Limited data, tested with land target immersed in speckle, vehicle or ship can easily “decohere”.

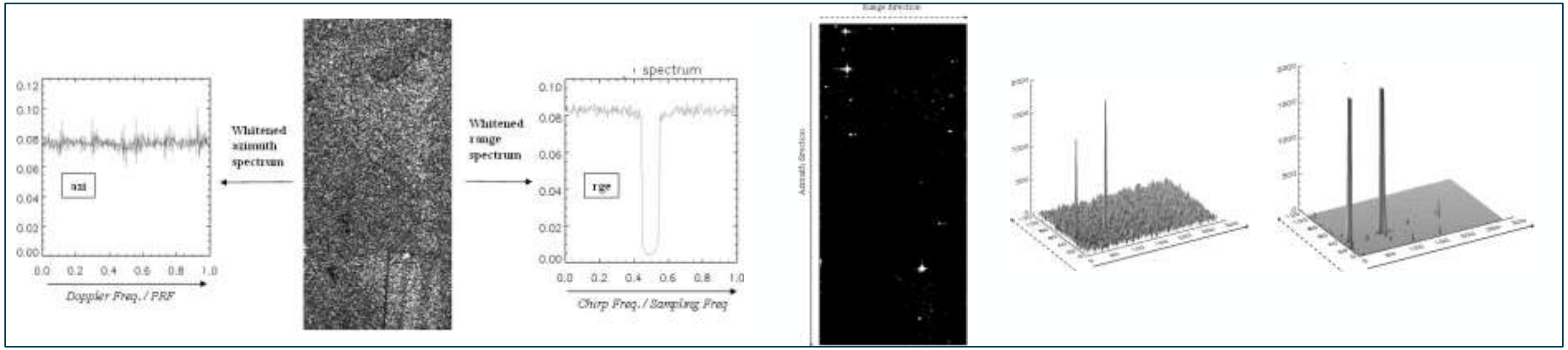

©J.-C. Souyris, C. Henry, and F. Adragna, “On the use of complex SAR image spectral analysis for target detection: assessment of polarimetry,” IEEE Trans. Geosci. Remote Sens., vol. 41, no. 12, pp. 2725–2734, Dicembre 2003.

SHIP DETECTION IN SLC DATA

- Greidanus '06:

  single-pol input, only azimuth direction and partitioning, 3 non-overlapping (1/3 $B_{Doppler}$), various combinations of the 3 complex signal output (multiplicative mean, CoV, local correlation, multi-look image). Small fishing vessel, no combination performed better than intensity, theoretical behavior. Limited data, no info on data oversampling, Doppler centroid correction and data weighting function.

- Brekke et. al. '13:

  single-pol input, azimuth direction and partitioning, 2 varying $B_{Doppler}$ and overlap, Doppler centroid correction, oversampling, complex correlation ρ_{herm}^{azi} Polarization dependency. Overlap effects. Medium size ship. Limited data and conditions tested.

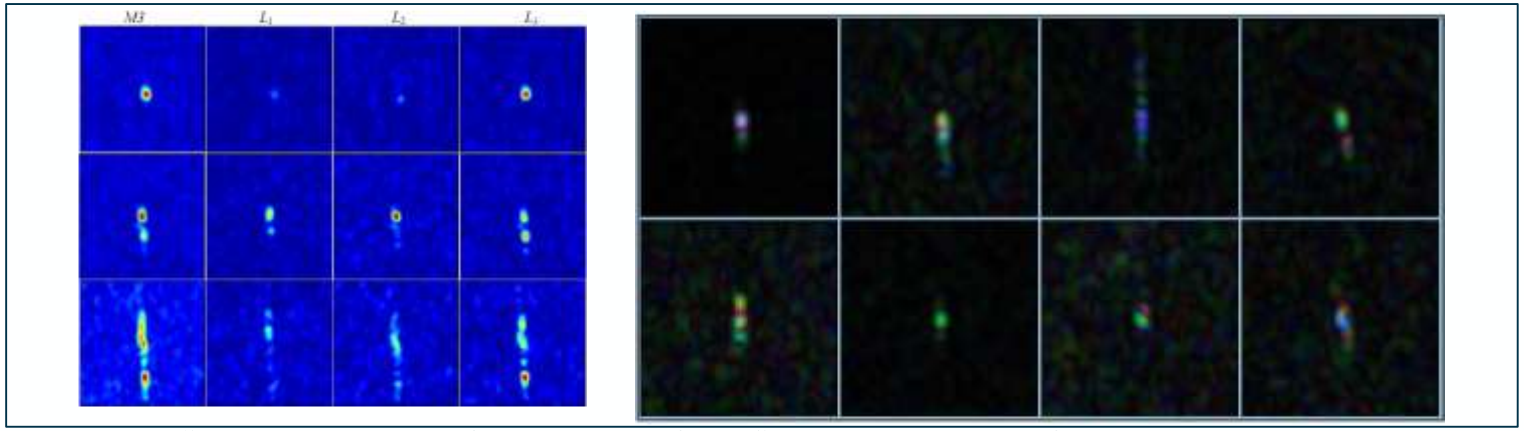

©H. Greidanus, "Sub-aperture Behavior of SAR Signatures of Ships," in IEEE International Conference on Geoscience and Remote Sensing Symposium, 2006. IGARSS 2006, 2006, pp. 3579–3582.

SHIP DETECTION IN SLC DATA

- Hu et. al. '13:

  quad-pol input, simultaneous azimuth and range direction and partitioning, 2 non-overlapping azimuth (halved $B_{Doppler}$) and 2 non-overlapping range (halved B_{chirp}), Doppler centroid correction, no-oversampling, TF-pol coherence ρ_{TF-pol} Ships vs island, ships vs ghost, ships vs sea ice, low SCR. Computational complexity, increased amount of memory, limited data.

- Marino et. al. '15:

  single-pol input, individual azimuth and range direction and partitioning, 2 or more azimuth (varying $B_{Doppler}$) and 2 or more range (varying B_{chirp}), set of overlapping bands, oversampling and pre-whitening, coherence, correlation, entropy, GLRT. L-, C- and X-band, large amount of ground truth ships, meteorological conditions. Dedicated to a general ship size.

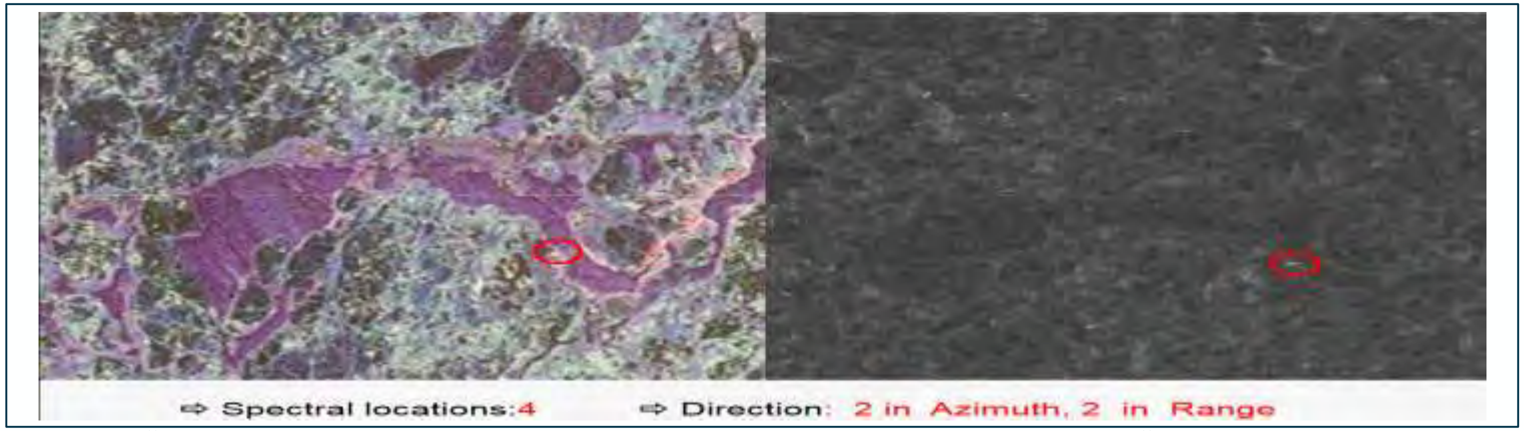

©C. Hu et al "Ship Discrimination Using Polarimetric SAR Data and Coherent Time-Frequency Analysis," Remote Sens., vol. 5, no. 12, pp. 6899–6920, Dec. 2013.

DUAL-POL REFLECTION SYMMETRY

Reflection symmetry approach applied to ship detection

- Man-made metallic target
- **Not symmetric**
- C has 9 non-0 elements

$$C_3 = \begin{bmatrix} \langle |\dot{S}_{hh}|^2 \rangle & \sqrt{2}\langle \dot{S}_{hh}\dot{S}_{hv}^{*} \rangle & \langle \dot{S}_{hh}\dot{S}_{vv}^{*} \rangle \\ \sqrt{2}\langle \dot{S}_{hv}\dot{S}_{hh}^{*} \rangle & 2\,\langle |\dot{S}_{hv}|^2 \rangle & \sqrt{2}\langle \dot{S}_{hv}\dot{S}_{vv}^{*} \rangle \\ \langle \dot{S}_{vv}\dot{S}_{hh}^{*} \rangle & \sqrt{2}\langle \dot{S}_{vv}\dot{S}_{hv}^{*} \rangle & \langle |\dot{S}_{vv}|^2 \rangle \end{bmatrix}$$

$$r = \left|\langle S_{xx}{S_{xy}}^{*} \rangle\right| \quad x, y \in \{h, v\}$$

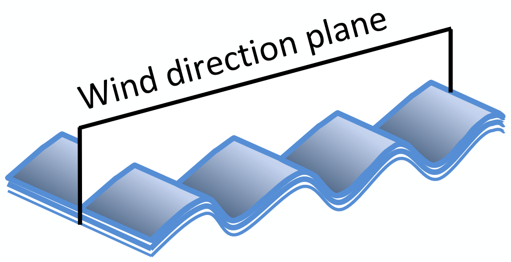

- Natural distributed target
- **Symmetric**
- C has 5 non-0 elements

$$C_3 = \begin{bmatrix} \langle |\dot{S}_{hh}|^2 \rangle & 0 & \langle \dot{S}_{hh}\dot{S}_{vv}^{*} \rangle \\ 0 & 2\,\langle |\dot{S}_{hv}|^2 \rangle & 0 \\ \langle \dot{S}_{vv}\dot{S}_{hh}^{*} \rangle & 0 & \langle |\dot{S}_{vv}|^2 \rangle \end{bmatrix}$$

DUAL-POL REFLECTION SYMMETRY – X-BAND

- Dual-Pol HH/HV $\vartheta = 30.51$
- Time: 2009-07-15 at 06:30 UTC
- Wind: 5.1 m/s SW
- Targets: 8; Ground truth: 7 Ships (AIS)

- Dual-Pol TS-X VV/VH Θ = 39.7
- Time: 2011-08-30 at 14:15 UTC
- Wind: 2.2 m/s SE
- Targets: 50; Ground truth: 21 (10 AIS)

DUAL-POL REFLECTION SYMMETRY – X-BAND

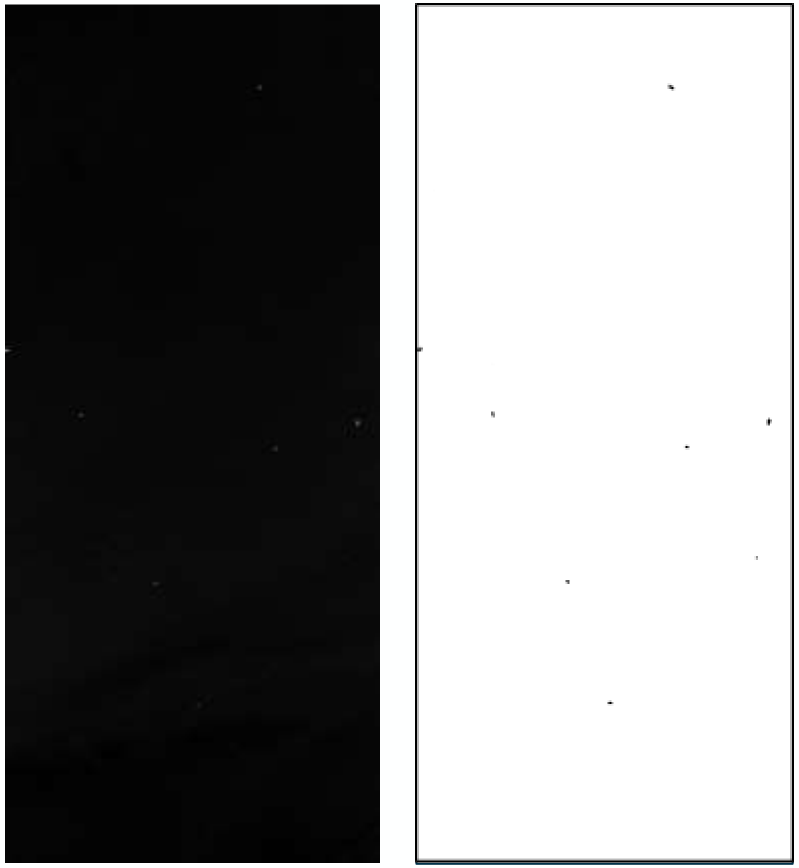

[Left] r image processed with 3x3 moving window based on dual-pol HH/HV.
[Right] Logical true-false output.

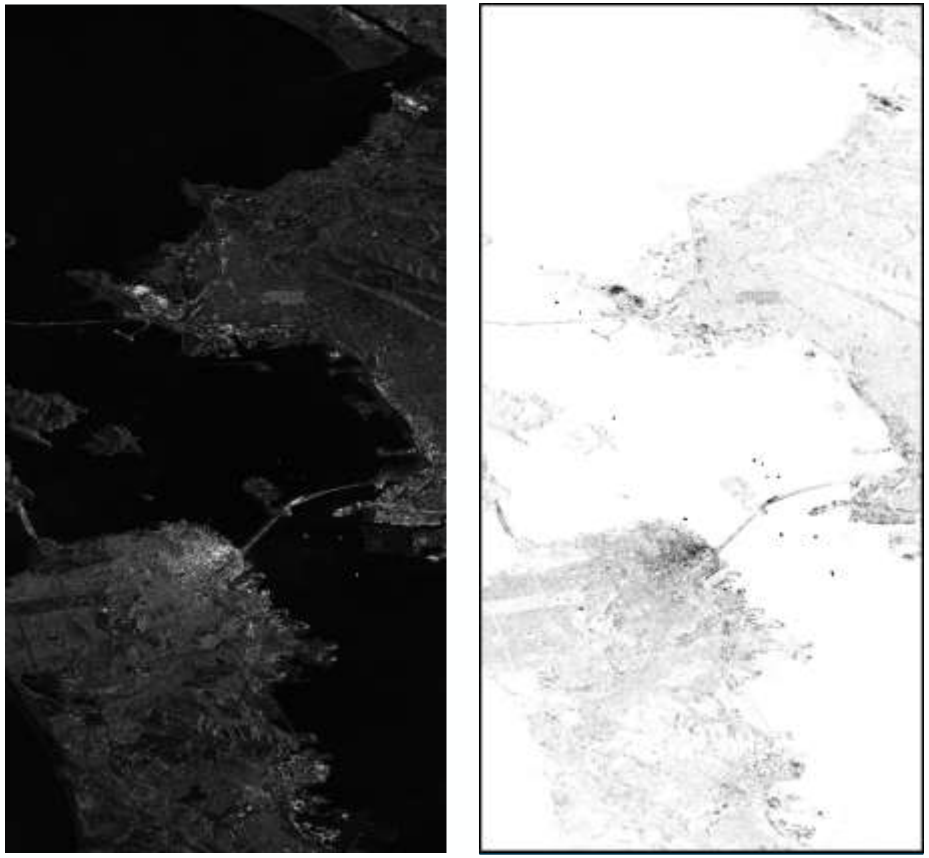

[Left] r image processed with 3x3 moving window based on dual-pol VV/VH.
[Right] Logical true-false output.

DUAL-POL REFLECTION SYMMETRY – X-BAND

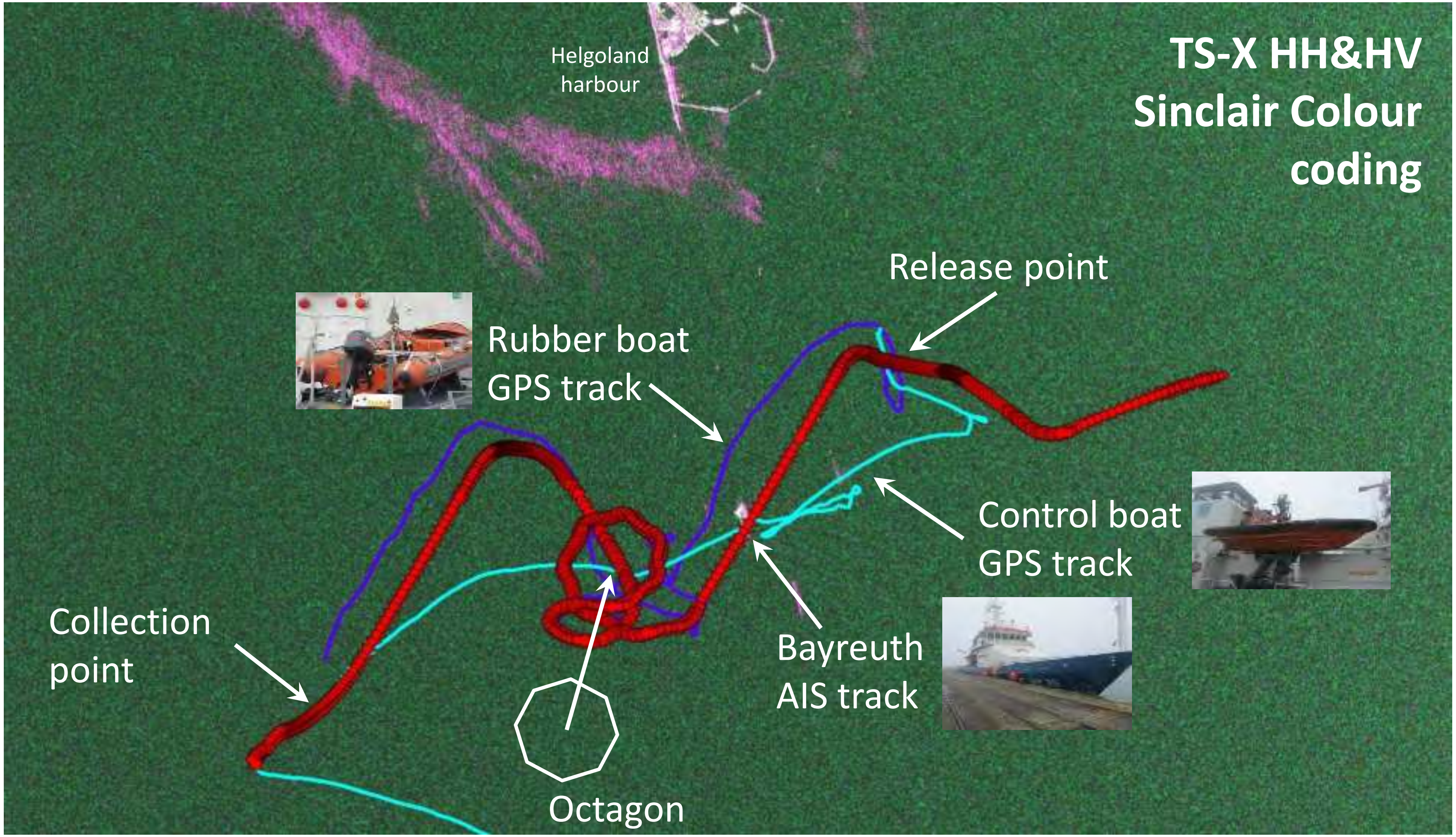

DUAL-POL REFLECTION SYMMETRY – X-BAND

Reflection symmetry approach tested during field experiment using a control boat

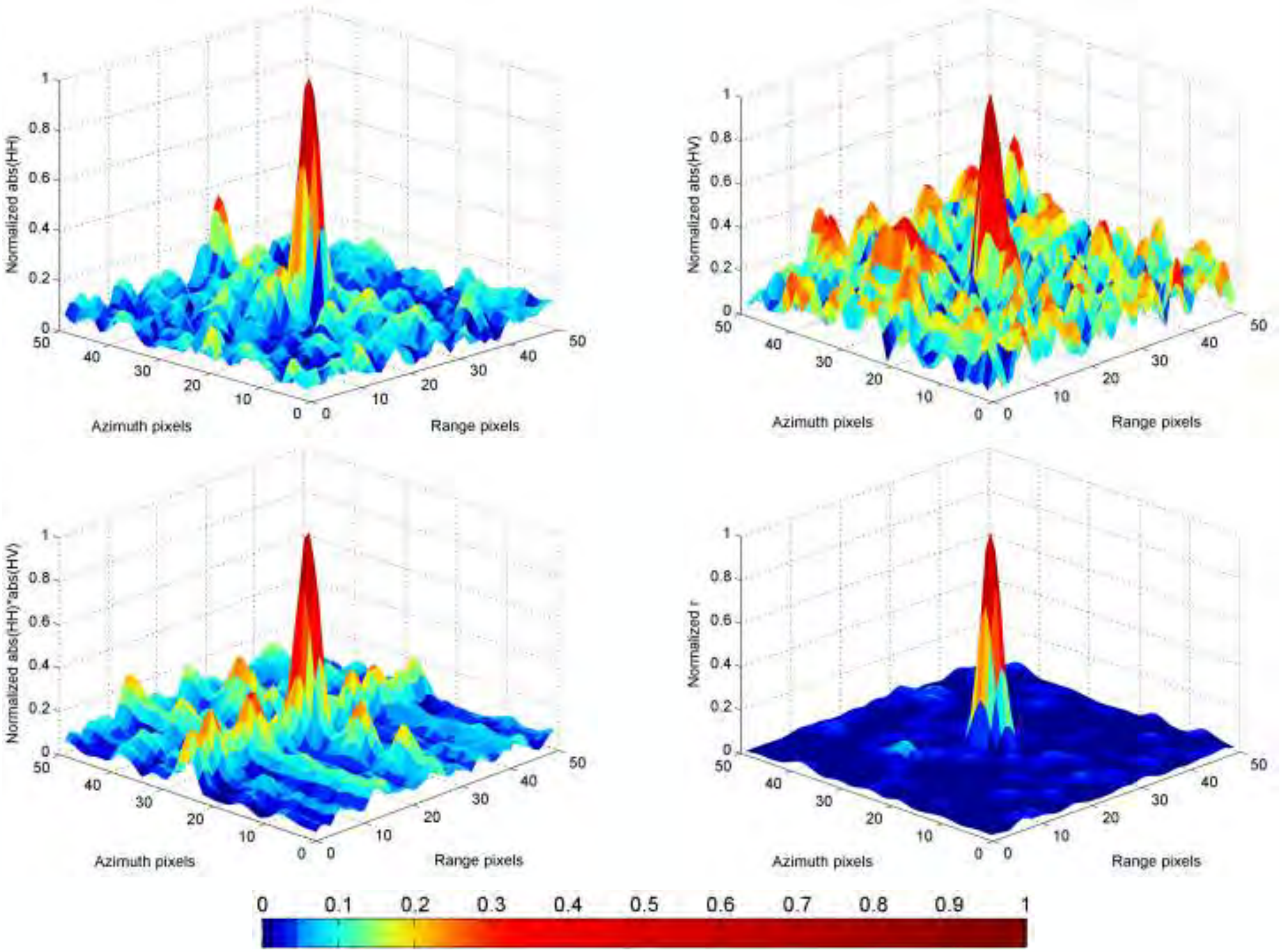

DUAL-POL REFLECTION SYMMETRY – X-BAND

Validation. Comparison to single-pol ship detection

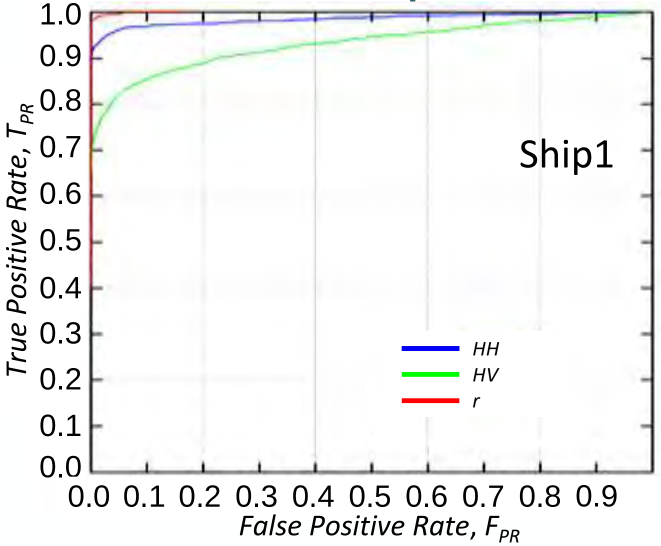

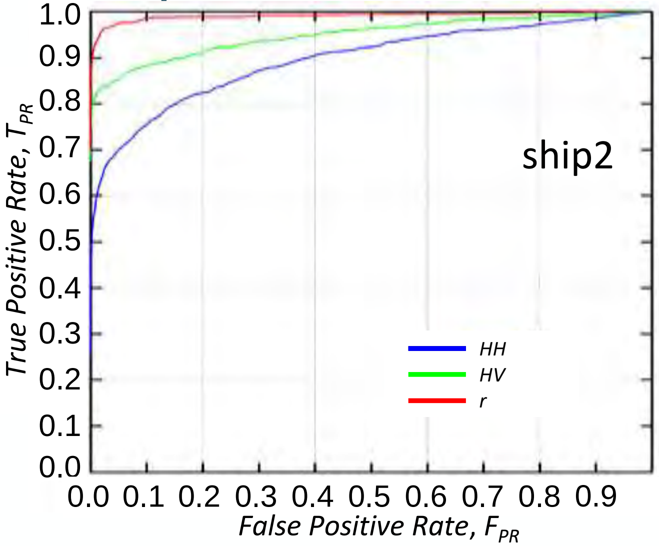

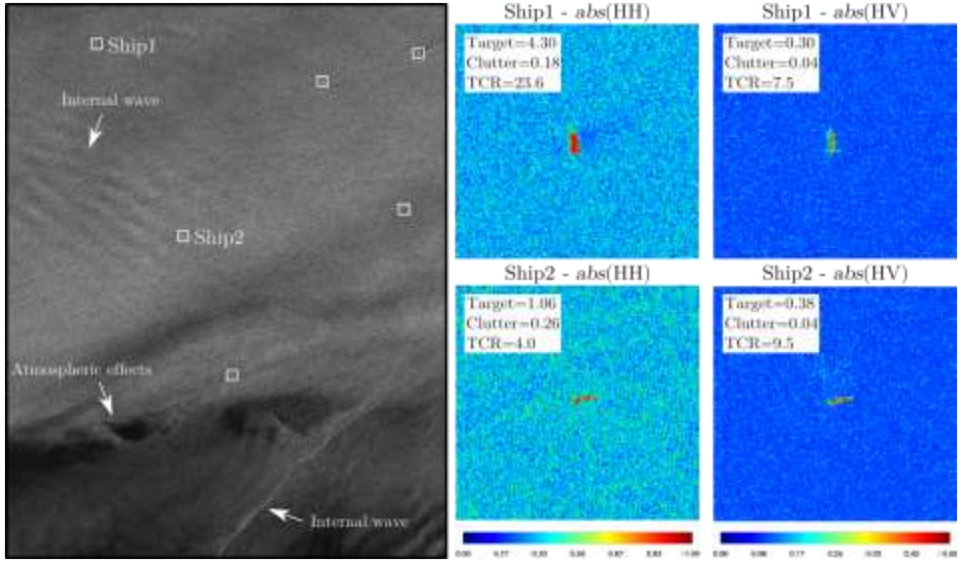

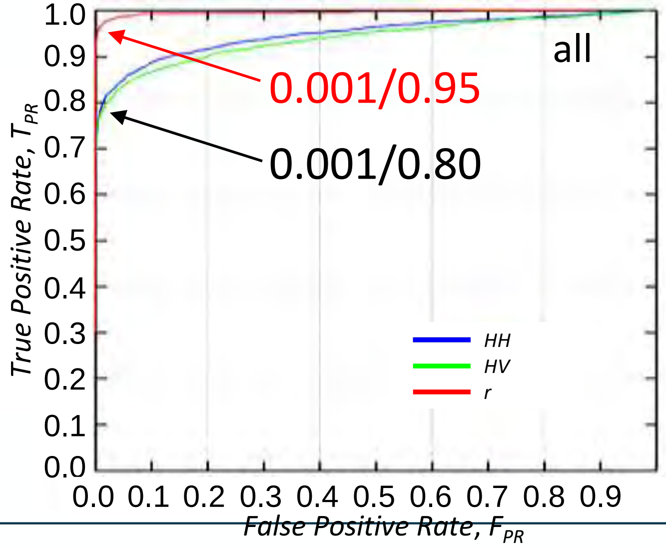

DUAL-POL REFLECTION SYMMETRY – L-BAND

Intensity HH

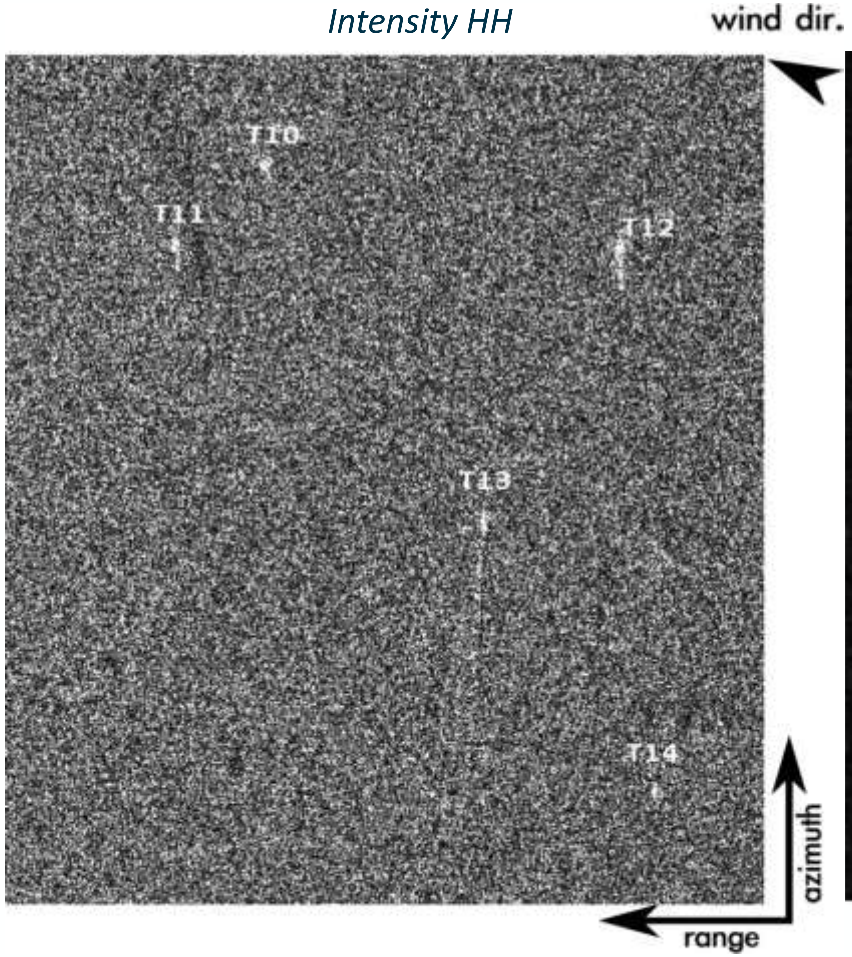

Reflection symmetry map

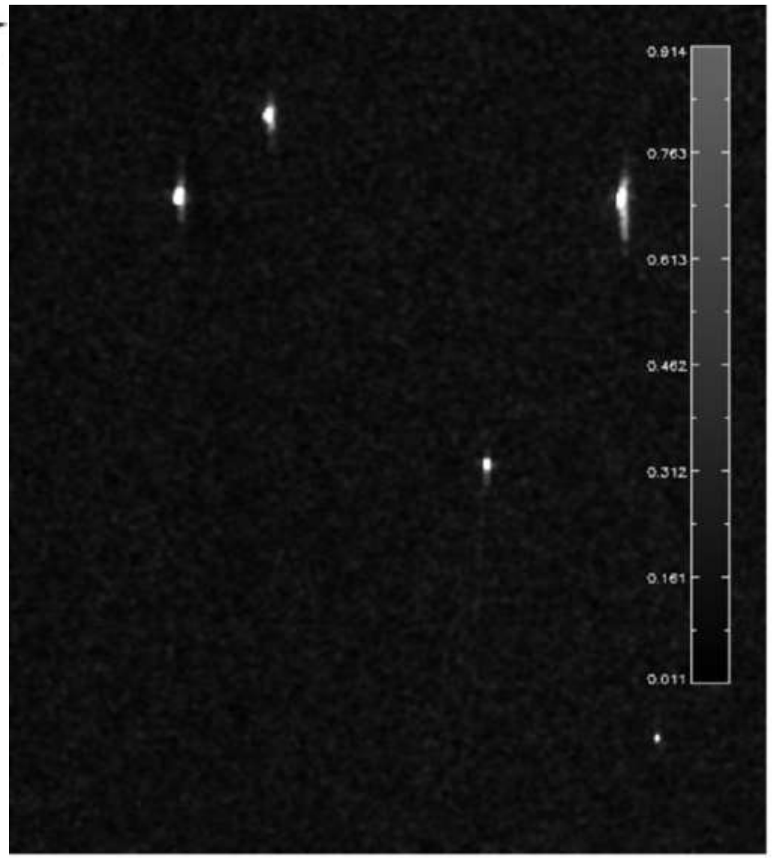

Detector output r>Thr

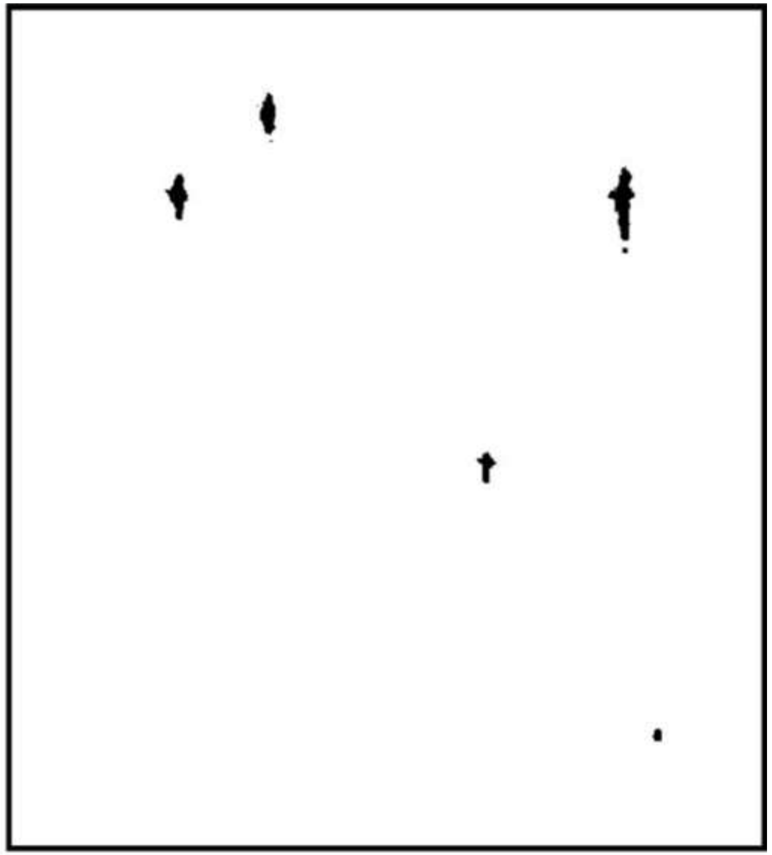

DUAL-POL REFLECTION SYMMETRY – C-BAND

Intensity HH

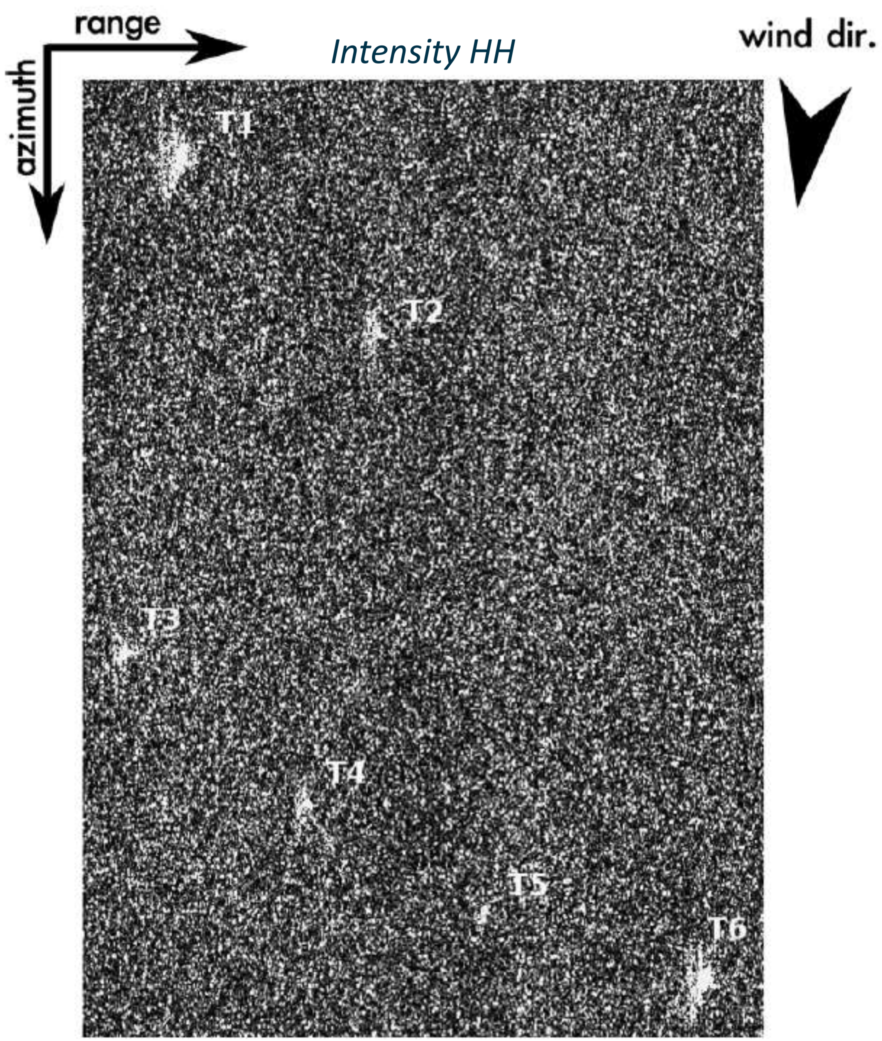

Reflection symmetry map

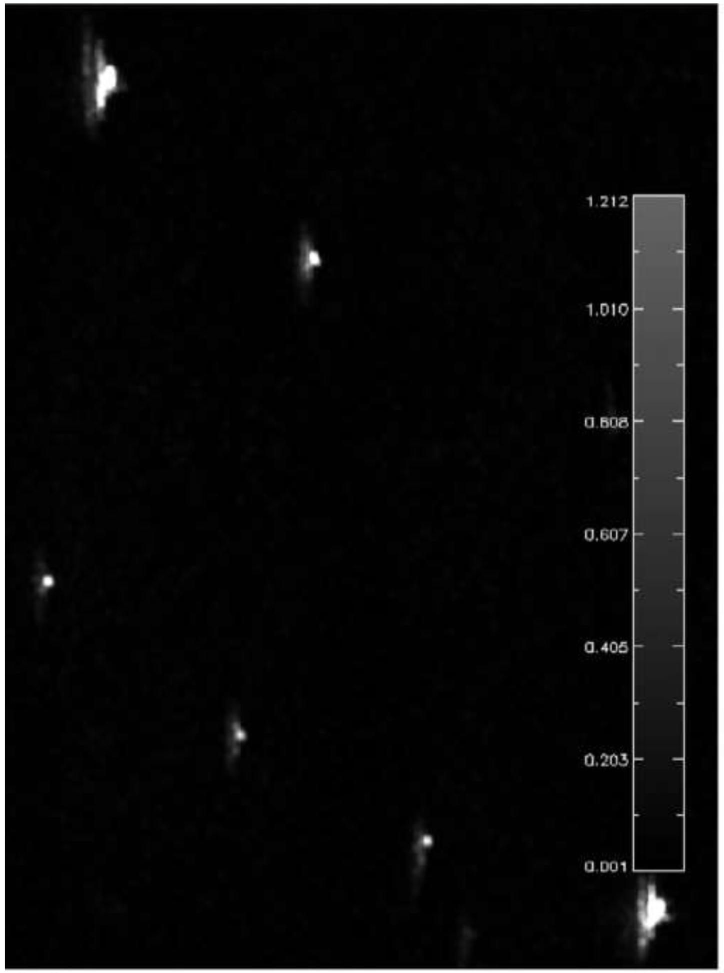

Detector output r>Thr

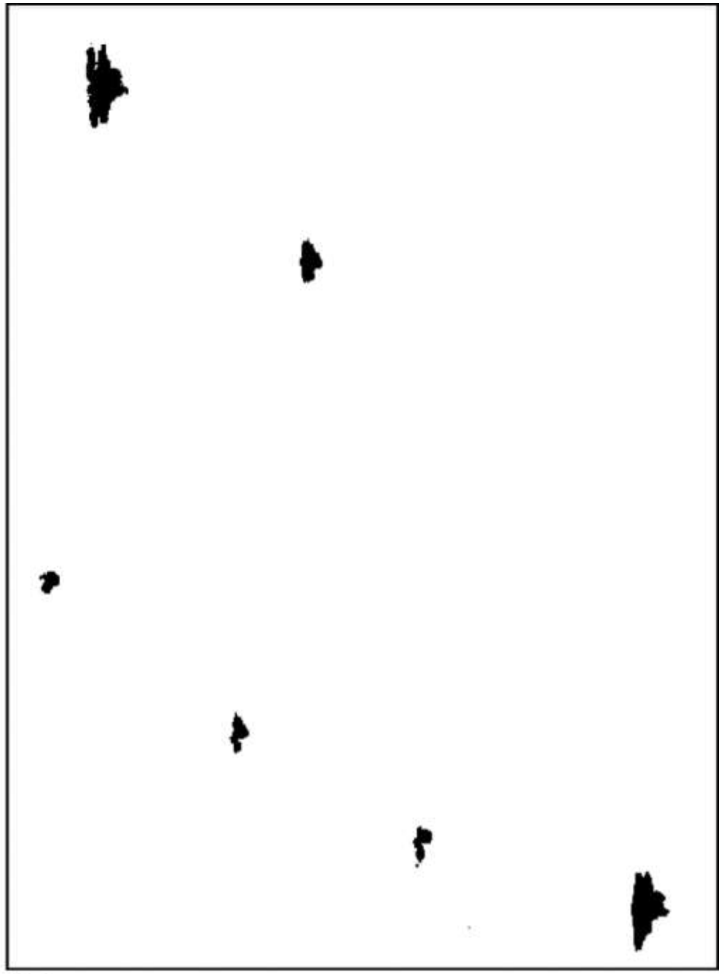

QUAD-POL AMBIGUITY FREE SHIP DETECTION

Spatial displacement of ghost replicas

$$\Delta x_{AZ} \approx \frac{mPRFv_S}{f_{\mathrm{DR}}}$$

$$\Delta x_{RG} = \frac{m\lambda PRF}{f_{\mathrm{DR}}}\left(f_{\mathrm{DC}} + \frac{mPRF}{2}\right)$$

and mutual relationship

$$\Delta x_{AZ} \approx m\frac{\lambda PRF}{2v_S}s_0$$

$$\Delta x_{RG} = \frac{(\Delta x_{AZ})^2}{2s_0}$$

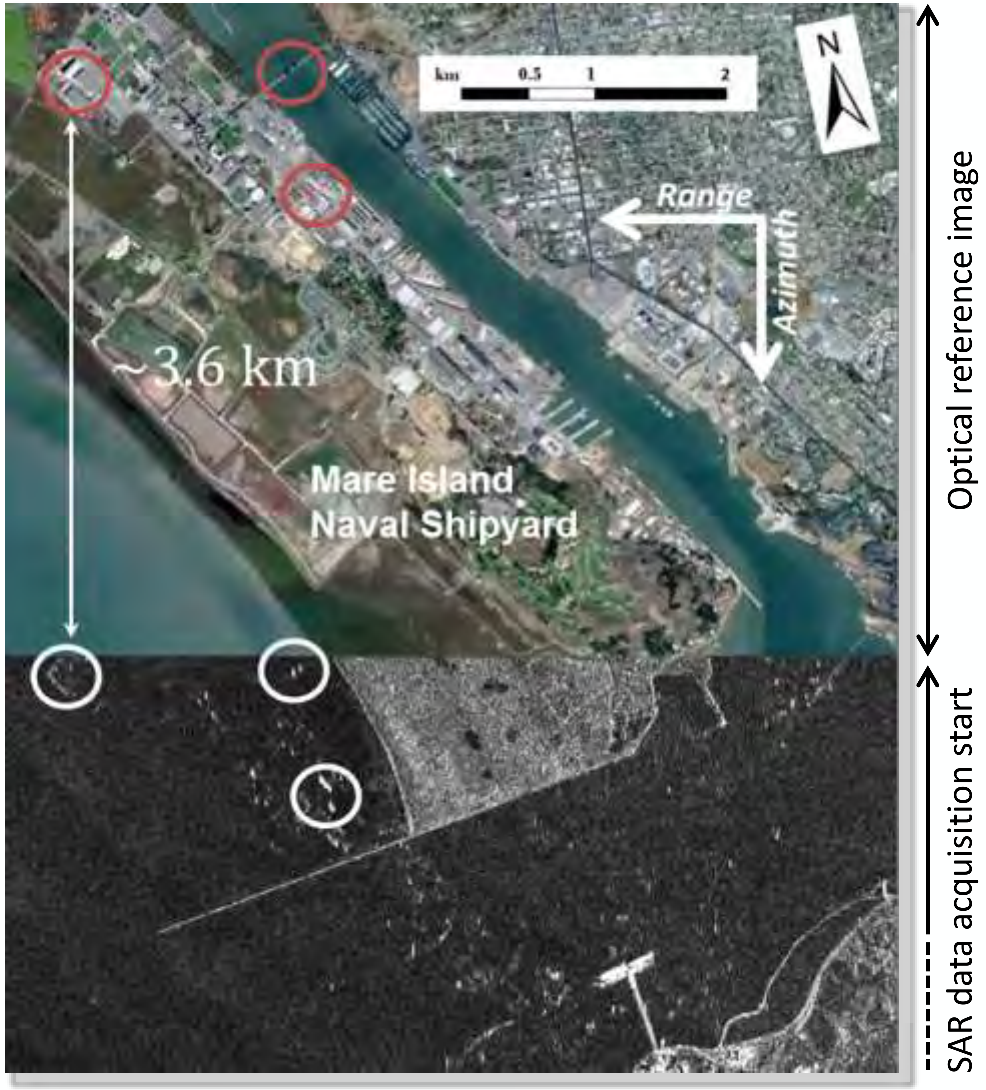

QUAD-POL AMBIGUITY FREE SHIP DETECTION

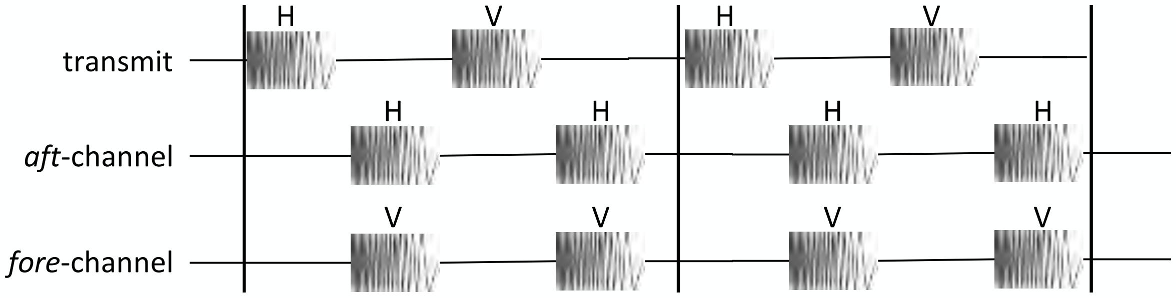

$\{s_{HH}, s_{HV}\}$ $\{s_{VH}, s_{VV}\}$ $\Rightarrow$ Time delay $PRI/2$

$x_n = v_S(n \cdot PRI)$ $\acute{x}_n = x_n + (v_S \cdot PRI/2)$ n-th azimuth line

$$s_{VH}(\tau, x_n) \cong s_{HV}(\tau, x_n) \quad \text{for} \quad x_n = x_T \Rightarrow \textbf{Targets}$$

$$s_{VH}(\tau, x_n) \cong -s_{HV}(\tau, x_n) \quad \text{for} \quad x_n = x_A^{\pm} \Rightarrow \textbf{Ambiguities}$$

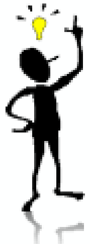

Ambiguities removal before target detection

$$HV_{free} = \frac{1}{2}\left[(\dot{S}_{hv} + \dot{S}_{vh})(\dot{S}_{hv} + \dot{S}_{vh})^*\right]$$

QUAD-POL AMBIGUITY FREE SHIP DETECTION

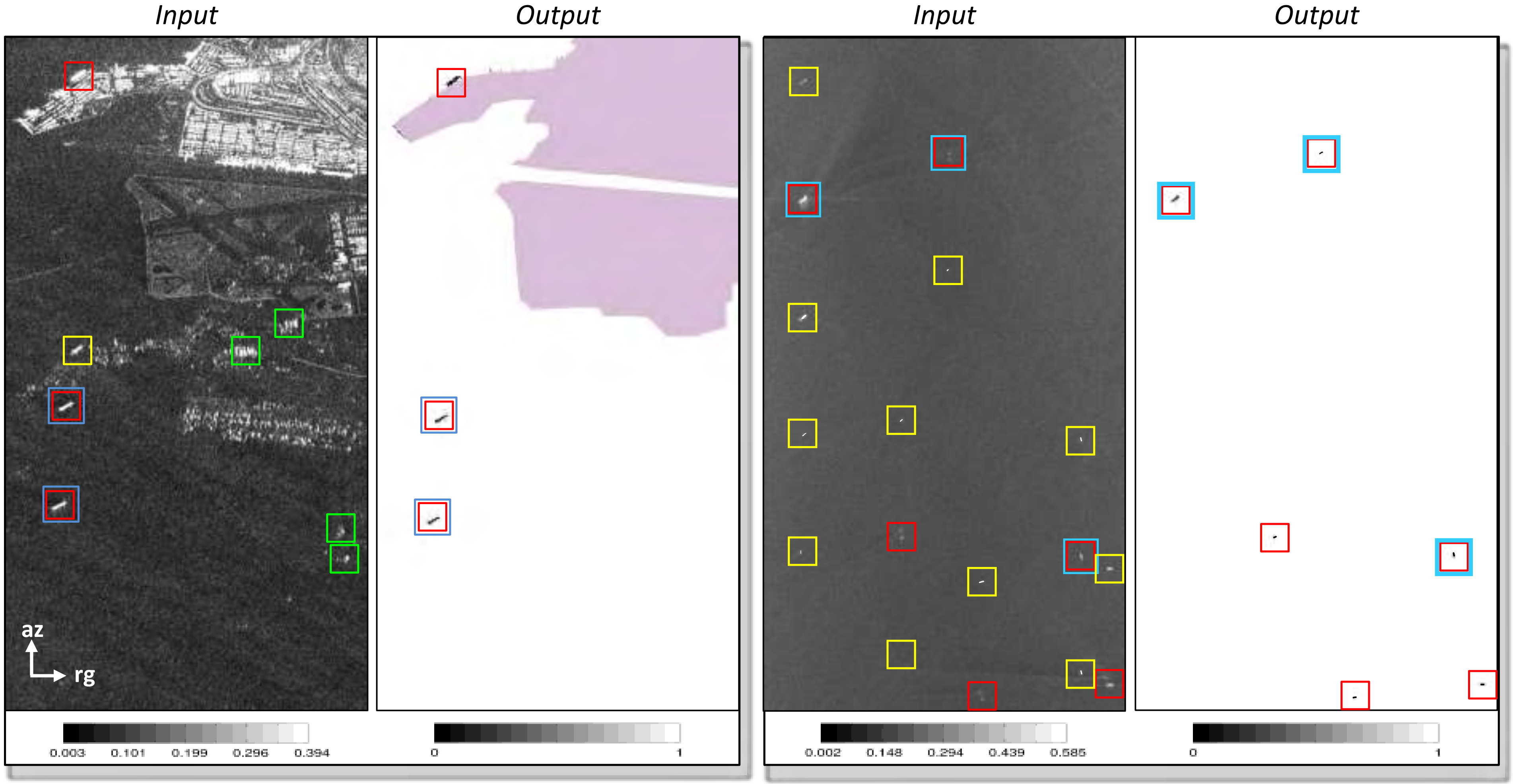

Legend Ships/Targets Ships Azimuth Ambiguities Land Azimuth Ambiguities Ships with available AIS

QUAD-POL AMBIGUITY FREE SHIP DETECTION

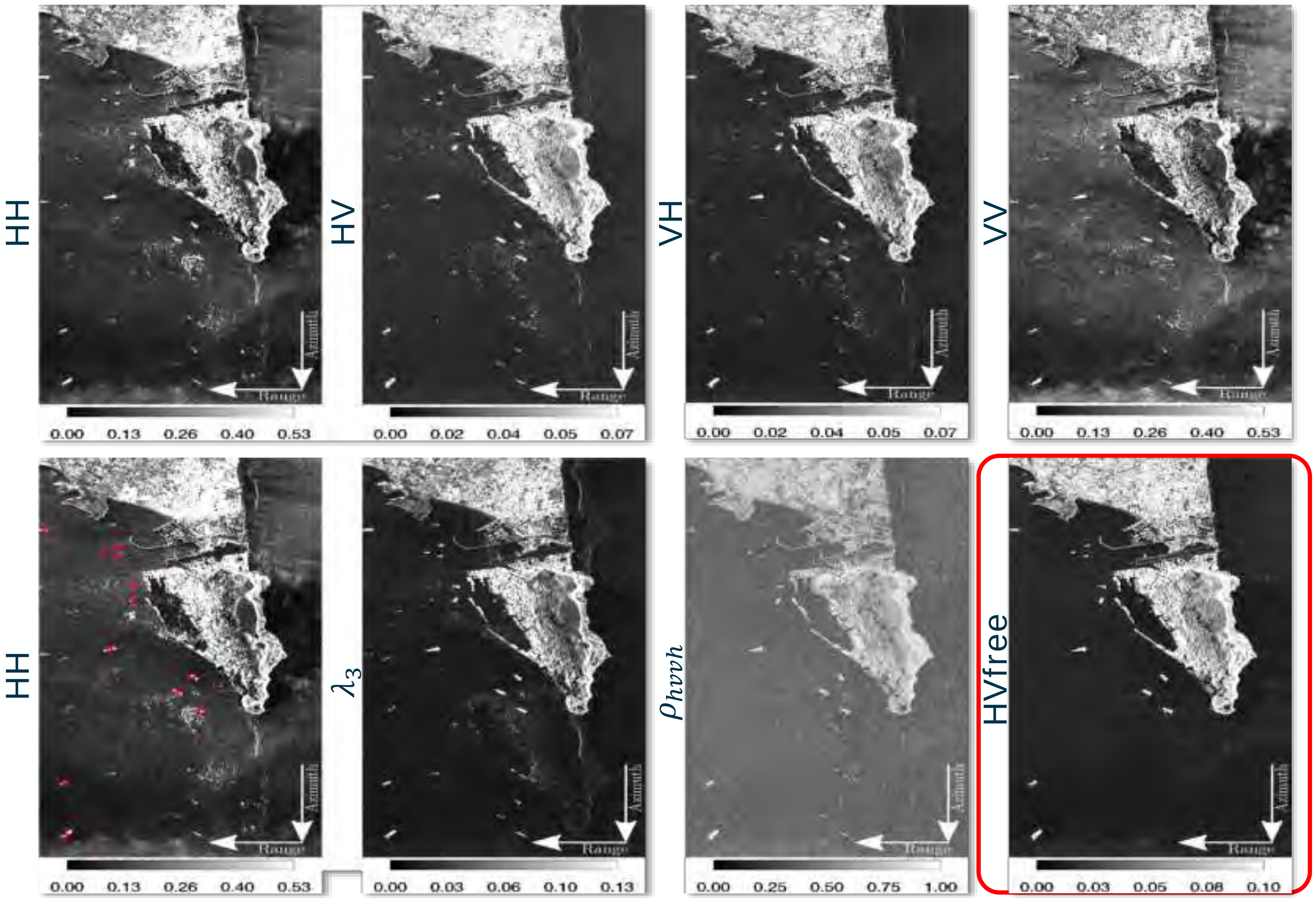

QUAD-POL AMBIGUITY FREE SHIP DETECTION

Validation. Comparison to other ambiguity free detectors

[3 x 1]

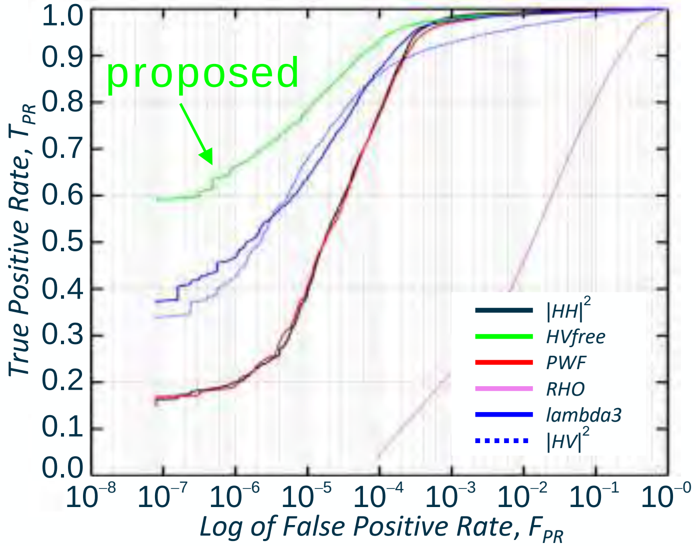

[5 x 3]

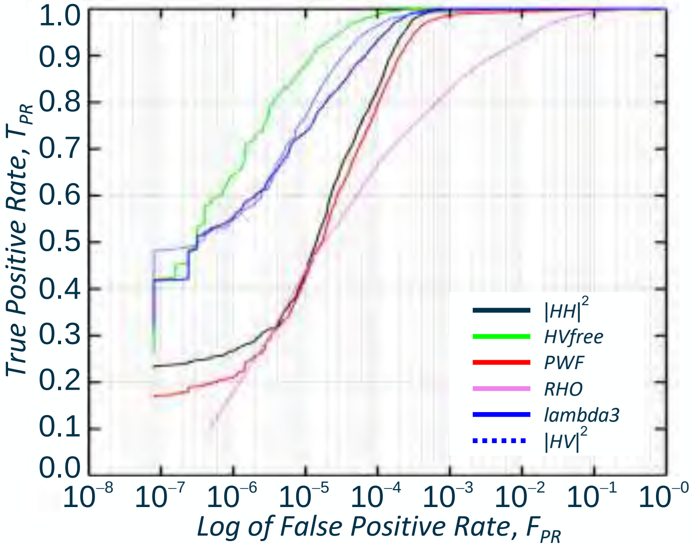

[7 x 5]

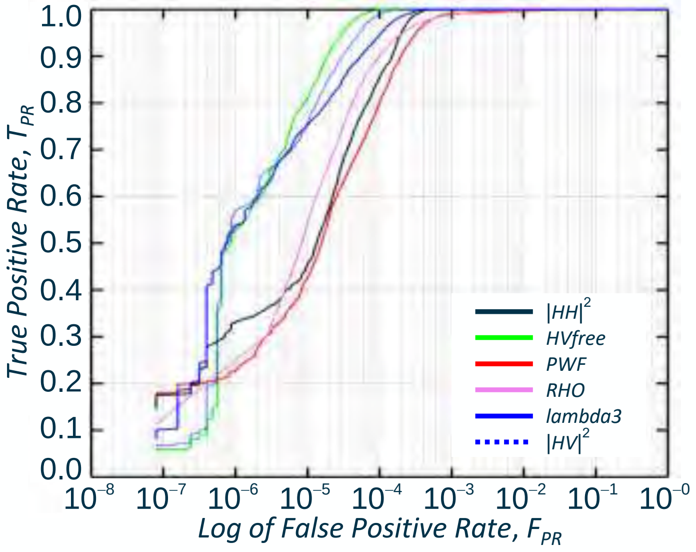

[9 x 7]

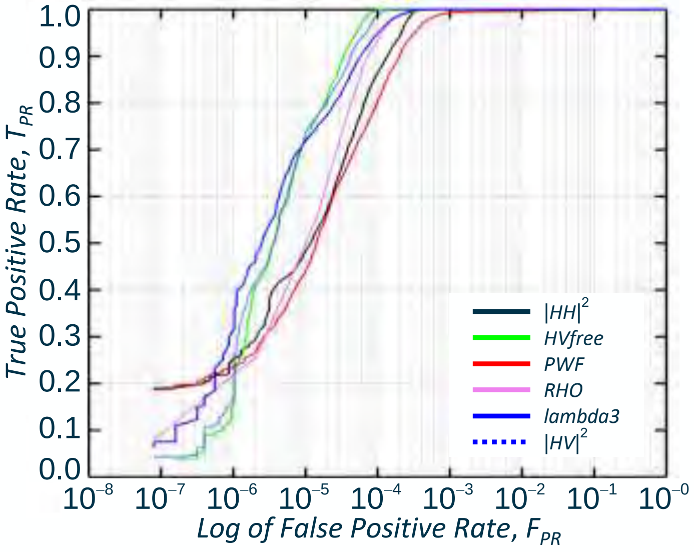

THANK YOU FOR YOUR ATTENTION!

Ship at sea exercise. Comparison of X-band SAR and X-band WaMoS®II wave radar system with added value of AIS tracks

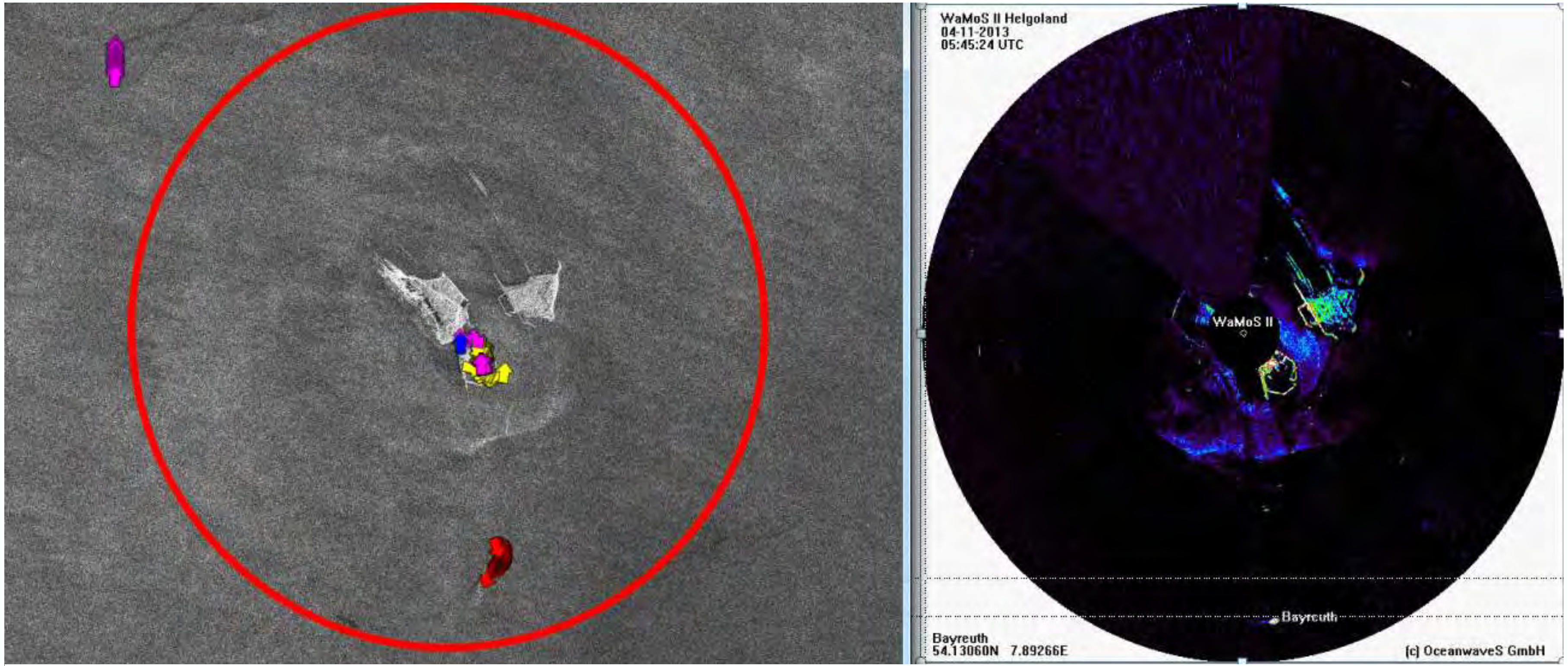

QUESTIONS?

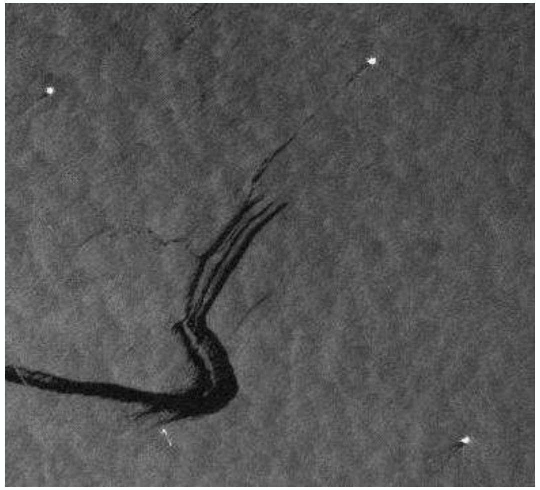

Oil spill, Seepage, Oil drift, Eddies

Ship detection, Wake

Land-Water line, Coastal erosion

Icebergs detection

Ice classification

Wind, Hurricane/Cyclone, Windfarm

Sea state, Wave breaking, Bathymetry

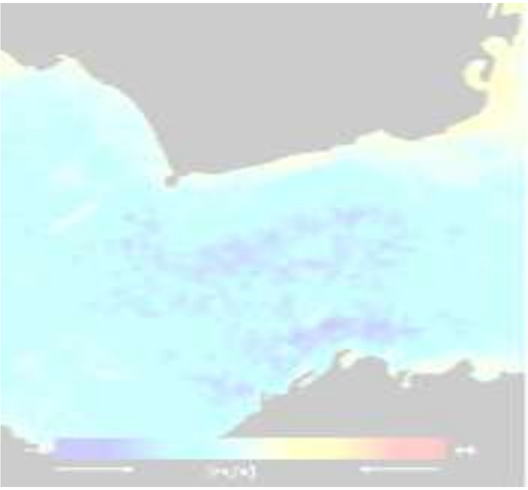

Surface current